DISCOVERY AND CHARACTERIZATION OF A NEW ZINC-BACTERIOCHLOROPHYLL BIOSYNTHETIC PATHWAY AND PHOTOSYSTEM IN A MAGNESIUM-CHELATASE MUTANT

by

Paul Richard Ayre Jaschke

B.Sc., The University of Alberta, June 4, 2003

A THESIS SUBMITTED IN PARTIAL FULFILLMENT OF THE
REQUIREMENTS FOR THE DEGREE OF
DOCTOR OF PHILOSOPHY

in

The Faculty of Graduate Studies

(Microbiology and Immunology)

THE UNIVERSITY OF BRITISH COLUMBIA

(Vancouver)

August 2010

Abstract

Porphyrins, for example heme and chlorophyll, are vital to biological processes such as respiration and photosynthesis. Both cofactors are synthesized through a common pathway to protoporphyrin IX (PPIX) which then branches: Fe^{2+} chelation into the macrocycle by ferrochelatase results in heme formation; by contrast, Mg^{2+} addition by Mg-chelatase commits the porphyrin to (bacterio)chlorophyll synthesis.

The purple bacterium *Rhodobacter sphaeroides* is a model for bacteriochlorophyll *a* (BChl) biosynthesis and type-2 reaction center (RC) structure and function. While studying RC protein assembly it was discovered that a *bchD* (Mg-chelatase) mutant did not produce BChl as wild-type (wt) cells do, but instead produced small quantities of an alternative BChl in which Mg^{2+} was substituted by Zn^{2+}. Zn-BChl *a* has been found in only one other organism before, the related acidophilic purple phototrophic bacterium *Acidiphilium rubrum*. The overall objectives of this thesis were two-fold: (1) to elucidate the Zn-BChl biosynthetic pathway; and (2) to utilize this biosynthesis as a tool to probe aspects of photosynthetic apparatus function.

The biosynthetic pathway of Zn-BChl in the *bchD* mutant was found to begin at ferrochelatase, which efficiently chelated Zn^{2+} into PPIX. The resultant Zn-PPIX was utilized by the BChl-biosynthetic pathway, with metabolites early in the pathway accumulating, but with low Zn-BChl levels. Two novel intermediates I described, protoporphyrin IX monomethyl ester and divinyl-protochlorophyllide, contained Zn^{2+} instead of Mg^{2+}. The demonstrated Zn-BChl biosynthetic pathway is a new way to make BChl and facilitates the further engineering of alternate forms of (Zn-)BChl.

The RC in the *bchD* mutant (Zn-RC) was found to bind six Zn-BChls, instead of the four Mg-BChls and two bacteriopheophytins of the WT-RC. Spectroscopic examination showed that electron transfer (ET) in the Zn-RC occurs at approximately the same rate as in the WT-RC, despite substitution of Zn-BChl for bacteriopheophytin *a*. We showed preservation of ET was due to the unusual tetracoordination state of the Zn-BChls in the bacteriopheophytin site. This discovery allows refinement of ET rules within pigment-

protein complexes by showing that the coordination state and conformation of cofactors can have an equally important role as the protein.

Table of Contents

List of Tables

List of Figures

ABBREVIATIONS

6His	6 histidine tag added to terminus of protein to aid in purification.
ALA	δ-aminolevulinic acid. Biosynthetic precursor to heme and bacteriochlorophyll.
Ap (Ap^R)	Ampicillin antibiotic (ampicillin resistance).
Apo-HRP	Apo-horseradish peroxidase.
B_A and B_B	Binding sites in reaction center that contain the accessory bacteriochlorophylls in the wild type. Subscript letters denote the physical location of the binding site on either the A- or B-branch of the cofactor pathway.
BChl	Bacteriochlorophyll *a*.
(B)Chl	(Bacterio)chlorophyll. Refers generically to both bacteriochlorophylls and chlorophylls.
BChlide	Bacteriochlorophyllide *a*. Bacteriochlorophyll-synthesis intermediate just prior to phytol addition.
BPhe	Bacteriopheophytin *a*. Structure of bacteriochlorophyll *a* but with metal removed.
BPheide	Bacteriopheophorbide *a*. Structure of bacteriochlorophyllide *a* but with the metal removed.
BN-PAGE	Blue-native polyacrylamide electrophoresis.

CFU	Colony forming unit of bacteria.
Chl	Chlorophyll *a*.
CPTS	Copper phthalocyanine 3,4′,4″,4‴-tetrasulfonic acid tetrasodium salt. A reversible protein stain for Western blot membranes.
Chromatophore	Specialized portion of cytoplasmic membrane in *Rb. sphaeroides* that is induced by low oxygen and that contains high concentration of photosynthetic complexes. See ICM.
DCTB	Chemical matrix used to crystallize material analyzed on MALDI-TOF mass spectrometry. Also known as (*trans*-2-[3-(4-tert-butylphenyl)-2-methyl-2-propenylidene]-malononitrile.
DDM	Dodecyl maltoside detergent.
DMSO	Dimethylsulfoxide.
DV-PChlide	Generic term referring to divinyl-protochlorophyllide *a*.
DV-Mg-PChlide	Divinyl-magnesium-protochlorophyllide *a*.
DV-Zn-PChlide	Divinyl-zinc-protochlorophyllide *a*.
ET	Electron transfer.
H_A and H_B	Binding sites in reaction center that contain bacteriopheophytins in the wild type. Subscript letters denote the physical location of the binding site on either the A- or B-branch of the cofactor pathway.

HEAR	Hexane-extracted acetone residue. The acetone/NH_4OH cell extract after carotenoids and chlorophylls are removed by extracting with hexane.
Heme	Ferrous iron-protoporphyrin IX.
ICM	Intracytoplasmic membrane of *Rb. sphaeroides*. Also known as chromatophores. They are a specialized portion of cytoplasmic membrane that is formed under low oxygen conditions and that contain a high concentration of photosynthetic complexes.
kb	Kilobase(s). 1000 DNA or RNA bases.
Km (Km^R)	Kanamycin antibiotic (kanamycin resistance).
LDAO	Lauryldimethylamine-oxide detergent.
LH1	Light-harvesting 1.
LH2	Light-harvesting 2.
Mg-PPIX	Magnesium-protoporphyrin IX.
Mg-PPIX-MME	Magnesium-protoporphyrin IX monomethyl ester.
MS	Mass spectrometry.
m/z	Mass to charge ratio.
MPC	Multiprotein complex.
Nm (Nm^R)	Neomycin antibiotic (neomycin resistance)
NMPP	N-methylprotoporphyrin IX. Ferrochelatase inhibitor.

OBTG	Octyl-β-D-thioglucopyranoside detergent.
OD	Optical density.
P	Binding sites in reaction center that contain the special pair bacteriochlorophyll dimer.
P*	Excited state of the special pair bacteriochlorophyll dimer in the photochemical reaction center.
PChlide	Protochlorophyllide *a*. Generic term for both monovinyl and divinyl version of the molecule.
PPIX	Protoporphyrin IX. Biosynthetic intermediate common to heme and bacteriochlorophyll synthesis pathways.
PS1	Photosystem 1.
PS2	Photosystem 2.
Q_X	The intermediate energy absorption band (transition) for chlorins and porphyrins.
Q_Y	The lowest energy absorption band (transition) for chlorins and porphyrins.
RC	Reaction center.
RCF	Relative centrifugal force.
SAM	S-adenosylmethionine. Methyl donor in enzymatic reactions.
SDS-PAGE	Sodium dodecyl sulfate polyacrylamide gel electrophoresis.

Soret peak	Strongest absorption band in the blue end of the visible spectrum.
Sp (Sp^R)	Spectinomycin antibiotic (spectinomycin resistance).
Tc (Tc^R)	Tetracycline antibiotic (tetracycline resistance).
wt	Wildtype.
Zn-BChl	Zinc-bacteriochlorophyll *a*. Structure of Magnesium-bacteriochlorophyll *a* but with Mg^{2+} replaced by Zn^{2+}.
Zn-PPIX	Zinc-protoporphyrin IX. Structure of Magnesium-protoporphyrin IX but with Mg^{2+} replaced by Zn^{2+}.
Zn-PPIX-MME	Zinc-protoporphyrin IX monomethyl ester. Structure of Magnesium-protoporphyrin IX monomethyl ester but with Mg^{2+} replaced by Zn^{2+}.

Acknowledgements

I would like to thank my supervisor Dr. Beatty for the excellent guidance. You gave me the freedom to explore many ideas. I couldn't imagine a better supervisor.

My committee was a stable guiding force that helped me learn the valuable lesson that science is too big to do everything. Past mentors have shaped the scientist I've become and I'm forever indebted to their guidance. Dr. Joseph Casey gave me my first break into science and allowed me to author my first paper. Dr. Marek Michalak taught me about dignity and respect, especially in the face of hardship, and is a model of the scientist I aspire to be.

I'd like to thank the Eltis, Jean, Murphy, and McIntosh Labs, who helped with equipment and expertise crucial to finishing this project. Many people helped provide the materials and services that kept my work going smoothly over the years and I'd like to acknowledge their hard work that enabled everything in this thesis.

In particular, five undergraduate students pushed my project forward and helped me become a better leader and mentor. I like to thank Elizabeth Digby who made and validated the double mutants, Amelia Hardjasa who performed heme assays and tried to make the *bchD* mutant photosynthetic, Tobie Patterson and Brandon Ash who also tried to make the *bchD* mutant photosynthetic, and Connie Lee who worked on RC protein association.

I will remember fondly all the members of the Beatty lab that I crossed paths with and I hope our paths will cross again. Also, I would like to thank Kris Shelswell for coming up with the idea to inhibit ferrochelatase. It was so I good I didn't listen the first time!

I owe a special debt of gratitude to Dr. Neil Hunter who provided me with the TB59 (*bchD*) strain that completely changed the direction of my thesis.

My Mom, Dad, and Brother have provided constant support through their genuine interest in my work. Thanks, that's all I needed!

My lovely wife Annette has provided constant encouragement through this journey, and always believed in me, even when I didn't.

1. Introduction

The Sun shines about 700 quadrillion (7×10^{17}) kilowatt-hours per year onto the Earth's surface, some of which is captured by the 10^{11} tons of chlorophylls synthesized by primary producers such as plants and photosynthetic bacteria (Scheer 2006). This captured energy provides the foundation for most of the inhabitants of Earth by driving carbon-fixation and conversion to biomass. One of the main issues remaining in our understanding of this vital process is the assembly and maintenance of the intramembrane complexes of chlorophylls and proteins responsible for the absorption and conversion of light into chemical energy by photosynthetic organisms. There is a wide diversity of photosynthetic organisms that synthesize four classes of antenna complexes and two types of reaction centers composed of a wide diversity of proteins, which convert photons to chemical energy. In addition to the diversity of photosynthesis proteins there are approximately 12 different types of chlorin pigments that bind these photocomplexes, with the most diversity found in the anoxygenic phototrophs (Chew & Bryant 2007; Scheer 2006). The structures of these pigments can be divided roughly into the chlorophylls found in cyanobacteria and algae up through plants, and bacteriochlorophylls, which are only found in phototrophic bacteria (Scheer 2006). The main difference between these two types of pigments is in the saturation state of the porphyrin macrocycle, with bacteriochlorophylls having a more reduced (unsaturated) structure than chlorophylls. Many of the corresponding biosynthetic pathway details for these (bacterio)chlorophylls are still largely a mystery (Chew & Bryant 2007).

1.1. *Rhodobacter sphaeroides* is an important model organism for the study of photosynthesis

The purple non-sulfur bacterium *Rhodobacter sphaeroides* is a member of the α-proteobacterial class and has become a model system for studying both bacteriochlorophyll *a* (hereafter referred to as BChl) biosynthesis and assembly of bacterial photosynthetic complexes. This organism's features include a versatile metabolism, information from decades of spectroscopic analyses, and a wealth of structural data. The two-chromosome genome has been sequenced, and genes are easily

manipulated and introduced into knockout strains to study mutant proteins in the homologous host (Choudhary et al. 2007; Lavergne & Vermeglio 2009; Mackenzie et al. 2001; Parson & Warshel 2009; Sener & Schulten 2009; Williams & Taguchi 1995). Under oxic conditions in darkness, the bacterium utilizes O_2 as a final electron acceptor to generate energy via respiration, funneling electrons through the cytoplasmic membrane-bound cytochrome-bc_1 complex, soluble periplasmic cytochrome-c_2, and finally to oxygen via membrane-bound cytochrome-cbb_3 and -aa_3 terminal oxidase complexes (Oh & Kaplan 2000).

The presence of membrane-bound light-harvesting antenna and reaction center complexes (the photosynthetic apparatus) is repressed by high concentrations of oxygen, and induced in response to low concentrations of oxygen (Zeilstra-Ryalls et al. 1998). With a drop in oxygen levels, an intricate and highly coordinated response occurs as the organism shifts to anoxygenic phototrophic growth. Several regulators of photosynthesis genes sense a change in the redox state of the electron transport chain caused by oxygen deprivation, which in turn causes a derepression and activation of many genes involved in the synthesis of photosynthetic apparatus proteins, pigments, and membrane (Moskvin et al. 2005).

Photosynthetic apparatus assembly has been studied by shifting cultures from high to low O_2 growth conditions, to reveal the regulation of many genes involved in pigment biosynthesis and production of photosynthesis proteins (Zeilstra-Ryalls et al. 1998). As these photosynthetic proteins are inserted into the cell membrane, the membrane itself is thought to expand. These structures mature into an intracytoplasmic membrane (ICM) system of vesicular invaginations, both contiguous with the cytoplasmic membrane and completely separated vesicles within the cytoplasm (Chory et al. 1984; Tucker et al. 2010). The photosynthesis apparatus is housed in the ICM (Chory et al. 1984), and uses light energy to drive electron transfer (ET) reactions that result in the net transport of protons from the cytoplasm to the periplasm, which generates a transmembrane electrochemical gradient that is used primarily for ATP synthesis (Okamura et al. 2000).

1.2. The structure and function of the photosynthetic apparatus of *Rb. sphaeroides*.

1.2.1. Photosynthetic apparatus structure.

The core of the photosynthetic apparatus is a dimer of reaction center (RC) complexes surrounded by the light-harvesting 1 (LH1) complex and the PufX protein (Qian et al. 2005; Scheuring et al. 2005; Scheuring et al. 2004). The LH1 complex consists of α/β heterodimer subunits that each bind two coupled BChl that absorb at 875 nm (Kohler 2006). Between 24-28 of the heterodimers form an S-shaped structure surrounding the RC complexes (Figure 1-1). The location and exact function of PufX in the core-complex is unknown, although this protein is essential for photosynthetic electron and proton transfer reactions (Holden-Dye et al. 2008). One model places PufX adjacent to the RC quinone binding site (Qian et al. 2008; Qian et al. 2005), whereas another model features a PufX dimer linking the two RCs (Scheuring et al. 2005; Scheuring et al. 2004).

The RC contains three proteins called H, M and L; the structurally similar RC M and L proteins consist of five transmembrane helices with pseudo two-fold symmetry, whereas the RC H protein has only one transmembrane helix and a large cytoplasmic domain (Yeates et al. 1988) . In addition to possessing similar structure, the RC M and L proteins share 33% amino acid identity. The overlapping *pufM* and *pufL* genes encoding these RC proteins are located within the 66.7 kb region of chromosome 1 called the photosynthesis gene cluster, and are transcribed on a polycistronic mRNA. In contrast, the RC H gene *puhA* is transcribed from an operon 38 kb distant from *pufML* but still within the photosynthesis gene cluster (Figure 1-2).

In the ICM, RC-LH1-PufX dimers appear to form linear arrays that are surrounded by a pool of light-harvesting 2 (LH2) complexes which form an antenna that directs photonic energy towards the core-complex (Bahatyrova et al. 2004) (Figure 1-1). The LH2 complex consists of rings of nine α/β protein heterodimers that each bind a carotenoid and three BChl molecules; two BChls form a dimer that absorb at 850 nm, and the other BChl absorbs at 800 nm (Kohler 2006).

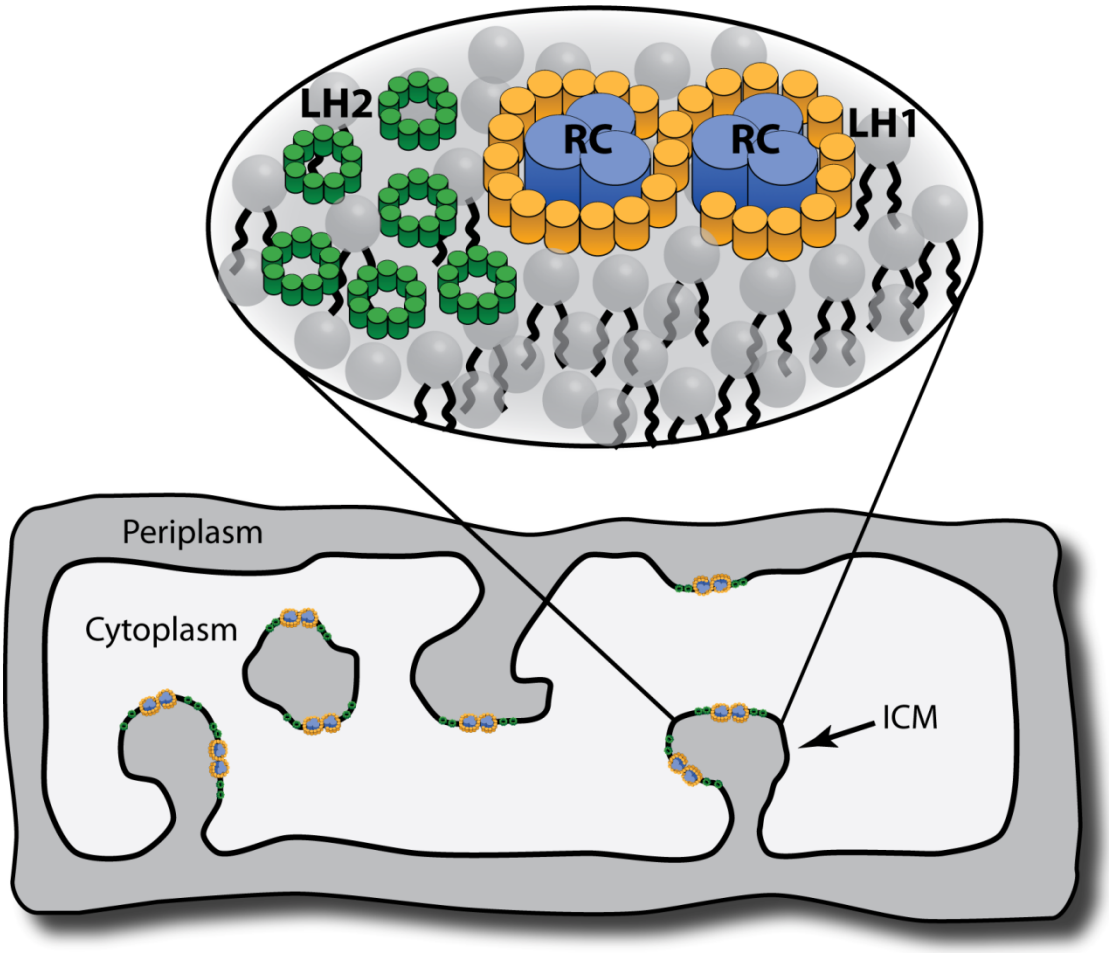

Figure 1-1. Membrane topology of *Rb. sphaeroides* photosynthetic apparatus.

Photosynthetic apparatus is located mainly in cytoplasmic membrane invaginations called ICM or chromatophores.

Figure 1-2. The 66.7 kb *Rb. sphaeroides* photosynthesis gene cluster. The gene cluster depicted is located on chromosome 1 between the displayed starting and ending coordinates. Each bar indicates a known gene or predicted open reading frame. Shading used to differentiate operons. Scale bar indicates distance of 1 kb of sequence. Arrow indicates location of the *bchD* gene mutation. Gene abbreviations are: *puf*, RC and LH1 structural proteins; *bch*, bacteriochlorophyll biosynthesis; *crt*, carotenoid biosynthesis; *acsF*, magnesium-protoporphyrin IX monomethyl ester oxidative cyclase ; *cyc*, cytochrome; *puhA*, RC H structural protein; *ure*, urea metabolism; *puc*, LH2 structural proteins; *hemN*, protoporphyrin IX synthesis; *amiR*, amidase regulator; *ppsR* and *ppaA*, photosynthesis gene regulators. Genome sequence for *Rb. sphaeroides* 2.4.1 chromosome 1 available from NCBI Entrez Genome database (accession number NC_007493.1).

1.2.2. Electron transfer in the reaction center.

The energetics of ET in the wild type RC (WT-RC) of *Rb. sphaeroides*, involve the generation of a strong reductant that can then inject electrons into the electron transfer chain. This strong reductant is the photon-excited special pair of (B)Chls in most photosynthetic organisms, including *Rb. sphaeroides*. The reductant is harnessed by two RC architectures, referred to as iron-sulfur (type 1) and pheophytin-quinone (type 2) RCs. Both RC types are thought to share a common ancestor (Schubert et al. 1998) although they have evolved to interact with different secondary-electron acceptors.

In type 1 RCs the excited 'special pair' of (B)Chls transfer an electron to a secondary (B)Chl acceptor called A_0, probably via an intermediate (B)Chl although it is not well established, and then on to several Fe-S binding proteins (Melkozernov & Blankenship 2006). The Fe-S proteins reduce $NADP^+$ to NADPH, and this reducing power is used for conversion of CO_2 into glucose (Romagnoli & Tabita 2009).

Type 2 RCs, as herein exemplified by the *Rb. sphaeroides* RC, contain a 'special pair' BChl dimer (sometimes called 'P') bound by RC M and L on the periplasmic side of the membrane (Figure 1-3A). The special pair is flanked by two accessory BChls bound to RC L (in the B_A site) and RC M (in the B_B site), which are the periplasmic ends of two cofactor branches called A and B. Two bacteriopheophytin *a* (hereafter referred to as BPhe) molecules (in the H_A and H_B sites) are located between the accessory BChls and two quinones (Q_A and Q_B), which are bound near the cytoplasmic side of the RC. An iron (Fe^{2+}) atom is located between Q_A and Q_B, and a carotenoid (not shown in Figure 1-3A) is bound near the special pair on the B-branch side (Lancaster & Blankenship 1995). Electrons are transferred exclusively through the A-branch pigments, from the special pair through the intermediate monomeric (B)Chl in the B_A position (Arlt et al. 1993), then onto the BPhe in the H_A-site, before finally passing on to the Q_A and Q_B quinones (Figure 1-3B) (Jones 2009).

The relative redox energies of the different pigments of the *Rb. sphaeroides* type 2 RC are among the best understood of any photosynthetic complex, due to their simplicity and ease of spectroscopic measurement (Williams & Allen 2009; Woodbury et al. 1995). Furthermore, as can be seen in Figure 1-3C, the relative redox midpoint potentials of each step in the A-branch result in a series of energetically favorable downhill reactions. The times for ET from $P^* \rightarrow H_A \rightarrow Q_A \rightarrow Q_B$ are 3 ps, 200 ps and 200 μs, respectively. These times

reflect the relative redox potentials of the pigments involved because this trait is the fundamental driving force of the reaction, although recently work has suggested that protein dynamics play a huge role in the overall kinetics of the reaction (Wang et al. 2007).

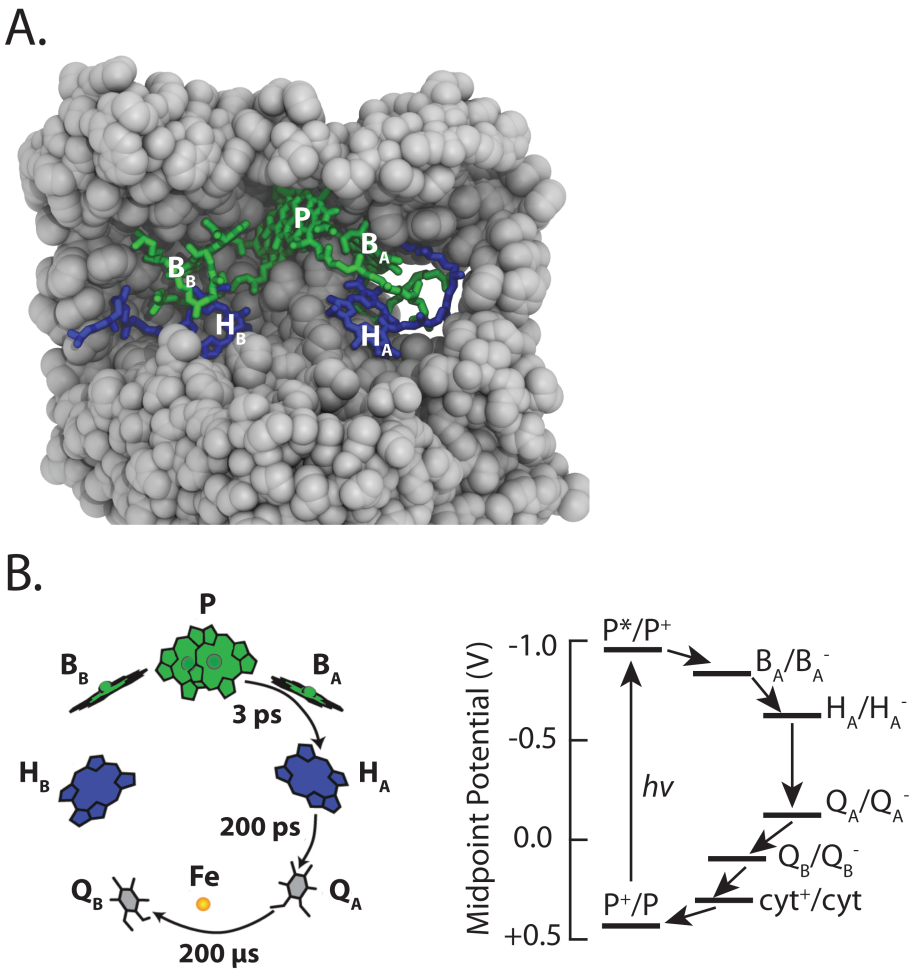

Figure 1-3. RC structure and ET rates. (A) Cofactor arrangement in RC complex. Protein surface in grey and oriented in a slice taken through structure to reveal inner cavity. Model oriented so that the periplasm is on top and cytoplasm is on bottom. Molecular model created from PDB file 2UWV (Koepke et al. 2007) using Visual Molecular Dynamics program with default settings (Humphrey et al. 1996). (B) ET pathway and relative cofactor energies. ET rates indicated beside arrows. P, special pair BChls; B, accessory BChls; H, BPhes; Q, quinones; cyt, cytochrome c_2; Fe, non-heme iron; *hv*, light. Figure adapted from (Jones 2009; Lin et al. 2009a).

1.2.3. Light harvesting and cyclic electron transfer in the photosynthetic apparatus.

After absorption of a photon of light by LH2, energy is moved via exiton transfer through the LH1 to the special pair of BChls in the RC, generating an excited state called P* (Sener & Schulten 2009). From P* an electron is transferred through the A-branch pigments of the RC, and thence to the Q_B quinone. After two electron and two proton transfers to Q_B, the resultant Q_BH_2 (quinol) leaves the RC and is oxidized in the cytochrome bc_1 complex, resulting in a net increase of protons in the periplasm (Okamura et al. 2000). Cytochrome c_2, which is a soluble periplasmic protein, shuttles back and forth between the RC and the cytochrome bc_1 complex, re-reducing the oxidized P cofactors to complete the photochemical cycle (Lavergne & Vermeglio 2009) (Figure 1-4).

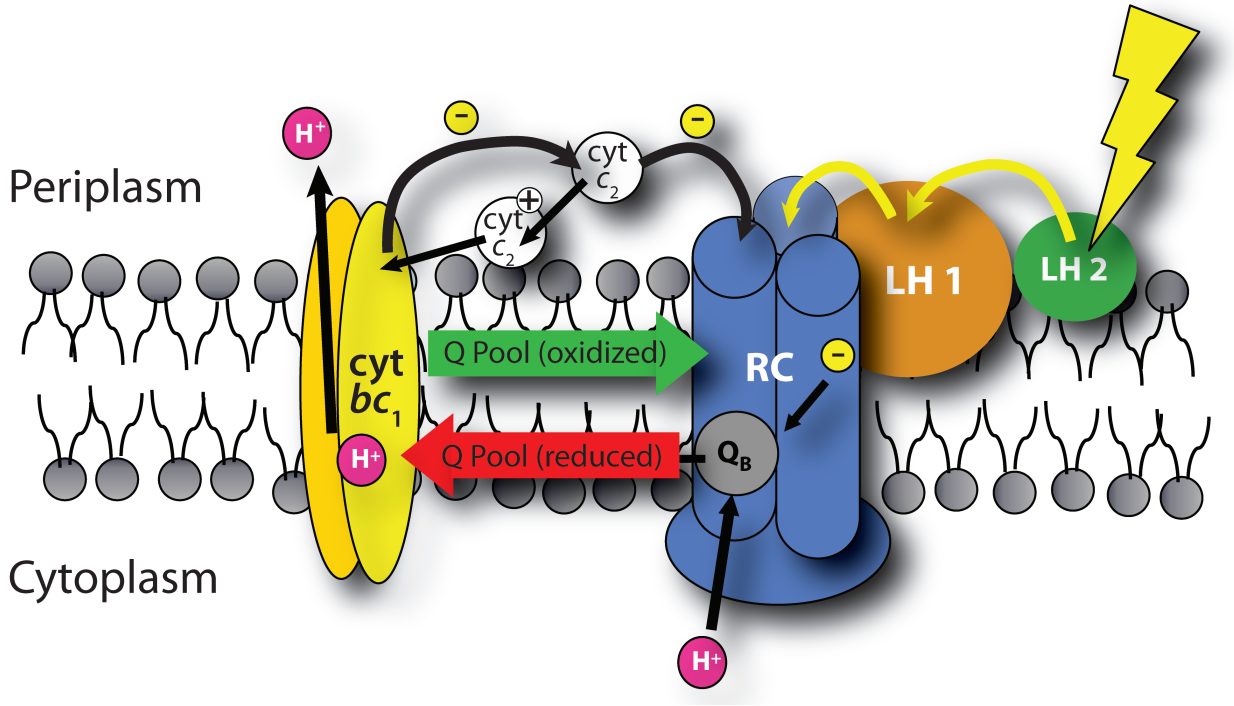

Figure 1-4. Light-driven cyclic electron transfer of the *Rb. sphaeroides* photosynthetic apparatus imbedded in a lipid bilayer. H^+, protons; -, electrons; RC, reaction center; cyt bc_1, cytochrome bc_1 complex; cyt c_2, cytochrome c_2 protein; LH1, light-harvesting 1 complex; LH2, light-harvesting 2 complex; Q_B, quinone/quinol; yellow arrow, exciton energy transfer; red and green arrows represent the flow of quinone molecules between the RC and cyt bc_1 complexes.

1.2.4. Biosynthesis and assembly of the photosynthetic complexes.

For functional photosynthetic complexes to be assembled, each protein must be synthesized from an mRNA, targeted to the membrane, inserted, folded, associated with cofactors, and physically bound with other members of the complex. During several of these stages the photosynthetic proteins likely interact with protein-based targeting, insertion and assembly factors. The BChl cofactors are likely to be delivered to the complexes at some point during the folding process because fully-assembled complexes cannot have their cofactors exchanged without the use of chemicals, such as acetone, and heat to denature the proteins (Scheer & Hartwich 1995).

Some evidence from studies of the closely related bacterium *Rhodobacter capsulatus* indicates that the RC proteins require assembly factors to form a functional complex. A knockout of the *puhB* gene immediately downstream of *puhA* (encoding RC H), causes an RC-specific assembly defect that appears to have a secondary effect, disrupting LH1 and PufX incorporation into the core-complex structure (Aklujkar et al. 2000; Aklujkar et al. 2005a). It is anticipated that this protein plays the same role in *Rb. sphaeroides* because these homologues share 42% identity. Other components of the photosynthetic machinery seem to require assembly factors as well. A large membrane protein called LhaA has a role in LH1 assembly (Young & Beatty 1998; Young et al. 1998), while the homologous protein called PucC plays a role in both LH2 assembly (Leblanc & Beatty 1993; LeBlanc & Beatty 1996; Tichy et al. 1991) and in shepherding the LH1 and LH2 complexes to keep them assembling separately (Jaschke et al. 2008).

1.3. Biosynthesis of bacteriochlorophylls and heme.

Cyclic tetrapyrroles, also known as porphyrins, are a large family of structures characterized by four pyrrole rings connected by methine (R_2=CH-R_1) or methylene (R_1-CH_2-R_2) bridges. Exploration of the structure of tetrapyrroles has been at the forefront of chromatographic and synthetic techniques for over 100 years (Scheer 2006).

In *Rb. sphaeroides*, the biosynthesis of tetrapyrroles begins with δ-aminolevulinic acid (ALA), which is converted through several enzymatic steps to protoporphyrin IX (PPIX), a precursor of both heme and BChl (Beale 1995). The first committed step of BChl

synthesis is the insertion of Mg^{2+} into the macrocycle of PPIX by the Mg-chelatase enzyme. Multiple enzymatic reactions convert magnesium-protoporphyrin IX (Mg-PPIX) to BChl, with all but the first step associated with the cytoplasmic or intracytoplasmic membrane (Gibson & Hunter 1994; Gibson et al. 1995; Hunter et al. 2005; Suzuki et al. 1997).

1.3.1. δ-aminolevulinic acid and protoporphyrin IX synthesis.

Rb. sphaeroides synthesizes ALA via the Shemin pathway by condensation of glycine and succinyl-coenzyme A. This pathway is shared between vertebrates, non-photosynthetic eukaryotes and the α-proteobacteria. Interestingly, most bacteria, photosynthetic eukaryotes and archaea, synthesize ALA through the alternative glutamyl-tRNA pathway, which uses two enzymes to release glutamate-1-semialdehyde from tRNA and transfer the amino group to an adjacent carbon to generate ALA (Willows & Kriegel 2009). In the Shemin pathway the enzyme ALA-synthase catalyzes the condensation reaction (Figure 1-5). Studies on *Rb. sphaeroides* indicated that there are two ALA-synthase isoforms with separable kinetic properties. These enzymes are encoded by the functionally redundant *hemA* and *hemT* paralogs located on separate chromosomes, and differentially regulated (Kikuchi et al. 1958; Neidle & Kaplan 1993; Tuboi et al. 1970a; Tuboi et al. 1970b).

The generation of ALA seems to be a major regulatory point for downstream pathways leading to heme and BChl. The tetrapyrrole needs of the *Rb. sphaeroides* cell change significantly when it shifts from aerobic to photosynthetic growth, with total tetrapyrroles increasing 200-fold (Lascelles 1968). Oxygen represses ALA-synthase transcription, but upon a lowering of oxygen levels, a 3- to 4-fold increase in *hemA* and *hemT* transcription occurs (Pappas et al. 2004). Light also seems to modulate ALA production, although the effect is small compared to oxygen (Oelze 1988). Downstream products of the pathway also seem to be important for post-transcriptional regulation because heme, Mg-PPIX and PPIX have all been shown *in vitro* to act as inhibitors of ALA-synthase (Burnham & Lascelles 1963; Yubisui & Yoneyama 1972).

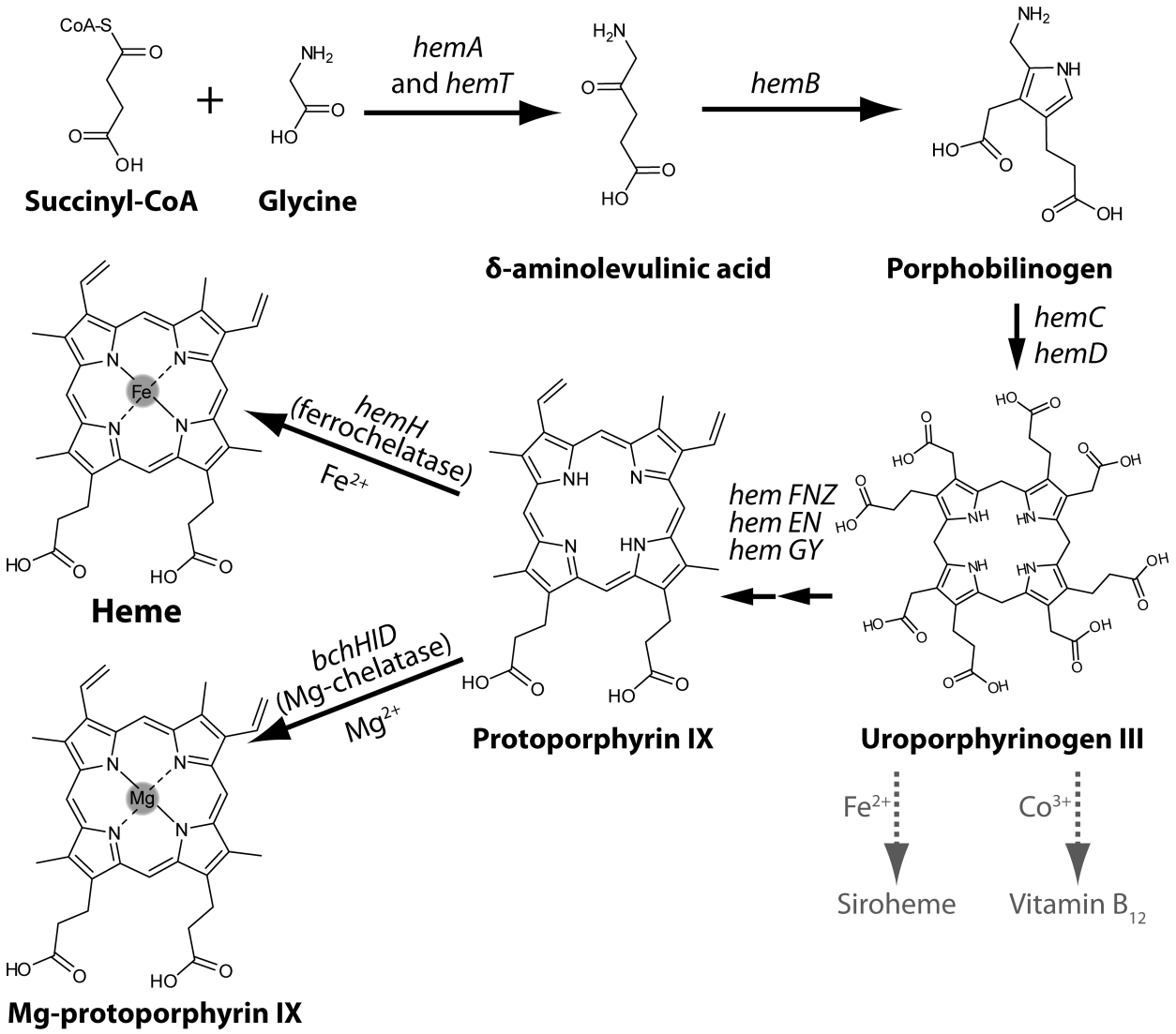

Figure 1-5. Porphyrin biosynthetic pathway from glycine to protoporphyrin IX and heme and BChl branches. Shading shows changes from previous intermediate. Figure derived from a prior scheme (Willows & Kriegel 2009). *hemA* and *hemT,* ALA-synthase; *hemB*, ALA dehydratase; *hemC,* hydroxymethylbilane synthase; *hemD*, uroporphryinogen III synthase; *hemE*, uroporphryinogen III decarboxylase; *hemFNZ*, coproporphryinogen oxidase; *hemGY*, protoporphyrinogen oxidase; *hemH*, ferrochelatase; *bchHID*, Mg-chelatase.

A series of linked condensation reactions that take place in the cytoplasm, catalyzed by seven different enzymes, link ALA to PPIX (Figure 1-5). Two other metal-chelated cofactor biosynthetic pathways branch off at the level of uroporphyrinogen III, leading to siroheme (Fe^{2+}) used in sulfite and nitrite reductases (Murphy & Siegel 1973; Murphy et al. 1974), and vitamin B_{12} (Co^{3+}) used in homocysteine methyltransferase and possibly Mg-

protoporphyrin IX monomethyl ester cyclase (BchE) (Beale 1995). Very little of the total flux through this pathway is diverted to siroheme or vitamin B_{12} in *Rb. sphaeroides* (Beale 1995), and instead proceeds to PPIX, which lies at a major branch point: if PPIX is used as a substrate by ferrochelatase (HemH) it becomes heme, whereas if PPIX is acted on by Mg-chelatase (BchHID) it leads to BChl.

1.3.2. Heme synthesis.

Ferrochelatase catalyzes the insertion of ferrous iron into PPIX to form heme (Figure 1-5). In *Rb. sphaeroides*, the enzyme is a monomer and binds to the inner face of the cytoplasmic membrane, although there is a wide diversity of subunit composition and localization in different organisms (Barrett & Jones 1978). The enzyme is encoded by the *hemH* gene, and its transcript levels seem to stay constant over the growth cycle, although shifting from aerobic to anaerobic photosynthetic growth results in a modest 2-fold increase in heme levels (dwarfed by a 200-fold increase in total tetrapyrroles) (Kanazireva & Biel 1996; Lascelles 1956; Pappas et al. 2004).

In vitro work on ferrochelatase from *Rb. sphaeroides* has shown that the enzyme uses PPIX as a substrate, and can catalyze both Zn^{2+} and Fe^{2+} chelation without ATP addition (Dailey 1982; Johnson & Jones 1964; Mazanows et al. 1966; Neuberger & Tait 1964; Wacker et al. 1965). One report showed that *Rb. sphaeroides* ferrochelatase had a specific activity for Zn^{2+} 1.6 fold lower than Fe^{2+}, although it is difficult to directly compare the activities because the assay used Zn^{2+} at 5 µM while the concentration of Fe^{2+} was much higher (40 µM) (Jones & Jones 1970). Under certain physiological conditions such as glucose starvation, zinc-protoporphyrin IX (Zn-PPIX) in addition to heme, has been found to accumulate in yeast (Grimal & Labbe-Bois 1980). Mutations that increase total porphyrin levels and decrease cytochrome levels have also been found to drastically increase levels of Zn-PPIX in yeast (Pretlow & Sherman 1967). Moreover, Zn-PPIX production in Rat hepatocytes occurred after addition of ALA to cultures and ceased when the ferrochelatase inhibitor N-methylmesoporphyrin was added, pointing to ferrochelatase as the source of Zn-PPIX (Jacobs et al. 1998).

1.3.3. Bacteriochlorophyll synthesis.

In *Rb. sphaeroides*, in addition to the heme pathway, PPIX is the substrate of the BChl biosynthetic pathway's first committed step, the insertion of Mg^{2+} into PPIX by the Mg-chelatase complex (BchHID). This enzyme complex, or a close homologue, is found in all known photosynthetic organisms, and has been extensively studied (Gibson et al. 1995; Kannangara et al. 1997; Papenbrock et al. 1997; Sawicki & Willows 2008).

The structure of Mg-chelatase is slowly starting to emerge. The crystal structure of the Mg-chelatase BchI protein subunit, solved to 2.1 Å resolution, shows a wedge-shaped protein. A combination of structural and sequence analysis has led to its classification of the BchI subunit as a AAA+ protein (Fodje et al. 2001). The AAA+ classification (**A**TPase **A**ssociated with diverse cellular **A**ctivities) comprises a large superfamily characterized by a P-loop NTPase fold, and performance of diverse functions ranging from protein degradation to membrane fusion. One unifying feature of this superfamily is the hydrolysis of ATP to enable conformational changes in the protein (Iyer et al. 2004). Many AAA+ proteins form double hexameric ring structures. In the Mg-chelatase, BchI and BchD appear to form separate interacting hexameric rings in an ATP-dependent manner (Fodje et al. 2001). The Mg-chelatase also exhibits several features atypical of this superfamily including extra loops from the ATPase domain and a second domain that is distant from the ATPase domain (Fodje et al. 2001). The BchH subunit of the Mg-chelatase binds PPIX tightly, and *E. coli* cells that express *bchH* turn bright red from PPIX bound to BchH (Gibson et al. 1995).

In vitro enzyme assays of *Rb. sphaeroides* Mg-chelatase show that all three subunits are required for enzyme activity. BchH with PPIX bound acts as a substrate in the reaction with a K_m of approximately 1 µM. Furthermore, it was shown that pre-incubating the BchI and BchD proteins with ATP and Mg^{2+} prevents an activity lag period (Gibson et al. 1995). These results point to a mechanism in which the BchI and BchD proteins use ATP to generate a double ring structure, and the BchH-PPIX complex interacts with this ring structure to insert Mg^{2+} and transform bound PPIX to Mg-PPIX.

The second step of the BChl biosynthetic pathway is methylation of the ring III propionate of Mg-PPIX by the BchM enzyme (see Figure 1-6 for ring-numbering scheme). Cell-free extracts of *Rb. sphaeroides* methylate Mg-PPIX, Zn-PPIX and Ca-PPIX in an S-

adenosylmethionine (SAM) dependent manner, although methylation of Zn-PPIX was approximately half as efficient as for Mg-PPIX (Gibson et al. 1963). In the same study it was found that the system could not methylate metal-free protoporphyrin IX, ferric or ferrous-protoporphyrin IX, nor manganic or manganous protoporphyrin IX (Gibson et al. 1963). More recently, heterologous expression of the *bchM* gene from *Rb. sphaeroides* in *E. coli* confirmed that the BchM enzyme is an S-adenosylmethionine : magnesium protoporphyrin IX–O-methyltransferase (Gibson & Hunter 1994).

Following methylation of the propionate on ring III to yield Mg-PPIX-monomethyl ester (Mg-PPIX-MME), this area of the molecule is ready to be cyclized and joined to the side of ring III to make the fifth ring that is characteristic of all chlorophylls. The Mg-PPIX-MME cyclase enzymes AcsF and BchE generate this fifth ring along with the addition of a keto group in the 13^1 position. The origin of the keto-group depends on which enzyme catalyzes the reaction: BchE uses a hydratase activity that adds water, while the structurally unrelated AcsF enzyme uses oxygen (Porra et al. 1996). Some purple bacteria, such as *Rhodovulum sulfidophilum*, *Rubrivivax gelatinosus,* and *Rb. sphaeroides* contain both types of cyclases (Ouchane et al. 2004; Porra et al. 1998). Sequence analysis of the *bchE* gene revealed a putative vitamin B_{12}-binding site, and B_{12} involvement in the cyclization reaction was experimentally shown in vitamin B_{12}-biosynthesis-deficient mutants (Gough et al. 2000). Disruption of the *bchE* gene in *Rb. sphaeroides* results in the cellular accumulation of Mg-PPIX-MME under semiaerobic growth conditions (Hunter & Coomber 1988), in accordance with the scheme shown in Figure 1-6. Expression from a *bchE-lacZ* transcriptional fusion increased 10-fold upon transitioning from aerobic (30% O_2) to semiaerobic (2% O_2) conditions (Oh et al. 2000). Since AcsF is normally active under aerobic conditions, it would seem that its role, if any, in *Rb. sphaeroides* is to allow a quicker transition from aerobic to semiaerobic conditions by allowing some protochlorophyllide to be produced while the cell is adapting to semiaerobic or anaerobic conditions.

Previously, the gene *bchJ* was thought to be involved in the conversion of divinyl- to monovinyl-protochlorophyllide, because *bchJ*-disrupted *Rb. capsulatus* cells have lowered mono/divinyl-protochlorophyllide ratios (Bollivar et al. 1994; Suzuki & Bauer 1995). Recently, this interpretation has been questioned, as evidence from work on an ortholog of *bchJ* in the green sulfur bacterium *Chlorobium tepidum* instead indicated a

substrate channeling function for this protein (Chew & Bryant 2007). In this same work, the gene CT1063 (subsequently named *bciA*) was shown to be the true divinyl-reductase in this organism. Both *in vitro* and *in vivo* evidence showed it was responsible for this reaction. Although unannotated in the *Rb. sphaeroides genome*, a *bciA* homolog (RSP_3070) was found on chromosome 2, with 95% of its sequence aligning to the *bciA* gene from *C. tepidum* with an e-value of $2e^{-98}$ and 54% identity (Bryant 2010).

Following the reduction of divinyl-protochlorophyllide to monovinyl-protochlorophyllide, the pathway becomes less linear. The enzymes appear to have more relaxed substrate specificity, so that conversion of the 3-vinyl group to a ketone, and a reduction of ring II, is able to occur in a variety of orders. As a result, single gene knockouts accumulate more than one intermediate, and different enzymatic steps seem to occur in different orders depending on which enzyme activity is knocked out. The products of *bchF* and *bchC* convert the 3-vinyl group first to a hydroxyl and then to a ketone by unknown mechanisms (Bollivar et al. 1994; McGlynn & Hunter 1993; Pudek & Richards 1975; Wellington & Beatty 1989).

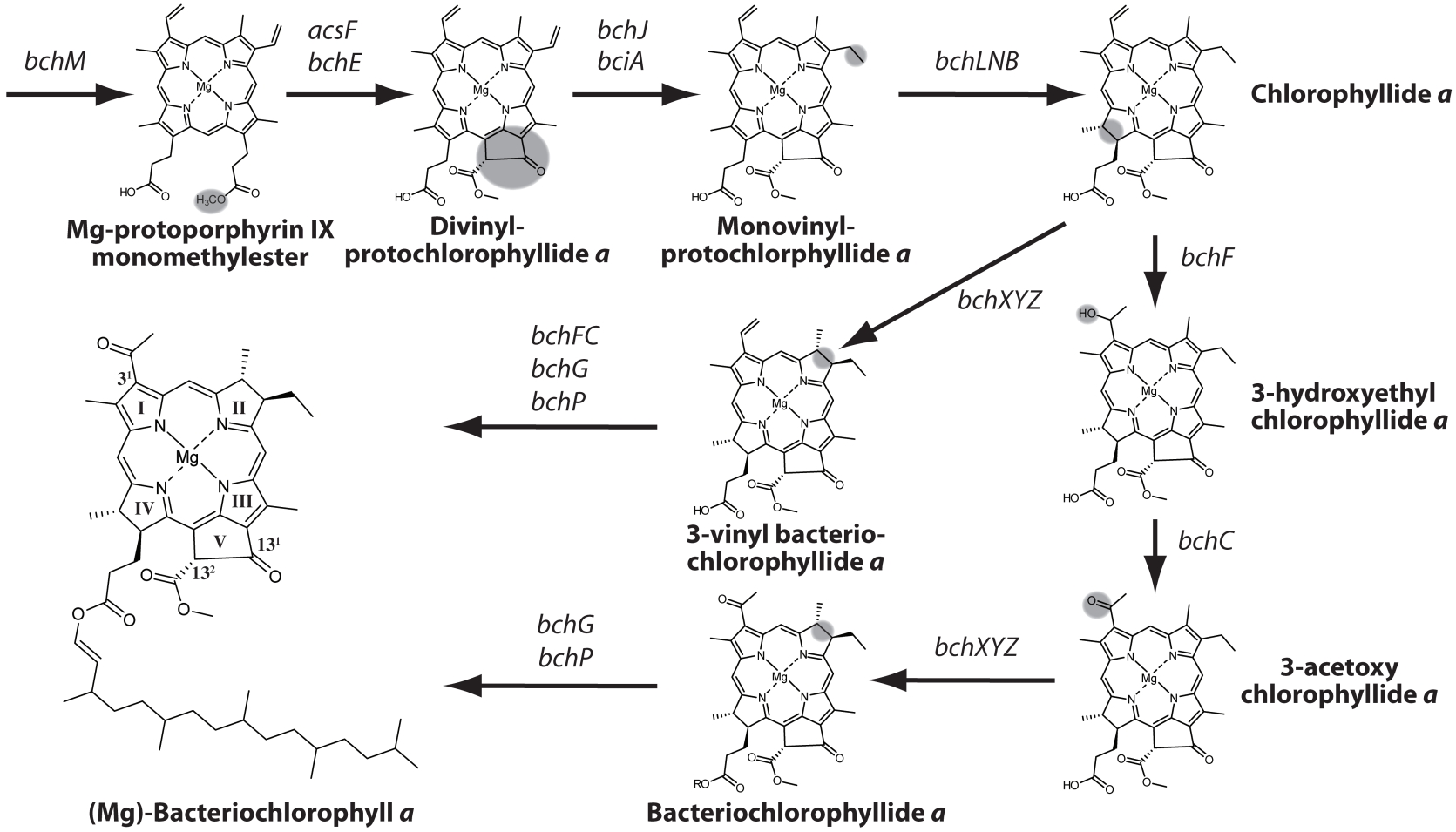

Figure 1-6. Bacteriochlorophyll biosynthetic pathway from protochlorophyllide to bacteriochlorophyll. Scheme derived from previous work (Willows & Kriegel 2009). Shaded circles indicate changes from previous intermediates. *bchM*, magnesium protoporphyrin IX: SAM O-methyltransferase; *acsF* and *bchE*, magnesium protoporphyrin IX monomethyl ester cyclases, *bchJ* and *bciA*, 8-vinyl reductase; *bchLNB*, protochlorophyllide reductase; *bchF*, 3-vinyl bacteriochlorophyllide *a* hydroxylase; *bchC*, 3-hydroxyethyl bacteriochlorophyllide *a* dehydrogenase; *bchXYZ*, chlorin reductase; *bchG*, bacteriochlorophyll synthase; *bchP*, geranylgeranyl reductase.

In parallel with the hydration of the 3-vinyl group, ring II and IV are reduced by two different but homologous enzyme complexes. The reductase complexes are encoded by *bchLNB* and *bchXYZ*, which share approximately 30% amino acid sequence identity with each other. These reductases are also homologous to the *nifHDK* genes of nitrogenase, and to *nifEN*, which encode proteins that synthesize the molybdenum cofactor used in one subunit of nitrogenase (Burke et al. 1993a; Burke et al. 1993b; Fujita & Bauer 2000; Nomata et al. 2006). The BchLNB enzyme complex is called the dark protochlorophyllide reductase, to distinguish it from the light-requiring, unrelated enzyme found in plants and many other photosynthetic organisms. Disruptions in these genes cause cells to accumulate protochlorophyllide (Bollivar et al. 1994; Burke et al. 1993b). The dark protochlorophyllide reductase structure of *Rb. capsulatus* (BchBLN) and *Rb. sphaeroides* (BchL only) has recently been solved and shows that BchL forms a homodimer and binds one [4Fe-4S] cluster while BchBN forms a heterotetramer binding two [2Fe-2S] clusters at their interfaces (Muraki et al. 2010; Sarma et al. 2008). The reaction involves BchB and BchN subunits forming a complex in an ATP-dependent manner, to create the catalytic site for protochlorophyllide reduction, with analogy to the NifK and NifD subunits of nitrogenase (Fujita & Bauer 2000). The second enzyme complex, BchXYZ, is called chlorophyllide reductase (Bollivar et al. 1994; McGlynn & Hunter 1993), and has recently been shown, using purified protein from *Rb. capsulatus*, to require ATP and dithionite for activity *in vitro*, with strict substrate specificity for chlorophyllide. Pheophorbide (demetallated chlorophyllide) and protochlorophyllide are not recognized as substrates by the enzyme (Nomata et al. 2006). Unfortunately, this work did not describe experiments using 3-acetoxy chlorophyllide or 3-hydroxyethyl chlorophyllide, both of which are postulated to be substrates for this enzyme *in vivo* (see Figure 1-6).

The BChl-synthase encoded by the *bchG* gene is responsible for the penultimate step in the pathway, attaching the non-polar geranylgeraniol tail to bacteriochlorophyllide to generate geranylgeranyl-bacteriochlorophyll (Addlesee et al. 2000; Coomber et al. 1990; Oster et al. 1997). Finally, BchP reduces this tail to phytol, creating BChl *a* (Addlesee & Hunter 1999).

1.3.4. Diversity of bacteriochlorophylls.

Many modifications to the carbon backbone of (B)Chls are seen in nature. These modifications affect absorption wavelength and ET properties of the cofactor, and are thought to have mainly originated from selective pressure within water columns where organisms shade each other. By developing pigments that absorbed wavelengths different from the organisms above them, under laying organisms could harvest energy from light that passed through competitors (Chew & Bryant 2007; Nisbet et al. 1995). Interestingly, almost all modifications begin with chlorophyllide, which seems to be a central molecule within the biosynthetic pathways of both Chl and BChl synthesis (Chew & Bryant 2007).

Apart from BChl *a*, phototrophic bacteria synthesize many different types of BChl. The purple bacteria *Blastochloris viridis* synthesizes BChl *b*, which has an ethylidene (=CH-CH_3) group at the C-8 carbon of ring 1. This modification to the carbon skeleton significantly red-shifts the absorption band of BChl *b* from that of BChl *a*, allowing RCs that bind this pigment to absorb at wavelengths greater than 1000 nm (Chew & Bryant 2007; Hoogewerf et al. 2003). Another derivative, called BChl *g,* containing a C-8 ethylidene in addition to a C-3 ethyl group, is blue-shifted from BChl *a* and is synthesized by the gram-positive *Heliobacterium chlorum* (Michalski et al. 1987). The green sulfur bacteria synthesize BChls *c*, *d*, and *e*, which are modified from chlorophyllide *a* through: addition of methyl groups at C-8^2/C-12^1/C-20 positions; farnesyl rather than phytol tails; and lacking the C-13^2 methylcarboxyl side chain found in all other (B)Chls (Chew & Bryant 2007).

Only one case of an organism that naturally uses a substituted metal in BChl has been seen before. The *Ac. rubrum* bacterium that makes this Zn-BChl *a*, is an α-proteobacterium that lives in acidic mine drainage areas, and is exposed to heavy metals and low pH (Itoh et al. 1998; Wakao et al. 1996). The Zn-BChl *a* structure is identical to BChl *a*, but with the Mg^{2+} substituted for Zn^{2+}. This structure appears to be favored in the acidic environment where these organisms live, due to 1000-fold higher resistance to metal-loss than the magnesium type of BChl (Kobayashi et al. 1998). *Ac. rubrum* does not seem to possess a Zn-chelatase (Masuda et al. 1999), relying instead on the Mg-chelatase and the

normal BChl-biosynthetic pathway to synthesize Mg-BChl *a*, which is then converted to Zn-BChl *a* through a demetallated (BPhe *a*) intermediate (Wakao et al. 1996). In this organism, Zn-BChl *a* is assembled into both the RC and LH1 complexes that are used to support aerobic anoxygenic photosynthetic growth (Tomi et al. 2007; Wakao et al. 1996). Some examples of substituted metals in Chls are seen in plants grown in areas with metal-contamination. Accumulation of various metals in their Chls decreases their ability to capture and transform light energy, perhaps because of the resultant heterogeneity of these photosystems, and indicates that this phenomenon is more likely a disorder than an adaptation as in *Ac. rubrum* (Kupper et al. 2006).

1.3.5. Cellular effects of BChl biosynthesis disruption.

Early work on *Rb. sphaeroides* mutants that were incapable of BChl biosynthesis showed a variety of phenotypes including: incomplete ICM maturation, reduced amounts of chromatophore vesicles, and inability to grow photosynthetically (Brown et al. 1972; Coomber et al. 1990). Both of these phenotypes are similar to the phenotype seen in chloroplast membranes of rice plants with a disruption of the gene homologous to *bchD* (subunit of the Mg-chelatase) (Zhang et al. 2006). All of these phenotypes can be traced back to a lack of proteins involved in the photosynthetic apparatus when (B)Chl is absent from the cell. Proteins of the photosynthetic apparatus seem to be stabilized by the presence of pigments in plants (Eichacker et al. 1990; Mullet et al. 1990) and bacteria (Varga & Kaplan 1993). Pulse-chase experiments on a *bchH* (subunit of the Mg-chelatase) mutant of *Rb. capsulatus* showed that the RC and LH proteins were synthesized and membrane-inserted, but the LH proteins were much less stable than in a wildtype strain (Brand & Drews 1997). Similarly, it was recently shown that in *bchI* (subunit of the Mg-chelatase) homolog knock-down tobacco plants, light-harvesting proteins were present in the chloroplast membrane at drastically reduced levels (Papenbrock et al. 2000). Experiments on *Rb. sphaeroides* mutants that uncharacteristically produce BChl under aerobic growth conditions indicated that the main stabilizing influence on the RC proteins is the presence of BChl, and not other factors relating to low O_2 levels during growth (Takemoto & Lascelles 1973; Varga & Kaplan 1993).

1.4. Thesis objectives and approach

Biosynthesis of the central RC-LH1-PufX core-complex of *Rb. sphaeroides'* photosynthetic apparatus has been studied with little success over the last 30 years. The determination of the high resolution crystal structure of the RC, low resolution structures of RC-LH1-PufX core-complex, and recent advances in other methodologies (Bahatyrova et al. 2004; Broglie et al. 1980; Qian et al. 2005; Scheuring et al. 2005; Tehrani & Beatty 2004; Tehrani et al. 2003; Yeates et al. 1988) have laid the foundations and provided the tools to tackle this problem head on.

My aim in this thesis was to address the question of how the core-complex proteins go from nascent polypeptides to an assembled membrane complex with incorporated cofactors. The first tool that I utilized to answer this question was a strain of *Rb. sphaeroides*, the *bchD* mutant, that had been shown to be BChl-less (Coomber et al. 1990) because of loss of function from the first enzyme of the BChl-biosynthetic pathway, the Mg-chelatase (BchHID). This strain was to enable experiments on the core-complex protein assembly process in the absence of BChl, to determine whether this pigment was necessary for protein association.

During work on this BChl-less mutant I discovered that the *bchD* mutant is a unique case because loss of the Mg-chelatase transforms it into a Zn-BChl producer, a phenotypic change never before seen in any photosynthetic organism. With this mutant in hand my revised overall objectives of this thesis were two-fold: (1) to elucidate the Zn-BChl biosynthetic pathway; and (2) to utilize this biosynthesis as a tool to probe aspects of photosynthetic apparatus function.

This unusual Zn-BChl was synthesized through a previously unknown BChl-biosynthetic pathway that utilized as its first step the ferrochelatase enzyme and Zn^{2+} rather than the Mg-chelatase and Mg^{2+}. This discovery has broad implications for the study of existing biosynthetic pathways, as well as the construction of *de novo* biosynthetic pathways, because it shows that substrates have the ability to shuttle between previously unrelated pathways. The Zn-BChl pathway may also be an example of

an ancestral biosynthetic pathway that has been superseded in modern organisms and is only revealed when the competing Mg-chelatase is removed.

Zn-BChl was also shown to bind to the RC in the *bchD* mutant and to transfer electrons similarly to the WT-RC despite having very different cofactors. This Zn-RC is the first example of a RC complex having characteristics of both type 1 and type 2 RC, and bridges the gap in both structure and function between these related photocomplexes. These results have provoked us to revise some of the previously held rules of ET in all types of RCs, and has led to a deeper understanding of the differences between type 1 and 2 RCs.

2. Materials and Methods

2.1. Bacterial

2.1.1. Culture conditions.

Rb. sphaeroides strains were grown as described previously (Tehrani et al. 2003), at 30°C using LB and RCV (Beatty et al. 1977) media. LB contained 5 g per litre granulated yeast extract (EMD), 10 g per litre of bactotryptone pancreatic digest of casein (BD) and 10 g per litre of NaCl, with a final pH 7.0 achieved by addition of 5 M NaOH. High to low aeration shifted cultures were initially grown in flasks filled to 8% of the nominal volume on a rotary shaker at 300 RPM (high aeration, aerobic growth) until exponential phase, then used to seed a flask filled to 80% of the nominal volume and shaken at 150 RPM (low aeration or semiaerobic growth). Antibiotics were used in *Rb. sphaeroides* cultures at the following working concentrations: spectinomycin (Sp) 50 μg/mL, tetracycline (Tc) 2 μg/mL, kanamycin (Km) 25 μg/mL, neomycin (Nm) 20 μg/mL. *E. coli* strains were grown at 37°C in LB at high aeration (shaking at least 200 RPM) with tubes and flasks filled less than 50% volume. Antibiotics were used at the following working concentrations: Sp 100 μg/mL, ampicillin (Ap) 150 μg/mL, Tc 10 μg/mL, Km 50 μg/mL.

2.1.2. Culture density measurements and colony forming unit determinations.

Culture densities for all strains were analyzed by measuring the absorbance at 650 nm on a UV/Vis spectrophotometer. Determinations of cell numbers for normalizing data were based on conversion of A_{650} readings to colony forming unit (CFU) per mL based on individual standard curves constructed for wt and *bchD* strains (Appendix I). Curves were constructed from several independent experiments where semiaerobic cultures were grown and samples removed at various points in the growth cycle. Each removed sample had A_{650} measurements taken, was diluted between 10^{-5} to 10^{-8}, and 100 μL was spread onto dry LB agar plates. Plates were scored for CFUs after three days growth at 30°C.

2.1.3. Strains.

The following strains were used in this study (Table 2-1).

Table 2-1. Strains used in this study.

	Strain	Description	Phenotype	Marker	Reference
E. coli	DH5α	standard cloning strain used for transformations.	-	-	(Meselson & Yuan 1968)
	S17-1	strain used for conjugation into *Rb. sphaeroides*.	-	-	(Simon et al. 1983)
	HB101(pRK2013)	helper strains for conjugation into *Rb. sphaeroides*.	-	Km^R	(Boyer & Roulland 1969)
Rb. sphaeroides	NCIB8253	wt strain.	RC+, LH1+, LH2+	-	ATCC 17023
	TB59	*bchD* mutant. NCIB8253 with Tn5 insertion into *bchD* gene.	RC+, LH1+, LH2+	Nm^R	(Coomber et al. 1990)
	β-mutant	site-directed mutant that binds BChl in H_A-site.	RC+, LH1+, LH2+	-	(Kirmaier et al. 1991)
	Δ*puhA*/Δ*puc*	unmarked *puhA* deletion and *neo* cartidge insertion into *puc* operon.	RC-, LH1+, LH2-	Nm^R	(Adelroth et al. 2001; Tehrani 2003)
	Δ*puhA*/Δ*puc*/Δ*bchD*	unmarked *puhA* deletion and *neo* cartridge insertion into *puc* operon, Ω cartridge inserted into native *NruI* site in *bchD* gene.	RC+, LH1+, LH2-	Km^R, Tc^R, Sp^R	This study
	TB303	*bchG* mutant. NCIB8253 with Tn5 insertion into *bchG* gene.	RC-, LH1-, LH2-	Nm^R	(Coomber et al. 1990)
	bchG/bchD	TB303 with Ω cartridge inserted into native *NruI* site in *bchD* gene.	RC-, LH1-, LH2-	Nm^R, Sp^R	This study
	TB04	*bchY* mutant. NCIB8253 with Tn5 insertion into *bchY* gene.	RC-, LH1-, LH2-	Nm^R	(Coomber et al. 1990)
	ΔRCLH	unmarked *puhA*, *pufQBALMX*, and *pucBA* deletion.	RC-, LH1-, LH2-	-	(Tehrani 2003)
	SB1003	wild type strain of *Rb. capsulatus*.	RC+, LH1+, LH2+	-	(Solioz & Marrs 1977)

2.1.4. Cell lysis and membrane isolation.

Cell lysis and membrane isolation was performed as described previously (Tehrani et al. 2003). Briefly, a *Rb. sphaeroides* culture was pelleted at 3000 RCF in a JA-type rotor at 4°C for 15 minutes. The supernatant was removed and cell pellet was resuspended in 10 mM Tris-HCl (pH 8.0). Cells were disrupted in a modified French press (Jaschke et al. 2009), and membranes isolated by ultracentrifugation in TLA 100.2 or 100.3 rotor at 424,480 or 355,040 RCF for 16 or 20 min, respectively. Membrane pellets were resuspended in the same buffer as above.

2.1.5. Aerobic growth in the light.

To measure the detrimental effects of growth in the presence of both light and oxygen, aerobically grown cultures were diluted 10^{-6} and 100 µL was spread onto dry LB plates. Plates were either wrapped in aluminum foil for the dark condition or left unwrapped for the light condition and placed in a plastic jar with partially covered lid within an aquarium light box setup for photosynthetic growth of *Rb. sphaeroides* cultures. Plates were incubated aerobically under illumination (75 µeinsteins/m^2s at 400-700 nm wavelength) and ~28°C for 4 days, followed by counting of CFUs.

CFU numbers were evaluated between light and dark conditions within each strain by first performing the Kolmogorov-Smirnov one sample test (Minitab) on the data to determine if they were normally distributed (Smirnov 1939). Data were analyzed with the SOCR Analysis program suite (Che et al. 2009) to perform the calculations using both the non-parametric two-independent sample Wilcoxon rank sum test which does not assume normality of the data (Mann & Whitney 1947; Stephens 2004) and the parametric 2-independent sample t-test (Student 1908) which assumes normally distributed data.

2.1.6. N-methylprotoporphyrin inhibition.

Wild type and *bchD* mutant cultures were grown aerobically in LB in flasks filled to 8% of the nominal volume and shaken at 300 RPM at 30°C until ~1.0 A_{650}. This aerobic seed was used to inoculate LB in a flask filled to 80% of the nominal volume to 0.20 A_{650}. Simultaneously, 1.8 mM N-methylprotoporphyrin (Frontier Scientific) stock dissolved in

20mM NaOH, 2% Tween-20 and filter sterilized, was added to a final concentration of 0.25, 0.50, 1.00 and 2.00 µM. The 0 µM condition had the same volume of solvent added as for the 2.00 µM condition, but lacking N-methylprotoporphyrin. Foil-wrapped culture flasks were shaken at 150 RPM/30°C for 3 days and then harvested by centrifugation.

2.1.7. Nicotinamide inhibition.

Wild type and *bchD* cultures were grown semiaerobically until ~1.0 A_{650} units, then nicotinamide (CAS 98-92-0, Sigma-Aldrich) dissolved in water and filter sterilized was added to a final concentration of 12 mM. Cultures were allowed to grow semiaerobically at 30°C and harvested by centrifugation 33 hours later (Gough et al. 2000).

2.2. DNA and cloning

2.2.1. Plasmids.

The following plasmids were used in this study (Table 2-2).

Table 2-2. Plasmids used in this study.

Plasmid	Description	Markers	Source or Reference
pATP19P	pRK415 derivative containing *puc* promoter.	Tc^R	(Tehrani & Beatty 2004)
p6His-C	pATP19P with *puhA* gene with six histidine codons on 3'-end of gene inserted downstream of *puc* promoter.	Tc^R	(Abresch et al. 2005)
pESHPUF	pATP19P with *puhA* and *pufQBALMX* inserted downstream of the *puc* promoter.	Tc^R	(Tehrani 2003)
pESHPFUM$^-$	pATP19P with *puhA* and *pufQBALX* inserted downstream of the *puc* promoter and *pufM* contains a translationally in-frame deletion.	Tc^R	(Tehrani 2003)
pHP45Ω	source of Ω cartridge as a *SmaI* fragment.	Ap^R, Sp^R	(Fellay et al. 1987)
pUC19(*bchD*Ω)	*bchD*Ω inserted as *Sac*I fragment.	Ap^R, Sp^R	This study
pNHG1	suicide vector used in *Rb. sphaeroides* to knockout chromosomal genes.	Tc^R, Km^R, *sacB*^{S}	(Jeffke et al. 1999)
pNHG1(*bchD*Ω)	*bchD*Ω inserted as *Sac*I fragment.	Tc^R, Km^R, *sacB*^{S}, Sp^R	This study

2.2.2. Primers.

The following primers were used in this study (Table 2-3). Primers were designed using NetPrimer (NetPrimer 2010). DNA sequences were visualized using Artemis (Rutherford et al. 2000).

Table 2-3. Primers used in this study.

Name	Description	Sequence ('5->'3)
bchD forward	binds to *Rb. sphaeroides* 2.4.1 chromosome 1 coordinates 1998332-1999721 and used to amplify the 3' end of *bchI* and half of *bchD* gene.	AAGACGCCGAACACCGTGCTG
bchD reverse		GCCTGCCCCAGAAGGAGCTC
NruI forward	binds to PCR product of *bchI* and *bchD* and amplifies area around natural *NruI* cut site.	CTCACCCTTCTCGCCATCG
NruI reverse		GGCCTCGACCAGCATCTCTT
sacB forward	used to amplify *sacB* gene.	GGCACTGTCGCAAACTATCACGGC
sacB reverse		CGCCGTTTGCTAACTCAGCCGTG

2.2.3. Construction of pNHG1 (*bchD*Ω) suicide vector.

Chromosomal DNA from wt *Rb. sphaeroides* strain NCIB8253 was purified from cells by incubating with 40 µg/mL proteinase K in dH_2O for 15 min at 55°C then 30 min at 85°C in a PCR machine. The sample was centrifuged at 14 000 RCF for 5 mins to pellet cell debris and the supernatant was used as a template for PCR amplification using primers *bchD* forward and reverse (Table 2-3) and the following parameters: Platinum Pfx polymerase (Invitrogen) using the manufacturer's standard conditions with the addition of 7% dimethylsulfoxide (DMSO) and initial denaturation of 94°C for 5 min, followed by 10 cycles of 94°C for 15 sec, 72 to 67°C (-0.5°C per cycle) touchdown for 30 sec, 72°C for 1 min 29 sec, followed by 20 cycles of 94°C for 15 sec, 63°C for 30 sec, 72°C for 1 min 29 sec, then 7 min at 72°C at the end of the run.

The PCR product was a 1485 bp section of chromosome 1 that corresponds to the coordinates 1998332 to 1999721. This section encompasses a 254 bp region of the 3' end

of the *bchI* gene, starting 72 bp upstream of a native *SacI* site, and runs 1231 bp into the 5' end of the *bchD* gene. This region also includes a native *NruI* site at coordinate 1999093. The reverse primer that binds within the *bchD* gene was engineered to introduce a *SacI* site through a single mismatch.

The PCR product was cut with *SacI* and ligated into a similarly cut pUC19 plasmid. Transformants were screened for white colonies on X-gal containing media, followed by restriction digest (*SacI*). The successful construct was called pUC19(*bchD*). A 2.0 kb *SmaI* fragment containing the Ω cartridge (which encodes Sp-resistance) was cut out of the plasmid pHP45Ω and gel purified. The pUC19(*bchD*) plasmid was cut with *NruI* and the *SmaI* Ω fragment was blunt ligated into the blunt cut *NruI* site. Transformants were selected for Sp-resistance and screened by *SacI* digestion of purified plasmid. The successful construct was called pUC19(*bchD*Ω). Plasmid pUC19(*bchD*Ω) was digested with *SacI* and the *bchD*Ω insert was gel purified. The *bchD*Ω *SacI* fragment was ligated into pNHG1 cut with *SacI*. Transformants were selected for Sp- and Tc-resistance and plasmids were screened with *SacI* digestion. The resulting plasmid was called pNHG1(*bchD*Ω), and a representation is shown in Figure 2-1.

2.2.4. Conjugation of plasmids into *Rb. sphaeroides*.

Plasmids were introduced into *Rb. sphaeroides* strains by conjugation using *E. coli* strain S17-1 as donor and HB101(pRK2013) as helper (Simon et al. 1983). Cells grown to mid-log phase were mixed in a 3:1:1 or 4:1:1 ratio of recipient to donor to helper culture volume and plated as 10 µL drops on dry RCV agar plates without selection. Plates were incubated for one day at 37°C, then shifted to 30°C for 2-3 days. This longer incubation time was found to be required for successful conjugation into several of the mutant strains used in this study, including *bchG* (Coomber et al. 1990) and *ΔpuhA/Δpuc* (Tehrani 2003). Cells from drops were spread onto RCV plates with selection and incubated for 3-5 days at 30°C. Single isolated colonies were picked and restreaked onto LB plates to test for *E. coli* contamination, followed by making freezer stocks of pure transformants. Methods of transformant screening are described below.

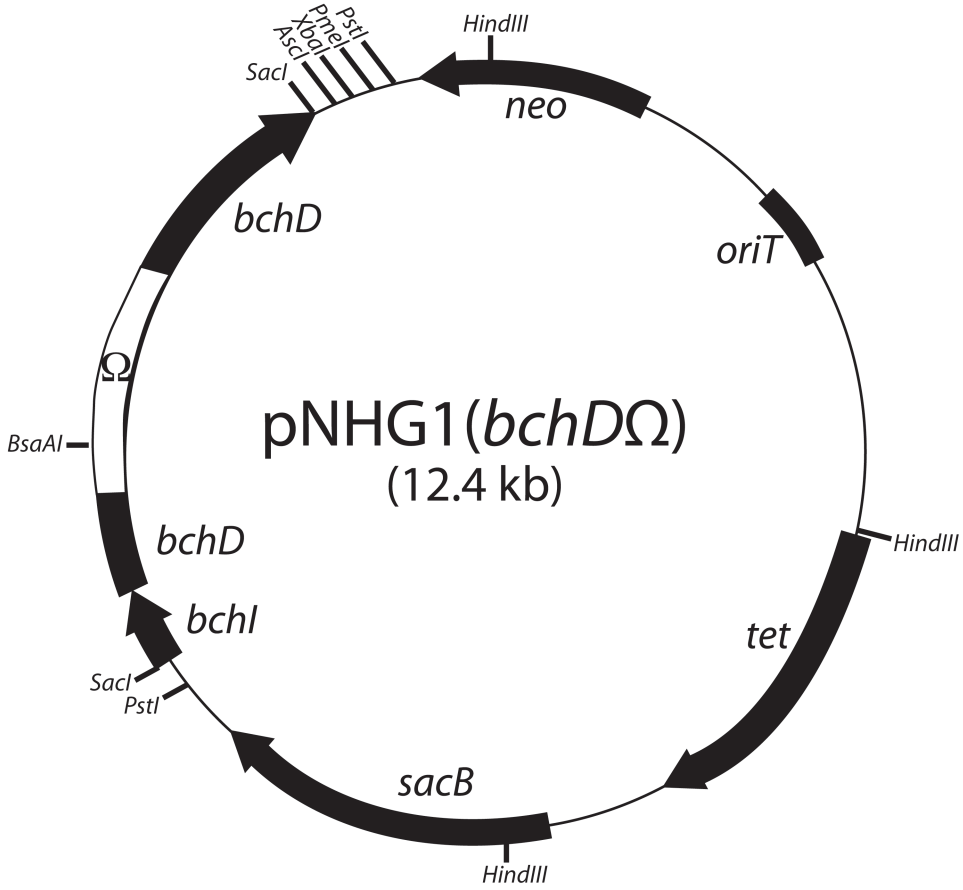

Figure 2-1. Map of pNHG1(*bchD*Ω) suicide vector. This plasmid was used to disrupt the chromosomal *bchD* gene by inserting the Ω cartridge into the native *NruI* site in *bchD*.

2.2.7. Creation of the Δ*puhA*/Δ*puc*/Δ*bchD*(p6His-C) strain.

The pNHG1(*bchD*Ω) suicide vector was conjugated into the *Rb. sphaeroides* strain Δ*puhA*/Δ*puc* (phenotype of RC^- $LH1^+$ $LH2^-$) previously made (Adelroth et al. 2001). The *ΔpuhA*/*Δpuc* strain has a *neo*-cartridge disrupting the *pucBA* operon (encoding α and β subunits of the LH2 complex) and a markerless deletion of the *puhA* (RC H) gene (Tehrani 2003).

Selection for single-crossovers of pNHG1(*bchD*Ω) into the chromosome was performed using growth on Sp-supplemented RCV agar. Candidate transconjugants were screened via PCR using the *sacB* forward and reverse primers (Table 2-3), which gives a 650 bp product for strains containing the *sacB* gene (positive transconjugants) and no product for those without (negative). As a further way to check if the putative transconjugants

contained the integrated pNHG1(*bchD*Ω) plasmid, *NruI* forward and reverse primers were used to identify the presence or absence of the 2.0 kb Ω cartridge (encoding Sp-resistance) inserted at a native *NruI* site approximately one-third of the way from the 5'-end of the *bchD* gene. Strains containing the pNHG1(*bchD*Ω) plasmid integrated into the chromosome showed a 2.8 kb product due to the Ω-disrupted *bchD* gene and a 795 bp product due to the wild type *bchD* gene, while those without the integrated plasmid only showed the 795 bp product.

Confirmed transconjugants were grown aerobically in Sp-supplemented RCV liquid medium for 5-7 days followed by plating on RCV agar supplemented with Sp and 15% sucrose to counterselect for loss of the pNHG1 plasmid from the chromosome. Strains that could grow in the presence of both Sp and sucrose (putative exconjugants) were further evaluated using the *sacB* forward and reverse primers and *NruI* forward and reverse primers as detailed above. Confirmed exconjugants were called Δ*puhA/Δpuc/ΔbchD*. The resulting Δ*puhA/Δpuc/ΔbchD* strain's phenotype is RC^- $LH1^+$ $LH2^-$ $bchD^-$.

The p6His-C plasmid was conjugated into the Δ*puhA*/Δ*puc*/Δ*bchD* strain using standard methods (see above) and plasmid presence selected for by Tc-resistance. The resulting Δ*puhA/Δpuc/ΔbchD*(p6His-C) strain's phenotype is RC^+ $LH1^+$ $LH2^-$ $bchD^-$.

2.2.8. Creation of the *bchG/bchD* strain.

The pNHG1(*bchD*Ω) plasmid was conjugated into the previously created TB303 (*bchG*) strain (Coomber et al. 1990). Selection and screening procedures were identical to those used for the creation of Δ*puhA*/Δ*puc*/Δ*bchD* above. The resulting double knockout strain is called *bchG/bchD*.

2.2.9. Sequencing.

To confirm the DNA sequence of all constructs made in this study, I performed minipreps of plasmids or phenol/chloroform chromosomal DNA extraction followed by PCR amplification of sections to be sequenced. These templates were used in reactions that consisted of: 3 µL BigDye 3.0 pre-mix, 10 ng DNA template, 5 pmol forward or reverse primer, 7% DMSO, and dH_2O to final volume of 10 µL. Reactions were cycled through a PCR

program consisting of 96°C for 1 min then 25 cycles of 96°C for 10 sec, 50°C for 5 sec, and 60°C for 4 min. Tubes were then submitted to the Nucleic Acid Protein Service Unit (NAPS) sequencing facility at UBC for cleanup and analysis.

2.3. Protein purification and analysis

2.3.1. SDS-PAGE and Western blotting.

Isolated membranes with protein amounts stated in figure legends, as determined by a modified Lowry assay (Peterson 1983) with bovine serum albumin as standard, were solubilized with sample buffers and run on SDS-PAGE or tricine-SDS-PAGE (Schagger & von Jagow 1987). Gels were stained directly with Sypro Ruby protein stain and visualized on a Typhoon 9600 scanner (Amersham Biosciences) to reveal protein bands, or electroblotted onto nitrocellulose membranes for probing with antibodies. Total protein on blots was detected by staining with copper phthalocyanine 3,4′,4″,4‴-tetrasulfonic acid tetrasodium salt (CPTS) (Bickar & Reid 1992). Immunodetection of proteins on blots was performed as recommended by Amersham ECL kit with antibodies raised against purified *Rb. sphaeroides* RC proteins kindly provided by S. Kaplan (University of Texas) and E. Abresch (University of California, San Diego). Quantification of protein bands detected by antibodies was done by scanning blots on a Versadoc multi-imager station (BioRad), with subsequent pixel analysis of bands using the QuantityOne (BioRad) program to measure the intensity of chemiluminescent light produced.

2.3.2. His-tag pulldowns.

I analyzed the relative amount of interacting RC proteins from an amount of membranes corresponding to 80 μg of protein from wt and *bchD* strains, as determined by a modified Lowry assay (Peterson 1983) using bovine serum albumin as a standard. The membranes were solubilized with 50 μL of 50 mM Tris-HCl (pH 8.0) buffer containing 0.5% LDAO, 12.5 mM imidazole and 1 M NaCl. After centrifugation (2500 RCF, 5 min), the supernatant fluids were bound for 30 minutes to Ni^{2+}-NTA agarose beads (Qiagen) previously equilibrated with the same buffer as used for solubilization. The beads were washed with three 200 μL portions of the same solution as for solubilization except that the concentration of LDAO

was reduced to 0.1%. Bound protein was eluted with three 20 μL portions of 50 mM Tris-HCl (pH 8.0) buffer containing 0.1% LDAO, 250 mM imidazole and 1 M NaCl. The elutions were pooled and proteins precipitated by diluting 4:1 with ice-cold 100% trichloroacetic acid. Precipitated proteins were washed with acetone, dried, and dissolved in SDS-PAGE sample buffer before analysis on SDS-PAGE and Western blotting. Large scale isolation of RCs for absorption spectroscopy and pigment analysis was performed as described previously (Goldsmith & Boxer 1996).

2.3.3. One- and two-dimensional blue-native polyacrylamide gel electrophoresis and electroblotting.

First dimension BN-PAGE gels were cast with 3.5% stacking and 6% resolving gels in a Mini-Protean II SDS-PAGE apparatus (BioRad). 40%T 3%C acrylamide for use with the gels was made from a mixture of 17.3% 19/1 acrylamide/bis-acrylamide and 82.7% 37.5/1 acrylamide/bis-acrylamide (Swamy et al. 2006).

Membrane samples were prepared using the normal methods above but were additionally dialyzed against BN-PAGE solubilization buffer containing 50 mM NaCl, 50 mM imidazole-HCl, 2 mM 6-aminohexanoic acid, 1 mM EDTA (pH 7.0). Membrane samples were solubilized by addition of dodecyl maltoside (DDM) or octyl-β-D-thioglucopyranoside (OBTG) detergent followed by 10 min incubation at room temperature. Unsolubilized material was removed by centrifuging for 30 min/81 800 RCF/4°C. The supernatant was mixed with glycerol (10% final concentration) and Coomassie G-250 dye solution and loaded onto the gel (Wittig et al. 2006; Wittig & Schagger 2008).

BN-PAGE gels were ran at 100 V constant voltage using Cathode Buffer B until the dye front had reached one-third into the gel. At this point, the cathode buffer was removed and replaced with Cathode Buffer B lacking Coomassie. The run continued until the dye front ran off the bottom of the gel. During the gel run several colored complexes could be seen separating out. The photosynthetic complexes seemed to have a red tint, likely due to the bound carotenoids. After the first-dimension run the lanes of interest were cut out of the gel and incubated with 1% SDS/1% mercaptoethanol for 15 min. The gel strip was rinsed several times to remove the mercaptoethanol and then pushed down

on top of a 13% tricine-SDS-PAGE gel. A 4% stacking gel was poured around the gel strip and allowed to polymerize (Schagger & von Jagow 1987; Wittig & Schagger 2008). After running the second dimension tricine-SDS-PAGE, the gel was electroblotted onto a PVDF membrane and probed sequentially with antibodies as described above.

2.4. Purification and analysis of bacteriochlorophylls, metalloprotoporphyrins IX, and heme

2.4.1. Bacteriochlorophylls.

BChls and BPhes were extracted from 50 mM Tris-HCl (pH 8.0) buffer washed cell pellets with ice-cold acetone/methanol (7/2, (v/v)), aided by sonication or vortexing. Crude extracts were concentrated at 25-35 °C using evaporation either from vacuum or nitrogen gas stream. Complex mixtures of BChls were pre-filtered through a 0.20 μm Millex filter and then separated by chromatography through a Prodigy ODS-prep column (Phenomenex) attached to a Waters 2695 HPLC fitted with 200-800 nm photodiode array detector. Pigments were eluted from the column using a gradient, changing from methanol/water/acetone (16/5/4) to acetone/methanol (9/1) over 20 minutes, then held at acetone/methanol (9/1) for 10 minutes, followed by washing and re-equilibration of the column.

Mass spectrometry of HPLC-purified BChls was performed at the UBC microanalysis and mass spectrometry facility using a biflex IV MALDI-TOF mass spectrometer (Bruker). Briefly, the sample and matrix (*trans*-2-[3-(4-tert-butylphenyl)-2-methyl-2-propenylidene]-malononitrile (DCTB) were dissolved in dichloromethane, either with or without acid, mixed in a ratio of 1:1, and 1 μl was applied to the target and dried in air. The sample was run using the reflector mode and pulsed ion extraction. Analysis of results was aided by Isotope Pattern Calculator v4.0 (Yan 2010).

2.4.2. Porphyrins.

Extraction of porphyrins was performed in three stages as previously described (Belanger & Rebeiz 1980; Masuda et al. 1999). Briefly, cell pellets from various amounts of cultures were washed with 10 mM Tris-HCl (pH 8.0), 150 mM NaCl, then 1 mL of 9/1 acetone/0.1 N

NH_4OH (v/v) was added per 2 mL culture, and the mixture was kept below 4°C and sonicated on power level 4 with a microtip (Misonix) for 3x30 sec with 1 min breaks. Cell fragments were pelleted by centrifugation at 3000 RCF for 15 min at 4°C.

The resulting supernatant was moved to a new tube and an equal volume of hexane was added and mixed. The resulting top hexane layer became orange or red with extracted carotenoids. This hexane extraction was repeated with 1/3 volume hexane. The remaining acetone layer is called hexane-extracted acetone residue (HEAR). To the remaining HEAR layer, 1/70 volume 0.5 M KH_2PO_4 and 1/17 volume saturated NaCl were added. To this mixture 1/5 volume ether was added and mixed, with the resulting top ether layer removed to a new tube and saved. The extraction was repeated two to four more times with 1/10 volume ether and all ether layers were pooled (Rebeiz 2002).

For separation of metalloprotoporphyrins IX and their monomethyl esters, ether extracts (obtained as above) from wt and the *bchD* mutant were pre-filtered through a 0.20 µm Millex filter and then separated by chromatography through a monomeric C18 column (Vydac) attached to a Varian Pro Star HPLC equipped with a fluorescence detector (module 363). Pigments were eluted from the column using 0.8 mL/min flow rate and a linear gradient changing from 80% solvent A (0.1 M ammonium acetate, pH 5.2), 20% solvent B (90% methanol, 0.1 M ammonium acetate, pH 5.2 (adjusted with glacial acetic acid)), to 0% solvent A, 100% solvent B over 10 minutes followed by 20 minutes of 100% solvent B (Masuda et al. 1999). Elution off the column was fluorometrically monitored via 418 nm excitation and 595 nm emission; peaks were identified using Mg-PPIX (Frontier Scientific) and Zn-PPIX (Sigma) standards.

Quantification of the relative amounts of Mg- and Zn-PPIX versus their corresponding monomethyl esters was done by comparing relative peak areas from HPLC injected ether extractions. Peak areas were calculated using Interactive Graphics v6.20 (Varian) with analysis of fluorescence emission at 595 nm from 418 nm excitation.

For separation of protochlorophyllides, the HEAR layer from wt and *bchD* cells treated with nicotinamide was pre-filtered through a 0.20 µm Millex filter and then separated by chromatography through a Luna C18(2) column (Phenomenex) attached to a Waters 2695 HPLC fitted with 200-800 nm photodiode array detector. Pigments were eluted from the column using 0.8 mL/min flow rate and a linear gradient changing from

80% solvent A (0.1 M ammonium acetate, pH 5.2), 20% solvent B (90% methanol, 0.1 M ammonium acetate, pH 5.2 (adjusted with glacial acetic acid)), to 0% solvent A, 100% solvent B over 3 minutes followed by 100% solvent B (Masuda et al. 1999). Elution off the column was monitored by measuring absorbance at 440 nm. Peaks were identified by comparison of absorption spectra to literature values (Shioi et al. 1988).

Mass spectrometry of HPLC-purified peaks from the *bchD* mutant extractions was performed at the UBC microanalysis and mass spectrometry facility using a biflex IV MALDI-TOF mass spectrometer (Bruker). Briefly, the sample and DCTB matrix were dissolved in dichloromethane and 1 μl was applied to the target and dried in air. The sample was run using the reflector mode and pulsed ion extraction. Analysis of results was aided by Isotope Pattern Calculator v4.0 (Yan 2010).

2.4.3. Heme.

Extraction of heme from cell pellets was accomplished by first extracting with 9/1 acetone/0.1 N NH_4OH followed by resuspension of the cell pellet in an 80% acetone wash, followed by resuspension of the pellet in 2% HCl (w/v) in acetone, followed by a final pelleting and removal of the acidified acetone supernatant which contains heme. This method was adapted from previous work (Stillman & Gassman 1978).

2.5. Spectroscopy

2.5.1. Absorption spectroscopy of bacteriochlorophylls and porphyrins.

Amounts of BChl were determined by absorption spectroscopy of acetone/methanol (7/2) extractions of purified membranes of known protein amount, using ε=75 $mM^{-1}cm^{-1}$ at 775 nm (Mg-BChl) and ε=56.3 $mM^{-1}cm^{-1}$ at 771 nm (Zn-BChl) (Hartwich et al. 1998). BChls and metalloporphyrins were analyzed by scanning 350-1000 nm in acetone/methanol (7/2) or ether on a Hitachi U-3010 spectrophotometer at 600 nm/min and 1 nm slit width with normal PMT settings. Spectral peaks were identified by comparison to standards and literature values (Dawson et al. 1986; Falk 1964). Absorption maxima were determined using estimation by eye as well as computational peak finding algorithms.

2.5.2. Absorption spectroscopy of photosynthetic apparatus.

For investigation of LH and RC complex assembly, purified membranes of *Rb. sphaeroides* grown under low aeration resuspended in 50 mM Tris-HCl (pH 8.0) were analyzed in a Hitachi U-3010 spectrophotometer. Data analysis was done using UV Solutions version 2.1 (Hitachi) and Microsoft Excel. The ratio of LH2 to LH1 was determined by using established peak deconvolution methods (Sturgis et al. 1988), with modification for the *bchD* mutant by substitution of 794, 836 and 859 nm in equations for 800, 849 and 875 nm values, using ε=75 $mM^{-1}cm^{-1}$ (Mg-BChl) and ε=56.3 $mM^{-1}cm^{-1}$ (Zn-BChl) (Hartwich et al. 1998). Determination of the number of BChls associated with RC complexes was based on extrapolation from total BChls associated with the LH1 complex. It was assumed that the RC-LH1 co-complex consists of 28 LH1 subunits binding 2 BChls per subunit, surrounding 2 RC complexes (Qian et al. 2005) that bind 4 BChls (WT-RC) or 6 Zn-BChls (Zn-RC) (Lin et al. 2009a). The number of moles of BChl associated with the LH1 complex in each strain was divided by 7 to get the number of moles of BChl associated with the WT-RC (8 BChls in RC/56 BChls in LH1) and was divided by 4.67 to get the number of moles of BChl associated with the Zn-RC (12 Zn-BChls in RC/56 BChls in LH1).

2.5.3. Fluorescence spectroscopy of porphyrins.

Total porphyrins were extracted from cells with 9/1 acetone/0.1 N NH_4OH and extracted twice with hexane to form HEAR. This residue was either scanned in this solvent or purified further by extraction with ether before scanning. These fractions were then subjected to excitation at characteristic wavelengths for each analyzed substance and an emission spectrum in the appropriate range was captured, see figure legends for details. Fluorescence spectra were captured on a Varian Carey Eclipse fluorescence spectrophotometer using 5-10 nm excitation and emission slit widths, medium photomultiplier tube setting, auto filters, and 600 nm/min scan speed. Analysis of spectra was performed using the Carey Eclipse scan application and Microsoft Excel.

2.5.4. Method used to quantify amounts of Mg-PPIX , Zn-PPIX , and their monomethyl esters, from cells.

This was accomplished by extracting cells with 9/1 acetone/0.1 N NH_4OH, and extracted twice with hexane to form HEAR. This was followed by capturing fluorescence emission spectra from 575-700 nm with excitation at 420 nm. Concentrations of metalloprotoporphyrins IX were determined through comparison of emission at 595 nm (Mg-PPIX) and 589 nm (Zn-PPIX) to a standard curve constructed from authentic standards in the same solvent.

2.5.5. Method used to quantify amounts of PPIX from cells.

This was done using an established spectral deconvolution method (Rebeiz 2002). Briefly, cells were extracted with 9/1 acetone/0.1 N NH_4OH and then extracted twice with hexane, yielding HEAR. Fluorescence emission spectra of each sample was captured from 575-700 nm with excitation at 400 and 440 nm. Fluorescence emission due only to PPIX was determined through the equation:

Proto (E400 F633) = 1.055F (E400 F633) – 0.1190F (E400 F622) – 0.442F (E440 F638)
– 0.0141F (E440 F675)

Where: E, excitation wavelength; F, fluorescence emission wavelength

This deconvolution removes the contributions from unwanted fluorescence from protochlorophyllide (Ex: 440 nm Em: 638 nm) and coproporphrinogen (Ex: 400 nm Em: 622 nm) from fluorescence intensity of PPIX (Ex: 400 nm Em: 633 nm). The resulting deconvoluted emission intensity at 633 nm is compared to a standard curve constructed from an authentic PPIX standard in the same solvent (Ex: 400 nm Em: 633 nm) to determine the concentration of PPIX in the sample.

The potentially detrimental effect of the ferrochelatase inhibitor N-methylprotoporphyrin IX (NMPP) on fluorescence measurement of extracted porphyrins from cells treated with this chemical was determined to be negligible. Although NMPP does fluoresce weakly at two wavelengths (Ex: 400 nm Em: 633 nm and 653 nm; and Ex: 440 nm Em: 653 nm), potentially adding to the (E400 F633) and (E440 F638) terms in the

above deconvolution formula, fluorescence scans of extractions from both wt and *bchD* strains treated with NMPP were shown to not contain characteristic emission peaks from NMPP at 653 nm upon 400 or 440 nm excitation (Appendix II). This finding indicates that NMPP was likely not extracted out of cells to any great extent by 9/1 acetone/0.1 N NH_4OH, or alternatively, was extracted out of the acetone layer by hexane.

2.5.6. Method used to quantify amounts of protochlorophyllide from cells.

This was done using an established spectral deconvolution method (Rebeiz 2002). Briefly, cells were extracted with 9/1 acetone/0.1 N NH_4OH then twice extracted with hexane, yielding HEAR. Fluorescence emission spectra of each sample was captured from 575-700 nm with excitation at 400 and 440 nm. Fluorescence emission due only to divinyl-protochlorophyllide (DV-PChlide) was determined through the equation:

DV-PChlide (wt, E440 F638; *bchD*, E440 F634) = 1.0080F (wt, E440 F638; *bchD*, E440 F634)
- 0.0141F (E440 F675) – 0.0197F (E400 F633)
+ 0.0028F (E440 F622)

Where: E, excitation wavelength; F, fluorescence emission wavelength; wt and *bchD* indicate different DV-Mg-PChlide and DV-Zn-PChlide emission wavelengths used.

This deconvolution removes the contributions from unwanted fluorescence due to chlorophyllide (Ex: 440 nm Em: 675 nm), protoporphyrin IX (Ex: 400 nm Em: 633 nm) and coproporphrinogen (Ex: 440 nm Em: 622 nm) from fluorescence intensity of DV-Mg-PChlide in the wt (Ex: 440 nm Em: 638 nm) and DV-Zn-PChlide in the *bchD* mutant (Ex: 440 nm Em: 634 nm). Since I do not have access to DV-PChlide standards, the fluorescence emission intensities were normalized based on the relative fluorescence intensities of Mg-PPIX versus Zn-PPIX, with the assumption that the 6.2-fold greater fluorescence intensity of Mg-PPIX over Zn-PPIX would also hold true for the DV-Mg-PChlide and DV-Zn-PChlide molecules.

2.5.7. Chemiluminescent method used to quantify amounts of heme.

Heme preparations extracted from cell pellets were used in a chemiluminescent heme assay (Masuda & Takahashi 2006; Takahashi & Masuda 2009). Briefly, a reaction mixture was made up to the following final concentrations: 2.5 nM apo-horseradish peroxidase (apo-HRP) (Biozyme), 100 mM Tris–HCl (pH 8.4), and heme extraction diluted 10^{-4} to 10^{-5} in 100 mM Tris-HCl (pH 8.4). The 100 µL reaction mixture for each sample was added to a 96-well plate and was incubated at room temperature for 30 min to allow heme reconstitution with the apo-HRP. Then 100 µL Immobilon Western HRP substrate (Millipore) was added to each well and the mixture was incubated for 10 min at room temperature. Chemiluminescence was read off the plate every 5 minutes, starting at 10 minutes post-incubation, until the chemiluminescent readings declined in intensity. Plates were read using a Victor^2 chemiluminescent plate reader (Perkin Elmer) set to 0.1 seconds integration. Standard curves were constructed using 20-800 pM heme standards (made up fresh in 10 mM KOH) and values for the samples were calculated from these curves.

2.5.8. RC steady state absorption spectroscopy.

Room-temperature absorption spectra of purified RCs in 15 mM Tris-HCl (pH 8.0), 1 mM EDTA, 0.025% LDAO, 150 mM NaCl were obtained in a Hitachi U-3010 spectrophotometer using 600 nm/min scan speed and 1 nm slit width. Low-temperature absorption spectra were recorded at 120 nm/min at 1 nm slit width (Cary 6000i, Varian Inc) with attached closed-cycle He cryostat (Omniplex OM-8, ARS Inc). RCs were prepared in 15 mM Tris-HCl (pH 8.0), 1 mM EDTA, 0.025% LDAO, and diluted 1:1 with glycerol so that the accessory BChl peak of the RC was at an OD of 1.0 with a 150 µm path length (Treynor et al. 2004). Samples were deposited between two quartz windows separated with a spacer. The assembly was then mounted on a sample rod and frozen rapidly to ~10 K, equilibrated for 15 minutes followed by absorption readings.

2.5.9. Spectral deconvolution.

Three Gaussian curves were used to model the three binding sites of the RC. The plotted curves are represented by the equation:

$$y = y_0 + s_0(x\text{-}1000) + \sum \left(\frac{A_i}{w_i \sqrt{(\Pi/2)}} \right) e^{-2\left(\frac{x\text{-}x_{ci}}{w_i}\right)^2}$$

Where:

y is the absorbance, x is the wavelength, y_0 is the baseline, s_0 is the slope of the line used to model the absorbance peak tails, A is the amplitude of each Gaussian distribution, w is the width of each Gaussian distribution, x_c is the center position of each Gaussian distribution, and *i* is the identifier for each of the three Gaussian curves.

2.5.10. Microsecond and millisecond kinetic measurements.

Kinetic measurements on μs to ms time scales were performed on a home-built spectrometer using a Nd:YAG laser (Opotek, Carlsbad, CA) for actinic excitation (40 mJ per pulse, 5 ns half-width) (Kleinfeld et al. 1984). Kinetic traces were recorded on a LeCroy oscilloscope and then transferred to a PC for analysis (Paddock et al. 2005).

2.5.11. Femtosecond transient spectroscopy.

The femtosecond transient absorption spectroscopy was performed using a pump-probe setup (Wang et al. 2007). Laser pulses of 1 mJ at a repetition rate of 1 KHz were generated from a regenerative amplifier system (Tsunami and Spitfire, Spectra-Physics). Part of the pulse energy (~10%) was used to generate a white light continuum for the probe beam. The remainder was used to pump an optical parametric amplifier (OPA-800, Spectra-Physics) generating excitation pulses at 860 nm. Transient absorption changes at various wavelengths were measured using a monochromator (SP150, Action Research Corp.) and a diode detector (Model 2032, New Focus Inc.). The relative polarization of the excitation and probe beams was set to the magic angle of 54.7° (Bydder et al. 2007). The excitation intensities were kept below 500 nJ per pulse and the excitation spot size was 0.5 mm in diameter. RC samples were loaded in a spinning wheel with an optical path length of 1.2 mm, and a final optical density of ~ 0.3 at 792 nm was used. Kinetic traces were fitted with a sum of exponentials using a local written program ASUFIT (Katilius 2009).

2.5.12. P_{Zn}/P_{Zn+} redox midpoint potential.

Measurements were made at room temperature using a thin-layer electrochemical cell as previously described (Allen et al. 1996; Lin et al. 1994). RC samples were concentrated to an A_{792} of ~100 and poised in 60 mM KCl/15 mM Tris-HCl at pH 8. Potassium ferrocyanide (0.4 mM) and potassium tetracyano mono[1,10-phenanthroline]Fe(II)•4H2O (0.074 mM) were added as mediators. A spectrophotometer (Cary 5, Varian Inc.) was used to measure absorption spectra as the potential was systematically varied. The extent of reduction monitored at the maximum of the BChl dimer (P) Q_Y transition was fitted to the Nernst equation (n = 1) (Lin et al. 1994).

3. Results

Data in Sections 3.1 and 3.3 appeared in a peer-reviewed publication (Jaschke & Beatty 2007), planned with Dr. Beatty's assistance and with all experiments and writing executed by me. Data in Sections 3.1.8, 3.1.9, and 3.2 appeared in a peer-reviewed publication in collaboration with three other groups (Lin et al. 2009a). I participated in planning, experimental design, experimentation, and editing of the manuscript in conjunction with the other authors.

3.1. Composition of the *bchD* mutant photosynthetic apparatus.

3.1.1. Comparison of growth between the wt and *bchD* mutant strain.

To investigate the physiological effect of disruption of the *bchD* gene we measured growth of the mutant under aerobic, semiaerobic and anaerobic photosynthetic conditions. Under aerobic growth the wt and *bchD* strains had nearly identical growth curve shapes and corresponding doubling times (4.2 hours). However, the *bchD* mutant only reached densities of $2.4X10^9$ CFU/mL while the cultures of the wt strain contained over $3.6X10^9$ CFU/mL (Figure 3-1A). Semiaerobic growth showed a larger disparity between the maximum density reached in the wt ($2.3X10^9$ CFU/mL) and *bchD* mutant ($0.82X10^9$ CFU/mL). Nevertheless, doubling times (6.5 and 6.7 hours, respectively), were very similar (Figure 3-1B). Finally, the wt strain grew photosynthetically with a doubling time of 2.0 hours. In contrast, the *bchD* mutant showed no increase in cell density (Figure 3-1C).

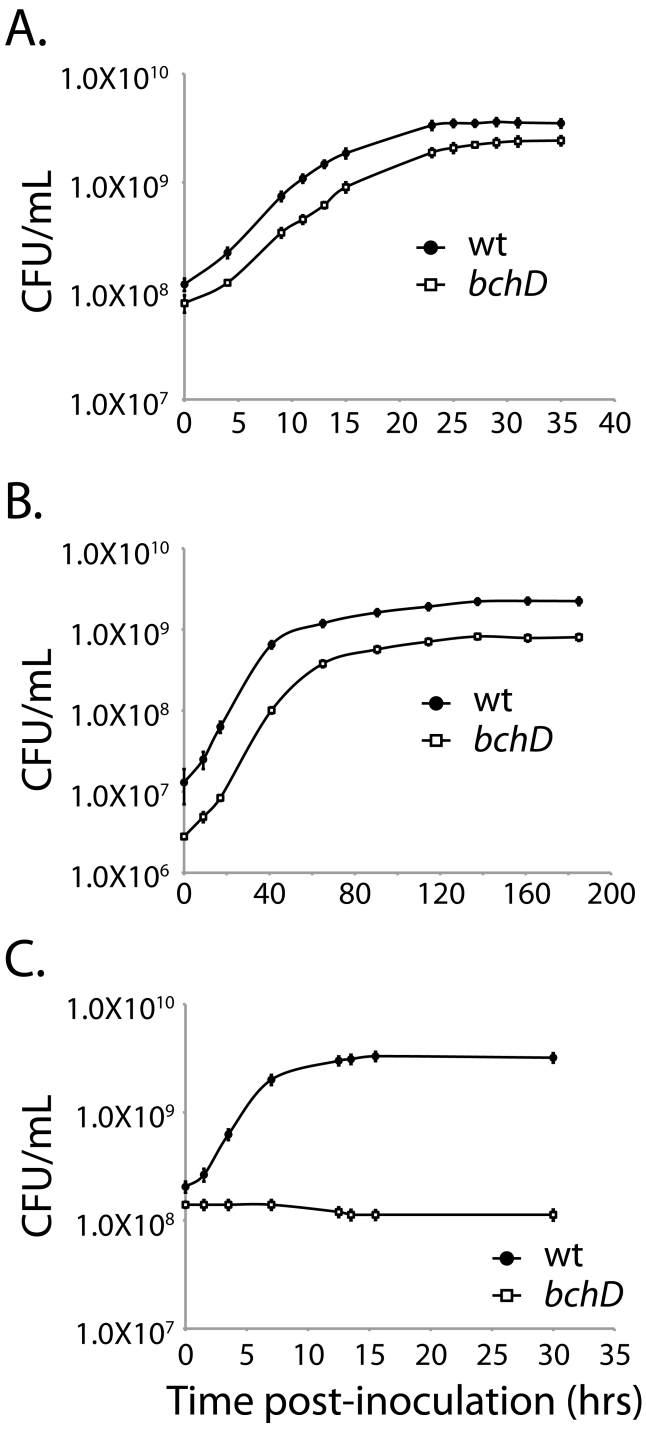

Figure 3-1. Aerobic, semiaerobic and photosynthetic growth of wt and *bchD* mutant strains. (A) Aerobic growth mode. Cultures grown on test tubes on a wheel spinning at 60 RPM. (B) Semiaerobic growth mode. Cultures grown in Erlenmeyer flasks filled to 80% capacity and shaken at 150 RPM. (C) Photosynthetic growth mode. Cultures grown in screw top tubes with light of 75 µEinsteins/m^2s. All cultures grown at 30°C. Black filled circles, wt strain; white filled squares, *bchD* mutant.

The growth curve results point to a growth mode-dependent disruption in the *bchD* mutant, which extends beyond simply not being able to synthesize BChl. The photosynthetic growth defect was reported when this strain was originally created (Coomber et al. 1990), but the effect on other growth modes is newly reported here. Since this mutant has been shown to not synthesize BChl, which is needed for photosynthetic growth, this result is not surprising, but the knock-on effect from the *bchD* mutation to other growth modes is unexpected. This effect manifested itself as a decrease in the maximal cell density the cultures could achieve during aerobic and semiaerobic growth. The *bchD* mutant reached approximately 66% the cell density of the wt strain during aerobic growth, but only reached 33% the density of the wt strain under semiaerobic growth. To assess additional reasons for the inability of the *bchD* mutant to grow photosynthetically, examination of photosynthetic protein levels was performed next.

3.1.2. Comparison of amounts and types of photosynthetic proteins present in the wt and *bchD* mutant.

Deletion of the Mg-chelatase (*bchD*) is expected to result in the abolition of BChl synthesis. The impact of this mutation on the amounts of photosynthetic proteins in the membrane fraction of semiaerobically-grown cells was evaluated. Western blotting showed significant amounts of RC H, M and L in the *bchD* mutant, although at lower levels than in the wt strain (Figure 3-2A). Measurement of the intensity of each RC band of the *bchD* mutant to wt showed that on average the RC H protein was present at the lowest amount (12% of that of the wild type), RC L was present at 32%, and RC M was present at the highest amount, 46% (Table 3-1, top three rows).

Antibodies to detect LH proteins in Western blots were not available. Consequently, tricine-SDS-PAGE was used to visualize LH1 and LH2 α and β protein bands (Figure 3-2B). This approach was possible because the LH1 and LH2 α/β proteins are small and well-resolved from the rest of the membrane proteins. Measurement of LH band intensities indicated that the level of LH1 α and LH2 α proteins on average was 52% of the wt, whereas the β proteins were present at 14% of wt (Table 3-1, bottom two rows).

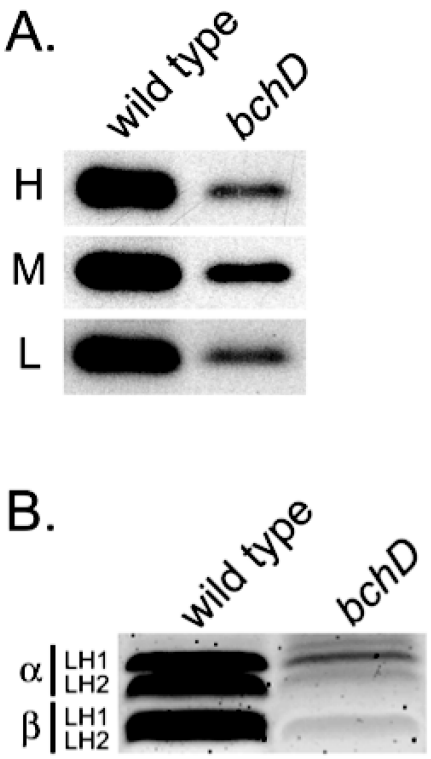

Figure 3-2. Relative amounts of photosynthetic proteins in wt and *bchD* membranes. (A) Western blot of wt and *bchD* membranes. Each lane contained 10 µg of membrane proteins. Blots were probed sequentially with anti-RC H/M/L antibodies. (B) Tricine-SDS-PAGE gel of wt and *bchD* membranes. Each lane contained 30 µg of membrane proteins.

Table 3-1. Relative amounts of photosynthetic proteins in *bchD* mutant membranes.

Protein	Amount relative to wild type (%)
RC H	12 (5)[a]
RC M	46 (2)[a]
RC L	32 (5)[a]
LH1/2-α	52 (1)[b]
LH1/2-β	14 (4)[b]

Values are means of three independent cultures, with standard deviations in parentheses. [a]Difference between protein band pixel volumes of wt and *bchD* mutant in Western blots. [b]Difference between protein band pixel volumes of wt and *bchD* mutant from stained tricine-SDS-PAGE gels.

To explore the possibility that RC proteins interact to form a complex in the *bchD* mutant, I used a six-histidine (6His) tag pulldown approach. A plasmid expressing the *puhA* (RC H) gene modified by addition of a C-terminal 6His tag was introduced into *bchD* and wt strains. Membrane proteins were solubilized with LDAO detergent, bound to Ni^{2+}-NTA beads, and eluted with imidazole. Western blot analysis of the elutions showed that all three RC proteins co-eluted from the Ni^{2+}-NTA beads incubated with solubilized membrane proteins from either *bchD* or wt cells expressing the 6His-tagged RC H, whereas none of the RC proteins were seen in the elutions of material from cells lacking the 6His-tagged RC H protein (Figure 3-3).

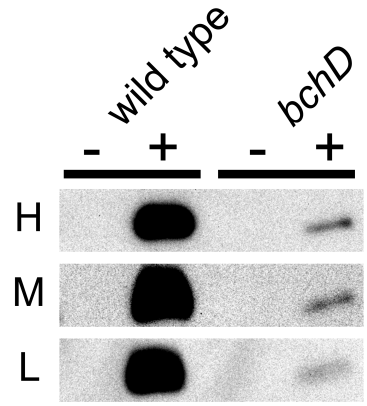

Figure 3-3. Relative amounts of interacting RC proteins in wt and *bchD* membranes. Western blot of 6His-tagged RC H pulldown elutions from wt and *bchD* solubilized membranes from cells containing either empty vector pATP19P (-), or p6His-C with RC H (*puhA*) gene encoding six C-terminal histidines (+). Equal amount of membrane proteins from each strain (80 µg) were solubilized and mixed with Ni^{2+}-NTA beads.

This co-elution of all three RC proteins indicates that the RC M and L proteins bind to RC H in *bchD* mutant cell membranes, and therefore form a complex. RC protein band intensities were quantified, and the data in Table 3-2 show that the average amounts of RC H, M and L that co-purified from the *bchD* mutant were 7 to 16% of the wt values. This result shows that not all of the RC protein present in the *bchD* mutant was successfully forming RC complexes.

Table 3-2. Relative amounts of RC proteins pulled down by 6His-tagged RC H.

Protein	Amount relative to wild type (%)[a, b]
RC H	7 (3)
RC M	12 (6)
RC L	16 (3)

[a]Difference between protein band pixel volumes of wt and *bchD* mutant elutions in Western blots. [b]Mean of experiments on three independent cultures, with standard deviations in parentheses.

3.1.3. Comparison of the types of pigments present in the wt and *bchD* mutant strains.

Since previous work had shown that, in mutants unable to make BChl, the photosynthetic proteins are very unstable (Klug et al. 1986), I wanted to see if residual BChl synthesized by the *bchD* mutant, caused by a leaky mutation or redundant paralog, was exerting a stabilizing influence on the small pool of LH and RC proteins observed. Pigment extractions from cells of wt and *bchD* mutant strains were separated by HPLC to investigate the differences in pigment composition (Figure 3-4A). As expected, BChl was the major component in the wt elution profile (retention time of 19.2 min), with a lesser amount of BPhe (retention time of 21.1 min). The absorption spectrum of BChl yielded major peaks at 364, 600 and 770 nm (Figure 3-4B), consistent with published values (Woodbury et al. 1995). The *bchD* mutant elution profile lacked BChl and BPhe peaks, although a carotenoid peak, also present in wt, at 20.4 min was seen. The major pigment eluted at 19.7 min, and is labeled as peak I in Figure 3-4A. Peak I had an absorption spectrum similar to BChl, but with blue-shifted peaks at 357, 569 and 766 nm (Figure 3-4B).

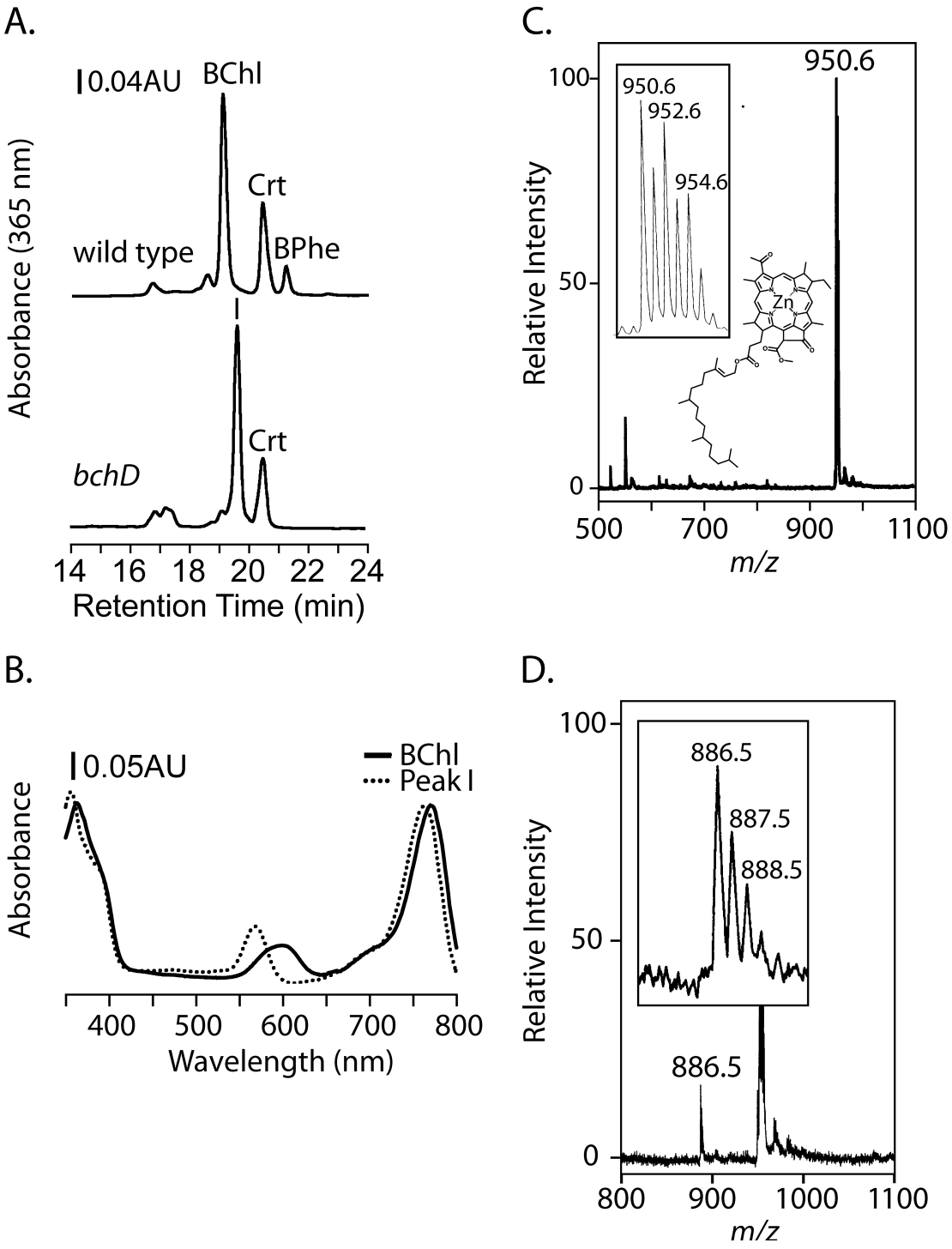

Figure 3-4. Isolation and identification of Zn-BChl from the *bchD* mutant.
(A) HPLC trace of wt (top) and *bchD* (bottom) whole cell acetone/methanol extractions. (B) Absorption spectra of BChl peak from wt and peak I from HPLC. (C) Mass spectrometry of peak I; insets, expanded region around peak 950.6 *m/z* and proposed structure of peak I. (D) Mass spectrometry of peak I material after acidic treatment; inset shows expanded region around newly created 886.5 *m/z* peak.

The material in peak I was subjected to MALDI-TOF mass spectrometry analysis to evaluate the identity of the pigment (Figure 3-4C). The mass to charge ratio (*m/z*) of the predominant peak was 950.6, which differs from the predicted BChl *m/z* of 911.5. However, the *m/z* of peak I (950.6) agrees well with the predicted *m/z* (950.5) of BChl that contains zinc instead of magnesium (Zn-BChl *a*). The pattern seen for the peaks surrounding the 950.6 *m/z* peak (Figure 3-4C, inset) are caused by two overlaid sub-patterns: the first, caused by the predominant isotopes of carbon, oxygen, and nitrogen (^{12}C (98.9%), ^{13}C(1.1%); ^{16}O(99.8%), ^{18}O(0.2%); ^{14}N(99.6%), ^{15}N(0.4%)) results in three peaks *one* mass unit apart that follow the ratio 1.00/0.37/0.07; the second pattern is caused by the most stable isotopes of zinc which are *two* neutrons apart (^{64}Zn (49%), ^{66}Zn (28%), and ^{68}Zn (19%)), and that 'add' onto the underlying isotope pattern (Heath 1981). The combination of the two sub-patterns is three series of three peaks with the same relative peak ratio as for the compound without zinc, one mass unit apart, but each series is offset by two mass units, caused by the isotopic characteristics of zinc. If the compound were to contain magnesium instead of zinc, the isotopes of magnesium (^{24}Mg (79%), ^{25}Mg (10%), and ^{26}Mg (11%)), which are all *one* mass unit apart would dominate the pattern causing the mass spectrum to look nearly identical to one that contains only carbon, nitrogen and oxygen (Heath 1981).

When peak I material was analyzed using an acidic matrix to remove chelated metals, the 950.6 *m/z* peak amplitude decreased and a new peak appeared at *m/z* 886.5 (Figure 3-4D). The 64.1 mass unit downshift agrees well with the predicted mass change due to loss of zinc (63.9 exact mass of most abundant isotope, ^{64}Zn). Furthermore, the isotopic pattern of the peaks surrounding the 886.5 *m/z* peak match those predicted for a compound containing only carbon, nitrogen and oxygen, as opposed to zinc (Figure 3-4D, inset). These findings further support my conclusion that peak I is Zn-BChl *a* (hereafter referred to as Zn-BChl).

Together, these data show that the *bchD* mutant contains low amounts of Zn-BChl in place of the normal Mg-BChl, but lacks BPhe. However, these data do not reveal whether some or all of the RC and LH complexes bind Zn-BChl.

3.1.4. Pigment composition of the light-harvesting complexes in the wt and *bchD* mutant strains.

To determine if Zn-BChl and other pigments were assembling with LH proteins in the *bchD* mutant, I performed absorption spectroscopy on purified membranes. Membrane absorption spectra reveal LH1 and LH2 complexes but cannot show the RC spectrum because it is hidden underneath the strong LH absorption peaks. Membranes of the wt strain grown to stationary phase under low aeration showed characteristic absorption peaks in the 450 to 550 nm region, which indicated the presence of carotenoids, and peaks in the 800 to 875 nm region, which indicated the presence of BChl bound to LH complexes. In addition to the presence of carotenoid peaks, the absorption spectrum of the *bchD* mutant revealed peaks at 793, 836 and 859 nm, which were blue-shifted 7 to 16 nm compared to the corresponding wt LH2 peaks at 800 and 850 nm, and the LH1 peak at 875 nm (Figure 3-5, top two traces). Interestingly, when grown under low aeration conditions, the LH2/LH1 peak ratio (0.50) of the putative *bchD* mutant complexes differs from the ratio (1.48) in identically grown wt cells, and is instead closer to the ratio (0.41) in wt cells at an early stage (8 hours) after shifting from high aeration (photosystem repressing) to low aeration (inducing) growth conditions (Figure 3-5, bottom trace).

These data showed that LH1 and LH2 complexes assembled in the *bchD* mutant, but bound a pigment that differed from the BChl found in complexes from identically grown wt cells. I propose that this pigment is the Zn-BChl described in Section 3.1.3.

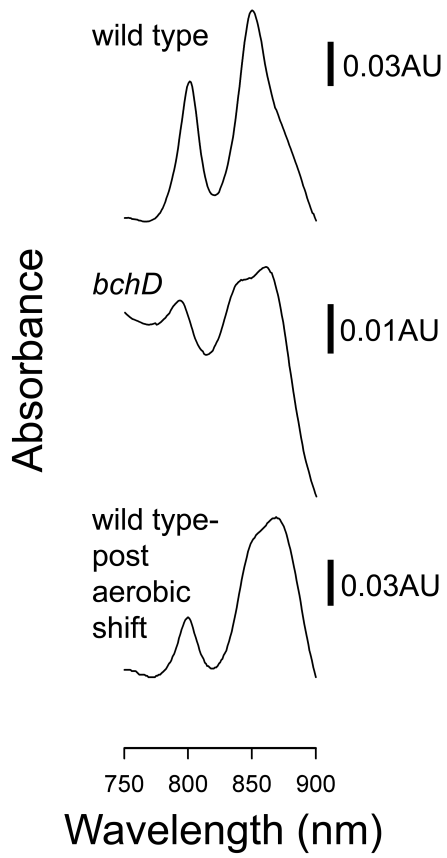

Figure 3-5. Comparison of LH complex absorption between the wt and *bchD* mutant. Absorption spectra of chromatophores from wt (top) and *bchD* cells (middle) grown to stationary phase under low aeration, and wt cells 8 hours after transition from photosystem repressing (high aeration) to inducing (low aeration) conditions (bottom). Spectra were normalized to absorbance at 650 nm.

3.1.5. Pigment composition of the RC complex in wt and *bchD* mutant strains, studied by room temperature absorption spectroscopy.

Following up on the discovery that LH complexes in the *bchD* mutant appeared to bind a BChl-like pigment, presumably the Zn-BChl described in Section 3.1.3, a similar spectral analysis was performed on the RC. Because RC absorption peaks are hidden by the LH peaks in chromatophores, I purified RC complexes from wt and *bchD* cells. The absorption spectra of RC complexes purified from the wt and *bchD* mutant were similar, with both preparations yielding distinct peaks in the 700 to 900 nm region, and overlapping peaks in the 450 to 550 nm region (Figure 3-6A). However, there were three major differences between these RCs: (1) the BChl special pair peak, at 865 nm in the wt strain, was blue-

shifted to 855 nm in the *bchD* mutant; (2) the accessory BChl peak, at 803 nm in the wt, was shifted to 795 nm in the *bchD* mutant; (3) the *bchD* mutant spectrum lacked a peak at 760 nm corresponding to BPhe absorption in the wt RC (Woodbury et al. 1995).

3.1.6. Pigment composition of the RC complex in wt and *bchD* mutant strains, studied by pigment extraction.

To better understand the nature of the pigments bound to the RC from the *bchD* mutant the purified RC was extracted with acetone/methanol (7/2). The absorption spectrum of pigments extracted from the *bchD* RC showed a major far-red peak at 766 nm, whereas pigments extracted from the wt RC absorbed maximally in the far-red region at 759 nm (Figure 3-6B). The wt peak results from the combined absorption of a 2:1 ratio of BChl (771 nm) to BPhe (750 nm).

However, the absorption spectrum of the intact *bchD* RC (see Figure 3-6) indicated that it lacks BPhe, and so the spectrum of the extracted BChl-like pigment appears to have an absorption peak at 766 nm, blue-shifted by 5 nm relative to BChl and matching the spectrum of Zn-BChl, purified from the *bchD* mutant in Section 3.1.3. Furthermore, absorption peaks in the 450 to 550 nm region showed the presence of carotenoid in the *bchD* RC. The ratios of the far-red to the far-blue peak between wt and the *bchD* mutant also highlighted the difference between these two pigment extracts. The wt peak at the blue-side of the spectra was much higher compared to the red-peak, whereas the peaks were almost equal heights in the *bchD* mutant extraction. Equal peak heights are indicative of BChls while much higher far-blue peaks are more indicative of demetallated molecules such as BPhe. Thus, I found that the *bchD* mutant assembled a RC that contained Zn-BChl and carotenoid but lacks BPhe, and is called the Zn-RC for the rest of this work.

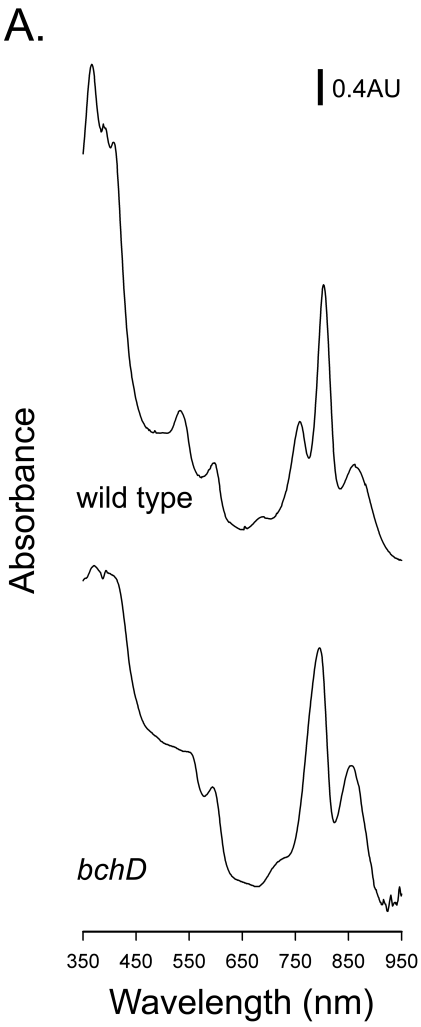

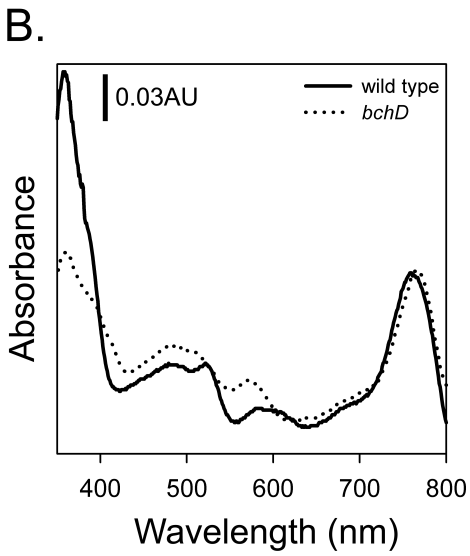

Figure 3-6. Comparison of RC composition between wt and *bchD* mutant. (A) Absorption spectra of purified RC complexes isolated using His-tagged RC H. (B) Absorption spectra of acetone/methanol extraction of RCs.

3.1.7. Analysis of photosynthetic apparatus mutants to determine the origin of BPhe.

The origin of BPhe in *Rb. sphaeroides* has for some time been a mystery, and its absence in the *bchD* strain was unexpected. This result is a unique finding in *Rb. sphaeroides*. One previous hypothesis of the origin of BPhe is that the RC itself is a dechelatase that removes the Mg^{2+} of BChl when it binds to the H-sites. To determine if the RC is needed for BPhe production, several strains of *Rb. sphaeroides* with photosynthetic apparatus gene deletions were examined.

Semiaerobically grown cells were extracted with acetone/methanol and the extract was examined with absorption spectroscopy. The spectral signature of the wt strain extraction showed the absorption of BChl at 771 nm (Figure 3-7). In contrast, the ΔRCLH::pESHPUFM$^-$ strain which lacks the LH2 and RC M genes, but still has RC HL, and LH1 (Tehrani & Beatty 2004), had an absorption peak at 753 nm that was close to the 750 nm BPhe peak, but was red-shifted towards that of BChl (Figure 3-7). Pigments in the ΔRCLH strain, which lacks the RC, LH1 and LH2 genes, absorbed at 752 nm, similar to BPhe (Figure 3-7). This result was perhaps not that surprising coming from the ΔRCLH strain which does not assemble any photosynthetic complexes, but it was very surprising from the ΔRCLH::pESHPUFM$^-$ which has been shown to assemble the LH1 complex (Tehrani 2003). The absorption peak of extractions from ΔRCLH::pESHPUFM$^-$ suggested there was a huge excess of BPhe in the cell over BChl, because the absorption maximum was much more similar to BPhe than to BChl. This was unexpected because BChl binds and assembles with the LH1 complex in these cells, and since the strain lacks the RC complex, there was no reason to believe that any BPhe was present in the cells (Tehrani 2003).

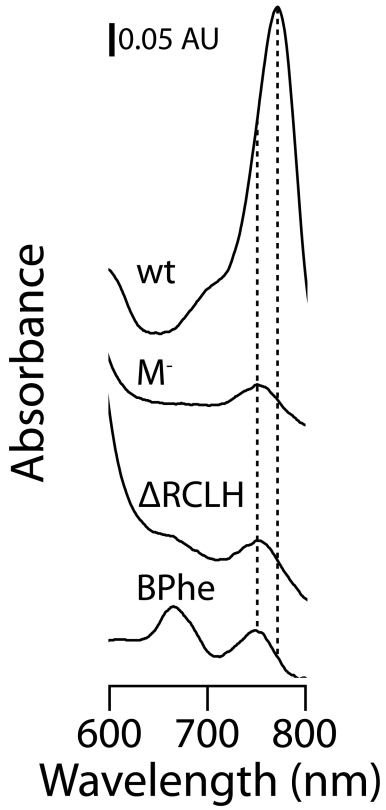

Figure 3-7. Pigment extraction of cells with RC component deletions. Whole cells extracted with 7/2 acetone/methanol then examined with absorption spectroscopy. wt, wild type *Rb. sphaeroides* strain; M^-, ΔRCLH::pESHPUFM$^-$; ΔRCLH, deletions in *puhA*, *puf*, and *puc* operons; BPhe, acid-treated wt extraction. Dotted lines indicate absorption maxima of Mg-BChl (771 nm) and BPhe (750 nm).

3.1.8. Pigment composition of the Zn-RC H-sites studied by room-temperature absorption spectroscopy and spectral deconvolution.

The absorption spectra of extracted pigments confirmed data from the intact RC spectra showing that the Zn-RC lacked BPhe but did not reveal if anything else was binding in its place. Looking deeper into the Zn-RC to explore the occupancy of the H-sites, which normally bind BPhe in the WT-RC, we performed room temperature absorption spectra again, but this time we also scanned the purified RC from the so called β-mutant, a strain of *Rb. sphaeroides* that has a single amino-acid change at the RC M protein residue 214 from Leu to His. This change adds a fifth stabilizing ligand for the Mg^{2+} in BChl that causes BChl to bind the H_A-site, where BPhe normally binds (Kirmaier et al. 1991). Therefore, the β-mutant has half the amount of BPhe present in the WT-RC, and 1.25 the

amount of BChl. By analogy, we hoped that the β-mutant RC would give us a hint whether Zn-BChl was binding to the H-sites or not.

The absorption spectra showed us that, compared to the WT-RC, the β-mutant RC had lower amplitude H-bands at 545 nm (short wavelength Q_X region) and 760 nm (long wavelength Q_Y region) due to BPhe. The changes in the H-band absorbance were accompanied by the appearance of a shoulder on the short wavelength side of the Q_Y band of the accessory BChl (B) at 804 nm, which was attributed to the single BChl binding to the H-site on the cofactor A-branch (Figure 3-8). Compared to the β-mutant RC, the Zn-RC absorption spectrum had a decrease of the 760 nm band and a corresponding increase of the ~775 nm shoulder on the B-band (Figure 3-8). Together, these data indicated that the Zn-RC likely lacked BPhe in the H-site, and contained a cofactor that absorbed at ~775 nm, analogous to the H_A-BChl in the β-mutant RC.

To model the absorption peaks that were evidently overlapping in Figure 3-8, we collaborated with Mark Paddock at the University of California, San Diego to perform spectral deconvolution of the room-temperature absorption spectra of the Zn-RC. This analysis yielded three absorption peaks that could account for the shoulder seen on the short-wavelength side of the accessory BChl peak of the Zn-RC (Figure 3-9). The results of the deconvolution indicated that there was a contribution to the absorption spectrum from a cofactor that absorbed at 783 nm, perhaps due to Zn-BChl bound at one or both of the H-sites. The combination of the room temperature absorption spectra and the spectral deconvolution suggested that Zn-BChl was bound to the Zn-RC where BPhe is normally bound.

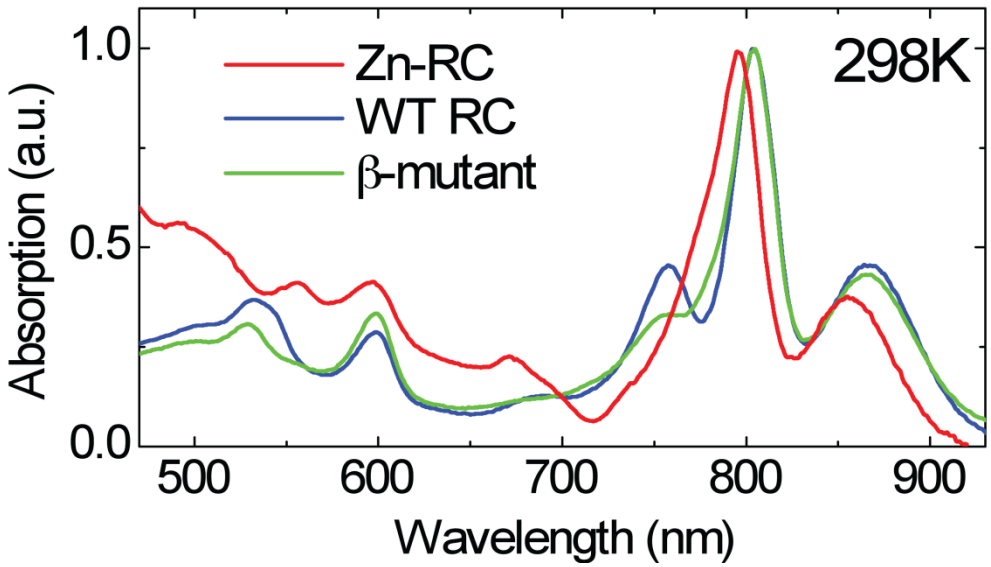

Figure 3-8. Room temperature absorption spectra of RCs from the wt, *bchD* mutant and β-mutant. Spectra of wt (blue), *bchD* mutant (red), and β-mutant (green), normalized at accessory BChl peak (800 nm for WT-RC and β-mutant RC, and 794 nm for the Zn-RC).

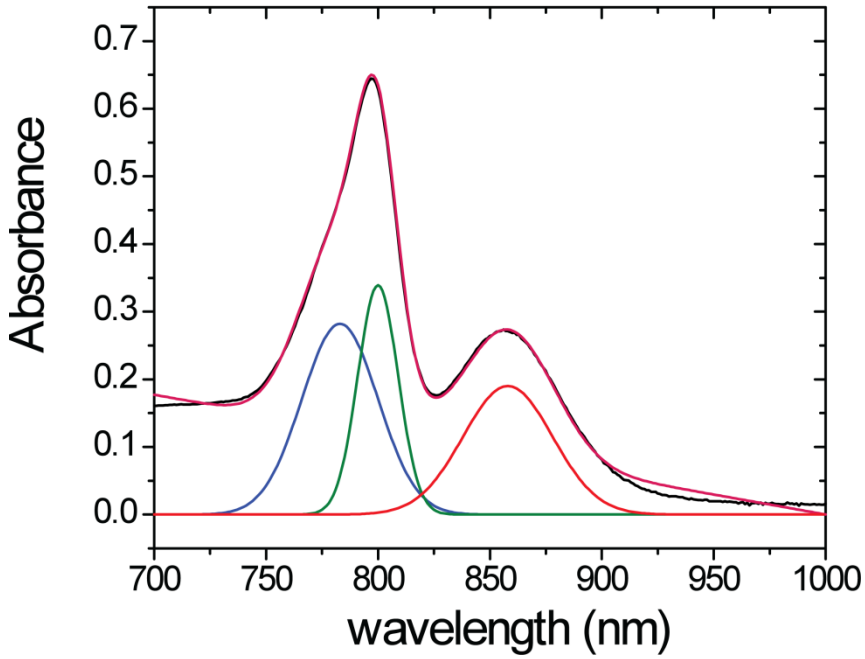

Figure 3-9. Spectral deconvolution of Zn-RC room temperature absorption spectra. Contributions from spectral components: blue, H-site ($H_{A,B}$) absorbance calculation; green, accessory site ($B_{A,B}$) absorbance calculation; red, special pair site (P) absorbance calculation; pink, total sum of calculated component curves; black, experimentally determined absorption spectra.

3.1.9. Pigment composition of the Zn-RC H-sites studied by low-temperature absorption spectroscopy.

To determine the identity of the cofactor binding to the H-sites of the Zn-RC we collaborated with Fred Roselle of the Mauk lab (Department of Biochemistry and Molecular Biology, UBC) to perform low-temperature absorption spectroscopy, which allows resolution of overlapping absorption bands that may not be resolved in room temperature scans.

These scans were highly informative, showing the Q_Y absorption band features of the WT-, β-mutant, and Zn-RC with much greater resolution (Figure 3-10A). At a temperature of 13 K, the shoulder around 775 nm became a peak in the absorption spectra of both the β-mutant and the Zn-RC. The amplitude of this band was about two times greater and slightly blue-shifted in the Zn-RC spectrum compared to the β-mutant RC spectrum. Figure 3-10B compares the Q_Y transition bands from the 13 K spectra of all 3 RCs normalized to the absorption maxima of their P bands in the 850 to 865 nm region, and with the spectrum of the Zn-RC mathematically shifted 9 nm to the red to make the P-band peaks coincident; a stepwise amplitude decrease of the 760 nm band and a corresponding increase of the ~ 775 nm band was shown clearly when comparing RCs containing 2 BPhe (WT-RC), 1 BPhe (β-mutant) and no BPhe (Zn-RC). Therefore, because of the increased peak height due to Zn-BChl(s) in the H-site(s), versus the one Mg-BChl seen in the H_A-site of the β-mutant, we believe these data confirm that the Zn-RC contained Zn-BChls in both of the H-sites.

In the Q_X transition region of the 13 K spectra the data further supported our original hypothesis that Zn-BChl was bound in place of BPhe (Figure 3-10A). The WT-RC showed bands at 533 and 546 nm, corresponding to the absorption of BPhe in the H_B and H_A positions, respectively (Woodbury et al. 1995). The Q_X transition bands of B_A, B_B, and P in the WT-RC were centered around 600 nm. The β-mutant RC had only one BPhe band (H_B, at 533 nm) because the H_A-BPhe had been replaced by BChl, resulting in an increased intensity of the 600 nm band. In the Zn-RC, only two Q_X bands were observed, at 560 and 600 nm. Because there were no BPhe or Mg-BChl cofactors in the Zn-RC, it followed that the 560 nm band must be due to a Zn-BChl, whereas the P and B-site Zn-BChl cofactors

absorbed near 600 nm. The 560 nm band, therefore, had to be the Q_X band of the H-site Zn-BChls, corresponding to the 775 nm peak of the Q_Y spectrum described above.

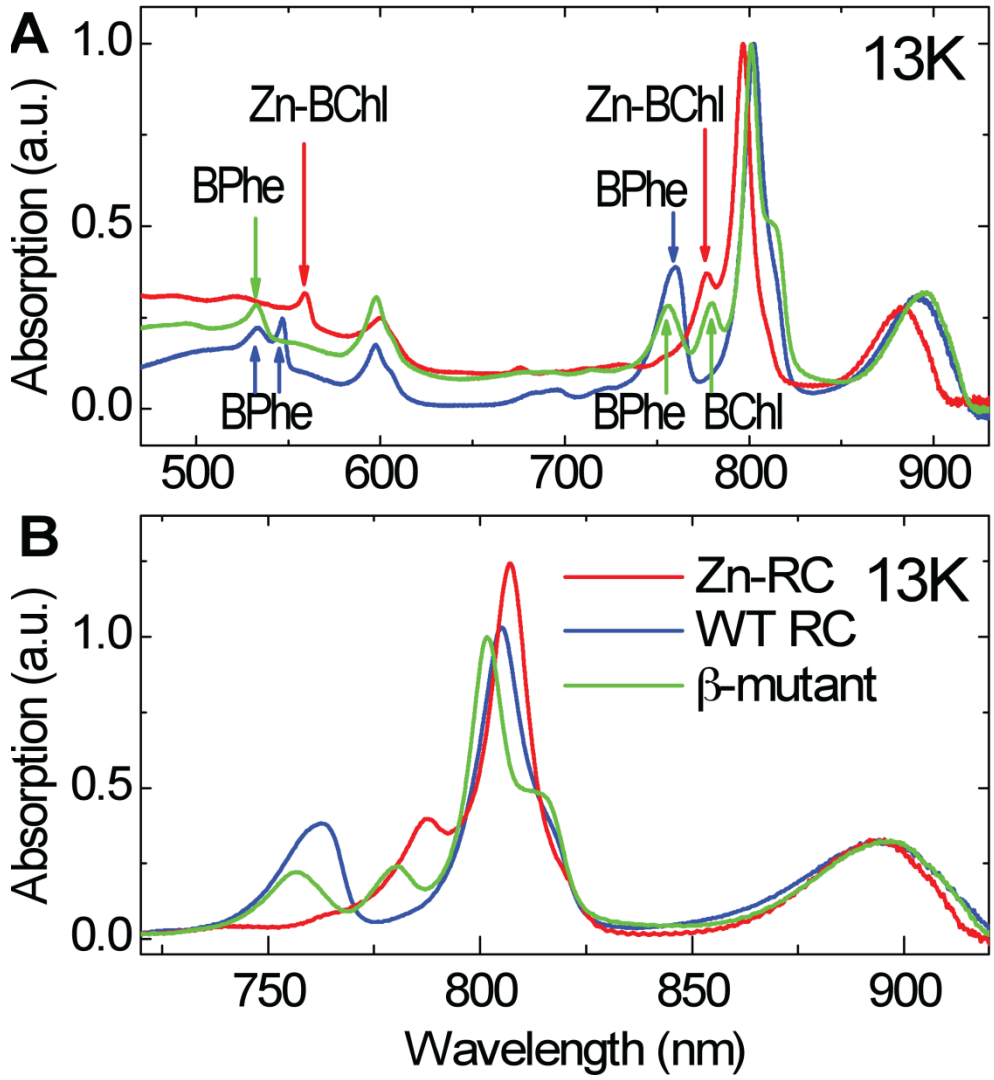

Figure 3-10. Low-temperature absorption spectra of RCs from the wt, *bchD* mutant and β-mutant. Spectra of wt (blue), *bchD* mutant (red), and β-mutant (green). (A) 13K spectra normalized at accessory BChl peak (800/794 nm). Arrows indicate both Q_X and Q_Y absorption peaks for pigments bound to the H-sites. (B) 13K spectra normalized at special pair peak (865 nm), with the Zn-RC spectrum mathematically red-shifted by 9 nm to align the special pair peaks.

3.1.10. The search for an alternative photosynthetic apparatus in other *bch* mutants.

Because of the surprising discovery of the Zn-BChl photosynthetic apparatus in the *bchD* mutant, other mutants in BChl-biosynthesis enzymes were examined to see if they also

contained proteins of the photosynthetic machinery. Two other Tn5 mutants made at the same time as the *bchD* mutant were analyzed. The *bchY* mutant is disrupted in the BchY subunit of the chlorophyllide reductase, while the *bchG* mutant is disrupted in the BChl-synthase (Coomber et al. 1990) (see Figure 1-6 for gene positions in the biosynthetic pathway). Both these mutants accumulate large amounts of intermediates upstream of their respective lesions in the BChl-biosynthetic pathway (Coomber et al. 1990).

The mutant strains were grown semiaerobically, lysed, and membranes were isolated from them. These membranes were run on tricine-SDS-PAGE, electroblotted, and probed with antibodies against various photosynthetic proteins. The *Rb. capsulatus* wild type strain SB1003 was included as a control because the LH2 antibody was raised against proteins from this species, and it was not certain whether it would cross-react with the *Rb. sphaeroides* proteins. In this experiment the anti-LH2 antibody was found to cross-react only with the β-subunit of *Rb. sphaeroides* LH2 (Figure 3-11). The ΔRCLH strain was included as a negative control, because the genes encoding all structural proteins of the photosynthetic apparatus have been deleted from the chromosome of this strain.

Analysis of photosynthetic proteins revealed that the RC, LH2 and PufX proteins were all present in the wt strains, in contrast to the ΔRCLH and *bchG* strains which lacked detectable amounts of RC, LH2, and PufX proteins (Figure 3-11). The *bchY* mutant strain did have a very small amount of the RC M protein but not any of the other proteins examined (Figure 3-11). This result fits with prior analysis that showed RC M is the most stable of the RC proteins and is capable of existing in the membrane without the other members of the RC (Tehrani & Beatty 2004). Without significant amounts of photosynthetic proteins accumulating, the *bchY* and *bchG* mutants could not assemble a photosynthetic apparatus, and so no further analysis was performed.

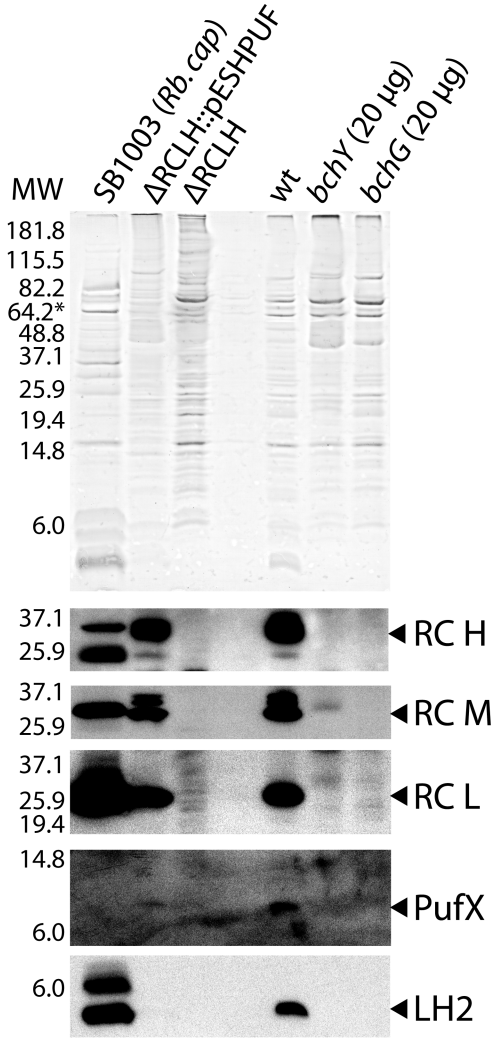

Figure 3-11. Photosynthetic proteins in the *bchY* and *bchG* mutants. Separation achieved on: 4% stacking/10% spacer/16% resolving gel tricine-SDS-PAGE system; then electroblotted onto membrane. Total proteins on the blot were visualized with CPTS stain, and the blot was sequentially probed for proteins with antibodies raised against *Rb. sphaeroides* proteins, except for the LH2 antibody which was raised against *Rb. capsulatus* proteins. Amount of protein loaded in each lane was 10 µg unless otherwise indicated. Membranes isolated from the following strains: SB1003, *Rb. capsulatus* wild type; ΔRCLH::pESHPUF, LH2-knockout; ΔRCLH, *puhA*, *puf*, *puc* deletion; wt, NCIB8253; *bchY*, TB04; *bchG*, TB303.

3.2. Electron transfer and redox properties of the Zn-RC.

To understand how ET occurs in the unusual cofactor arrangement of the Zn-RC, collaborations were established with Mark Paddock (University of California, San Diego), Su Lin, Haiyu Wang, Neil Woodbury, Aaron Tufts, and James Allen (Arizona State University). I helped plan and interpret experiments and purified WT- and Zn-RC. These experiments measured both time-resolved changes in absorption after a laser flash (ET), and redox titrations on the purified Zn-RC complex.

3.2.1. Midpoint potential of the special pair in the Zn-RC.

An important parameter for the driving force of ET in the RC is the special pair (P) redox potential, which contributes to the energy differential between the donating and accepting cofactors in the RC. A redox titration of P_{Zn}/P_{Zn}^{+} in the Zn-RC found the midpoint potential to be +515 ± 5 mV (Figure 3-12), only slightly more positive than the +505 ± 5 mV P_{Mg}/P_{Mg}^{+} midpoint potential in the WT-RC (Lin et al. 1994). The difference between the P_{Zn}/P_{Zn}^{+} midpoint potential of the Zn-RC and that of the WT-RC was only slightly off from what may have been predicted on the basis of the relative potentials of isolated Zn-BChl and Mg-BChl in organic solvents (monomeric axial-coordinated Zn-BChl ΔE^{1}_{Red} is 50 mV more positive than Mg-BChl under the same conditions) (Scheer & Hartwich 1995).

The P_{Zn}/P_{Zn}^{+} redox potential of isolated RC from the Zn-BChl producing *Ac. rubrum* were not available, but titrations against isolated membranes have been done to estimate the midpoint potential of P in this organism. These experiments found the midpoint potential of P_{Zn}/P_{Zn}^{+} in *Ac. rubrum* was +440 mV while those of *Rb. sphaeroides* P_{Mg}/P_{Mg}^{+} was +440-450 mV (Tomi et al. 2007), the relative difference being in close agreement with our result here between the WT- and Zn-RC special pair midpoint potentials. These findings are all consistent with the observation that only a minor increase in the midpoint potential is observed when Zn-BChls serve as the primary donor (P) in place of Mg-BChls.

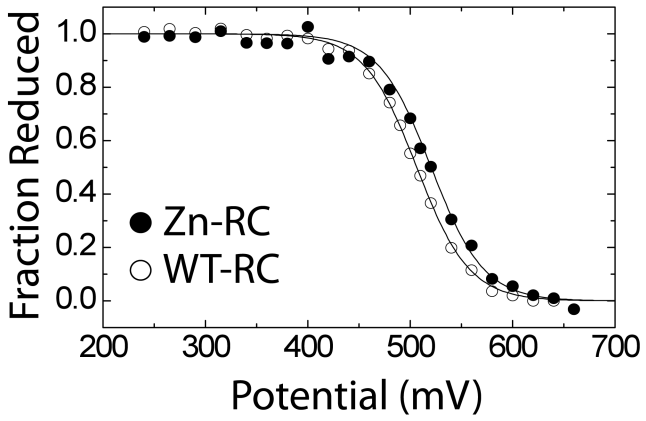

Figure 3-12. Electrochemical titration of WT- and Zn-RCs. The lines are fits to the Nernst equation with n equal to 1. The midpoint for the WT-RC (open circles) is 505 ± 5 mV and for the Zn-RC (filled circles) is 515 ± 5 mV. These values were obtained by averaging the midpoint potentials of five independent measurements of the Zn-RC and three of the WT-RC. For each titration, measurements were performed in both the oxidative and reductive directions to ensure reversibility.

3.2.2. Steady-state light-minus-dark absorption spectra of the Zn-RC.

The light-minus-dark difference absorbance spectrum was measured to examine the photoactivity of the Zn-RC over long time-scales (steady-state) (Figure 3-13). The spectrum showed the bleaching of the P bands at 600 and 855 nm upon formation of the P^+ state. Additionally, a positive band at 790 nm and a negative band at 805 nm resulted from a shift of the B band due to the oxidation of P. These spectral features were very similar to those observed with the Mg-BChl-containing WT-RC (Woodbury et al. 1995). This observation further confirms the assignment of the 600 and 855 nm peaks to P in the Zn-RC steady state absorption spectrum (Figure 3-10), and suggests that ET proceeds all the way from P through the A-branch cofactors to Q_A, producing a long-lived $P^+Q_A^-$ charge-separated state as is observed in the WT-RC (Woodbury et al. 1995). If ET to Q_A were not possible, the charge-separated state would decay too rapidly to be observed in a steady-state light-minus-dark difference spectrum.

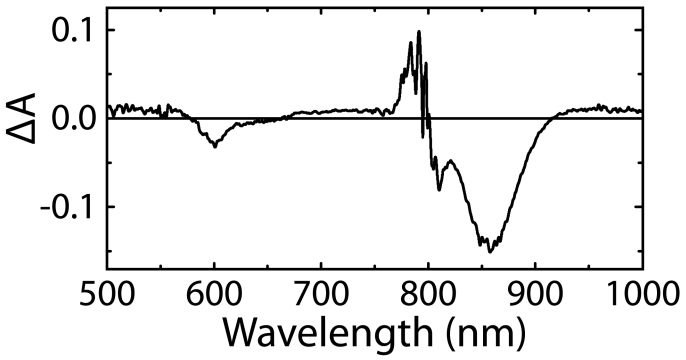

Figure 3-13. Absorption difference spectrum of the Zn-RC under light and dark conditions. The light-minus-dark spectrum of the Zn-RC, represents the P^+ state.

3.2.3. Kinetics of ET in the Zn-RC.

To characterize the primary ET processes following the photoexcitation of P (generating the P* excited state), ultrafast time-resolved absorbance spectroscopy was performed on the Zn-RC at room temperature. The excited state kinetics of $P^* \rightarrow P^+$ transition in the Zn-RC was monitored at 930 nm and compared to those obtained with the WT-RC (Figure 3-14A).

Multiple exponential fitting of the P* kinetics of the WT-RC (Table 3-3) returned three components of 2.8 $\pm$ 0.2 ps (86%) due to formation of $P^+H_A^-$, 10.1 $\pm$ 0.5 ps (18%) due to slow protein responses to catalyze and stabilize the $P^+H_A^-$ state, and a minor non-decaying component (~ 4%) thought to be due to spectral overlap between the P* signal and the P ground state bleaching signal (Lin et al. 1996). The Zn-RC kinetics of P* decay at 930 nm were surprisingly similar to those observed in the WT-RC, showing two dominant decay components of 2.6 $\pm$ 0.2 ps (78%) and 9.8 $\pm$ 0.5 ps (26%), along with a non-decaying component of 4% (Table 3-3). Comparison to the *Ac. rubrum* RC, which binds Zn-BChl, also finds similar kinetics with decay components of 3.3 ps (53%), and 16 ps (13%) (Tomi et al. 2007).

The stability of the charge-separated state ($P^+Q_A^-$) in the Zn-RC was monitored at 840 nm after a laser flash. While the WT-RC showed no recovery of the P^+ band over a 3 ns time scale (Figure 3-14B) because the $P^+Q_A^-$ state lived for thousands of nanoseconds, there was a slight recovery of the P bleaching at 840 nm in the Zn-RC during the same time frame

(Figure 3-14B). Despite this, the recovery was small with a time constant of 130 ps and an amplitude ~ 5% of the total bleaching signal observed (Figure 3-14B).

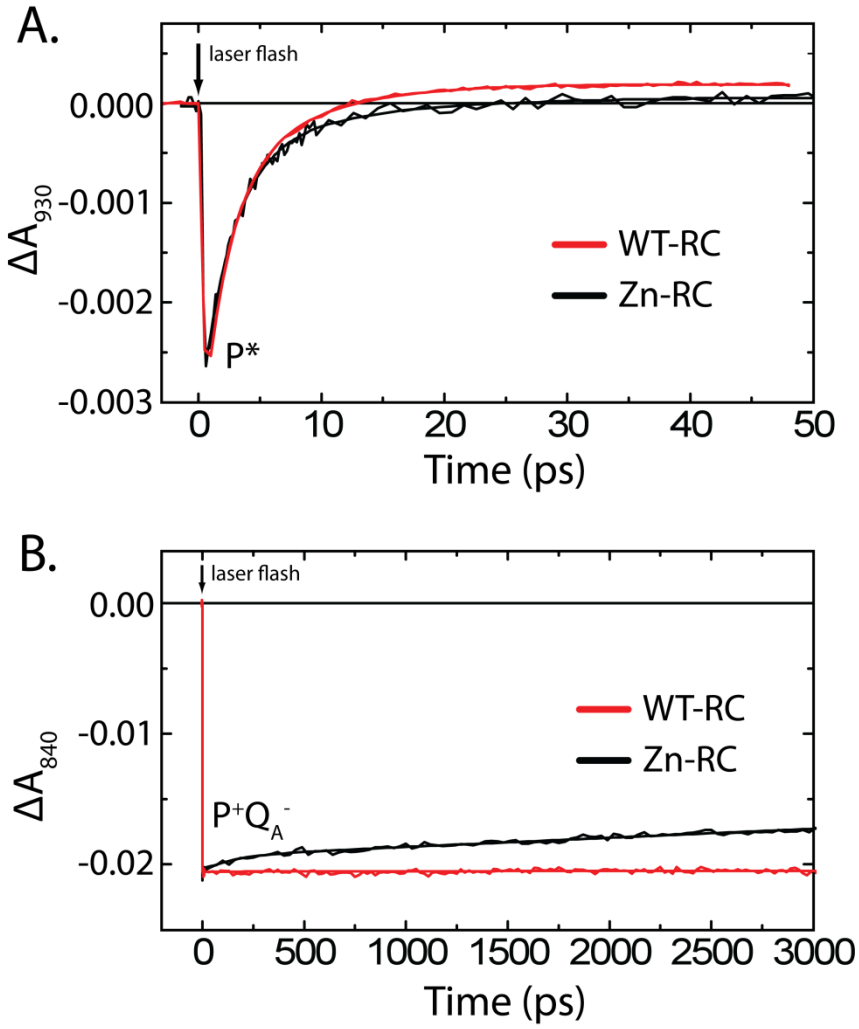

Figure 3-14. Kinetics of the special pair (P) after femtosecond laser excitation at 860 nm. Observed at (A) 930 nm (P*), and (B) 840 nm (P ground state bleaching). The smooth curves were obtained from multiple exponentials fitted to the data. The kinetic traces from the Zn-RC and the WT-RC were normalized at the maximum bleachings. The multiple exponential fitting parameters are listed in Table 3-3.

The slow recovery of the P ground state bleaching in the Zn-RC, in contrast to the dominant 2.6 ps P* decay kinetics, suggests a very high yield of P^+ formation (again similar to the WT-RC) with ~95% of the charge-separated state being stable for at least several nanoseconds. The small amount of P^+ decay on the hundreds of picoseconds time scale

probably reflected a yield loss, likely due to the recombination of $P^+B_A^-$ because it is known that $P^+H_A^-$ recombination is much slower (>1000 ps) (Feher et al. 1989). Nevertheless, there was a small amount of P^+ decay in the 1-3 ns time range that we cannot explain. Although this could in principle be due to recombination of P^+/H_A^-, it is also possible that the purified Zn-RC contained a contaminant that was capable of reducing P^+.

Table 3-3. Multiple exponential fitting parameters for kinetic curves in Figure 3-14.

Kinetics	Measured Wavelength	τ_1, A_1%	τ_2, A_2%	τ_3, A_3%
WT-RC	930 nm	2.8 ps, 86%	10.1 ps, 17.7%	ND, –3.7%
Zn-RC		2.6 ps, 78%	9.8 ps, 26.2%	ND, –4.2%
WT-RC	840 nm			ND, 100%
Zn-RC			130 ps, 5.5%	ND, 94.5%

ND: non-decaying component which has a lifetime more than 100 times longer than the time scales measured. τ_n, A_n% represent the exponential fitting parameters, from the equation for the sum of the three parameters $F(t)=\sum A_n e^{-t/\tau_n}$.

3.2.4. Spectroscopic dissection of the kinetics of H_A versus H_A^- states of the Zn-RC.

To examine the Zn-RC H_A states, light-minus-dark absorption spectrum changes at two time points after a laser flash were recorded (Figure 3-15A). The 15 ps spectral changes represented the $P^+H_A^-$ state with the characteristic bleachings at 560 nm (H) and 600 nm (P), and an absorption increase above 620 nm due to H_A^-, as previously shown for the WT-RC (Lin et al. 2001). The spectrum at 1 ns showed the recovery of the H band (at 560 nm) while the P band bleaching persisted, which was consistent with a $P^+Q_A^-$ spectrum; the absorption >620 nm decreased, indicating the change of $H_A^- \rightarrow H_A$.

The double difference spectrum, calculated by subtracting the 1 ns spectral changes from the 15 ps trace, represented the H_A^- minus H_A spectrum (Figure 3-15B). This spectrum obtained from the Zn-RC was similar to that obtained from the WT-RC (Lin et al. 1996), but with the major absorbance decrease at 560 nm red-shifted by about 20 nm from the WT-RC value, consistent with a change in the H_A cofactor from BPhe to Zn-BChl. These

data also lend further support for my assignment of the Q_X peaks in the low-temperature spectra in Section 3.1.9.

To further investigate ET processes involving H_A, the kinetics of absorbance changes at 560 nm and 660 nm in the Zn-RC were measured (Figure 3-16A and B). The kinetic trace at 560 nm represented bleaching of the Zn-BChl in the H_A site, whereas the kinetics at 660 nm reflected the formation and decay of H_A^-. The traces at both wavelengths could be adequately fitted by a 3 ps component corresponding to the formation of $P^+H_A^-$; a 250 $\pm$ 25 ps recovery likely due to the ET from H_A^- to Q_A; and a non-decaying component on the time scale measured, attributed to the long-lived P^+ state. The Zn-RC time constants were, again, very similar to those observed from the WT-RC (Lin et al. 1996).

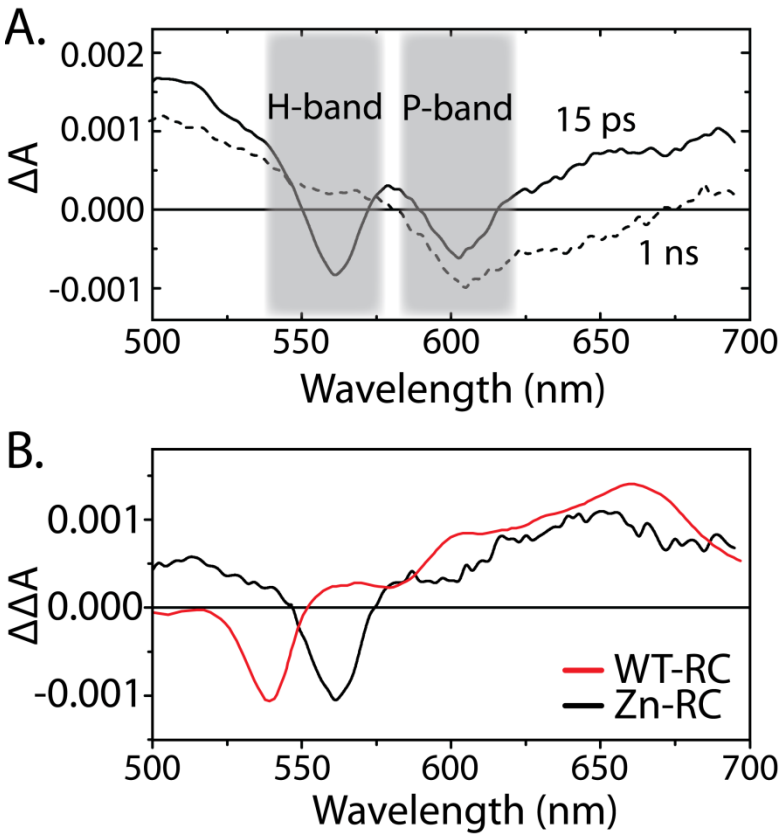

Figure 3-15. Q_X transition time-resolved absorption difference spectra reveal $P^+H_A^-$ and $P^+Q_A^-$ states of the Zn-RC. (A) Time-resolved absorbance changes in the Q_X wavelength region of the Zn-RC recorded at 15 ps (solid line, $P^+H_A^-$), and 1 ns (dashed line, $P^+Q_A^-$) after laser excitation. Traces were obtained by subtracting the dark spectrum from the illuminated spectrum, such that light-dependent bleaching is shown as negative absorption. (B) Double difference spectrum of WT- and Zn-RC. Calculated by subtracting 1 ns trace from 15 ps trace.

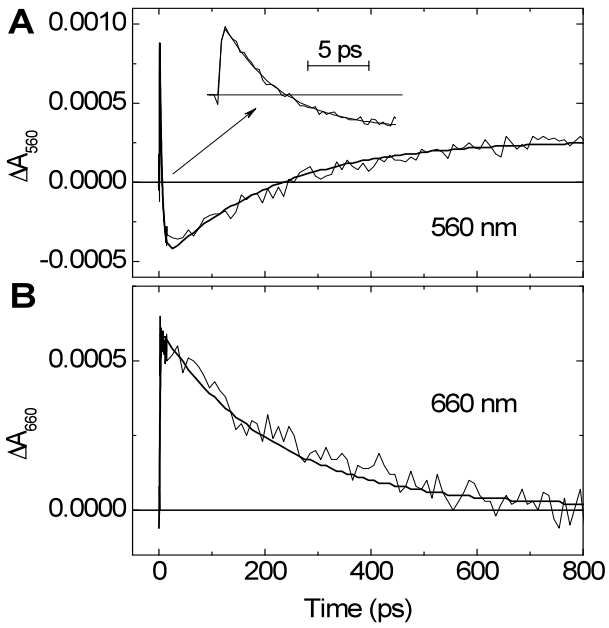

Figure 3-16. Kinetics of absorption changes in H_A after laser excitation of the Zn-RC. Observed at (A) 560 nm (appearance and decay of H_A), (B) 660 nm (appearance and decay of H_A^-). The smooth curves were obtained from multiple exponential fitted to the data. The inset in panel A gives the absorption changes over the first 15 ps plotted on an expanded time scale.

3.3. Photosynthetic growth potential of the *bchD* mutant.

3.3.1. Relative amounts of photosynthetic complexes and BChl in the wt and *bchD* strains.

Despite being able to synthesize Zn-BChl, assemble it into the RC, LH1 and LH2 complexes, and with the knowledge that the Zn-RC could transfer electrons with near WT-RC efficiency, it was not immediately clear why the *bchD* mutant was unable to grow photosynthetically. To understand the reasons behind these remaining questions, potential limiting factors to photosynthetic growth were investigated.

Photosynthetic growth in *Rb. sphaeroides* is dependent on the RC complex because this is where photon-driven charge separation is converted to the chemical intermediate that holds the energy in a form useable for growth. Mutants of *Rb. sphaeroides* that only contain the RC complex are able to grow photosynthetically under low-light conditions but at a reduced rate to those that contain both RC and LH1, although under high-light their growth is indistinguishable from wt cells (Jones et al. 1992). These mutants

synthesize an amount of RC equivalent to wt, and so the growth defect is believed to be from loss of stabilization of the RC charge separated state or less efficient photon capture when the LH1 ring that surrounds the RC is absent (Francia et al. 2004) (see Figure 1-1). The LH2 complex is mainly an antenna that increases the effective surface area of the cell used to capture photons, conducting them toward the RC-LH1 core-complex, and is dispensable for growth under high-light conditions (Tehrani 2003).

Levels of the assembled photosynthetic apparatus complexes LH1 and LH2 were quantified from membrane scans of semiaerobically grown cells to see if low levels were limiting photosynthetic growth potential. The low oxygen levels in the culture during this growth mode induced the photosynthetic machinery similarly to what would occur under purely anaerobic photosynthetic growth conditions, but allowed enough respiration to occur such that *Rb. sphaeroides* did not require energy from photosynthesis to grow. In fact, knockout strains with all the RC, LH1 and LH2 genes removed from the chromosome will grow with near wt rates semiaerobically but are totally unable to grow photosynthetically (Tehrani 2003). These measurements detect the complexes that contain both protein and BChl, as opposed to the previous protein measurements that only detected protein levels (Figure 3-2).

Analysis of membranes from the *bchD* strain cells showed that they develop only a tiny fraction of the LH1 and LH2 complexes that the wt strain does under semiaerobic growth conditions (Figure 3-17A and B). The *bchD* mutant membranes showed only 3.4% of LH2 and 9.1% of LH1 complexes relative to the wt strain. These values were similar to the relative amounts of total BChls, about 5.9% Zn-BChl in the *bchD* mutant compared to Mg-BChl in the wt. Unfortunately, membrane absorption spectroscopy could not directly quantify the relative amount of RC complexes between the wt and *bchD* mutant strains because the RC absorption peaks were hidden by the LH peaks. But, since the RC and LH1 complexes assemble in a fixed ratio, it is possible to estimate the amount of RC from the amount of LH1. This analysis revealed only 12.5% Zn-RC complex levels in the *bchD* mutant compared to wt RC levels (Figure 3-17A). Although the amount of BChls as measured by deconvolution of membrane complexes was significantly greater than the total BChl measured by extracting membranes with acetone/methanol, there appeared to be a systematic error that was consistent for both wt and *bchD* strains (Figure 3-17A). This

was shown by the nearly identical ratios between wt and the *bchD* mutant total BChls as determined by deconvolution of membrane scans versus direct measurement of BChls from extracted membranes (Figure 3-17B).

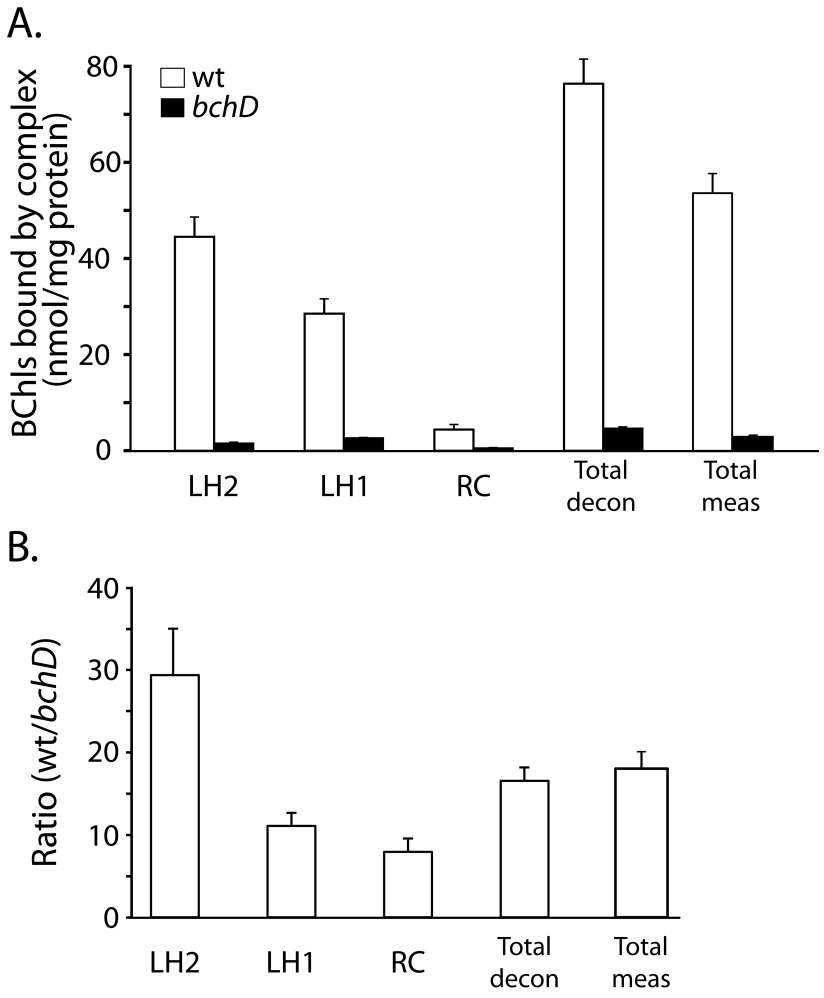

Figure 3-17. Comparison of photosynthetic apparatus assembly and BChl content of wt and *bchD* membranes. (A) LH1, LH2, and RC assembly. Amounts of LH determined by absorption spectra of membranes using LH2 and LH1 peaks. Total decon, BChl sum of LH2, LH1 and RC components calculated from deconvolution; Total meas, amount of BChl measured from membranes extracted with acetone/methanol. (B) Ratio (wt/*bchD*) of BChls calculated for each complex from part (A) above.

The amounts of LH and RC complexes and total Zn-BChl measured from membrane absorption and extraction, as a percentage of wt, were less than the RC proteins (12 to 46% of the wt levels) and LH proteins (14 to 52% of the wt levels) would allow (see Figure 3-2). Thus, it appeared that the production of Zn-BChl was the limiting factor in the

assembly of LH and RC complexes in *bchD* mutant cells. Based on the low photosynthetic apparatus amounts, it would seem likely that some minimal threshold of RC and LH complexes necessary for photosynthetic growth had not been reached in the *bchD* mutant.

3.3.2. Effect of LH2 loss on *bchD* mutant.

Since there was a limited pool of Zn-BChl in the *bchD* cells available for assembly with the RC, LH1 and LH2 complexes, one way to increase the amount of Zn-BChl available for the RC and LH1 complexes was to eliminate the LH2 complex, shown above to bind one-third of the total Zn-BChl (Figure 3-17A). It was hoped that this would increase the amount of the Zn-RC past minimal levels needed for photosynthetic growth.

An additional reason for removal of the LH2 complex comes from analogy of the *bchD* mutant with the only other species known to make Zn-BChl and assemble it with its photosynthetic apparatus; *Ac. rubrum* contains RC and LH1 proteins homologous to *Rb. sphaeroides'* but does not contain the LH2 complex, an absence shared by nearly all the bacteria in the α-1 proteobacterial phylogenetic group of *Ac. rubrum* (Hiraishi & Shimada 2001; Paulsen 2006). In contrast, the α-3 proteobacteria, to which *Rb. sphaeroides* belongs, usually contain the LH2 complex. Perhaps some feature of the LH2 complex assembled with Zn-BChl actually hindered photon capture, or some other process in energy transduction? Could this be why no LH2-containing species has been seen before with a Zn-BChl containing photosynthetic apparatus? Such a situation exists for the artificially synthesized Ni-BChl when assembled with LH1 complexes for *Rb. sphaeroides,* where it acts as a 'black hole', trapping and dissipating excitation energy faster than it can be transferred to the RC (Paulsen 2006).

Instead of knocking out the LH2 genes (*pucBA*) in the existing *bchD* strain, a *bchD* knockout in a previously made Δ*puhA*/Δ*puc* deletion strain ($RC^{-}LH1^{+}LH2^{-}$) was created (Adelroth et al. 2001). This was done by introduction of a suicide vector carrying the *bchD* gene disrupted by the Ω cartridge.

The absorption spectrum of the parental Δ*puhA*/Δ*puc* strain membrane fraction showed a major peak at 875 nm due to the LH1 complex, and a small peak at 771 nm due

to free Mg-BChl. In contrast, the Δ*puhA*/Δ*puc*/Δ*bchD* strain showed a major peak at 863 nm due to LH1, and blue-shifted by 12 nm from the wt complex (Figure 3-18A). The LH1 complex bound with Zn-BChl could now be resolved better than in the original *bchD* mutant, which had an LH2 peak at 836 nm obscuring the LH1 absorption peak at 863 nm. This result indicated that the Ω–cartridge insertion into the *bchD* gene had caused the same Zn-BChl production phenotype as the original Tn5 transposon mutant (*bchD*), and this strain lacked the LH2 and RC complex.

The recapitulation of the Zn-BChl production phenotype in the Δ*puhA*/Δ*puc*/Δ*bchD* strain using the targeted pNHG1::*bchD*Ω construct lent support to the mapping of the Tn5 in the original *bchD* mutant to the *bchD* gene (Coomber et al. 1990). Furthermore, single-crossovers examined during the generation of the Δ*puhA*/Δ*puc*/Δ*bchD* strain, possessing one wild type and one mutant copy of the *bchD* gene, had wt strain Mg-BChl biosynthesis phenotypes, indicating that the *bchD* mutation was recessive. This genetic relationship seems to indicate that the truncated *bchD* protein was not able to affect Mg-chelatase activity in the cell.

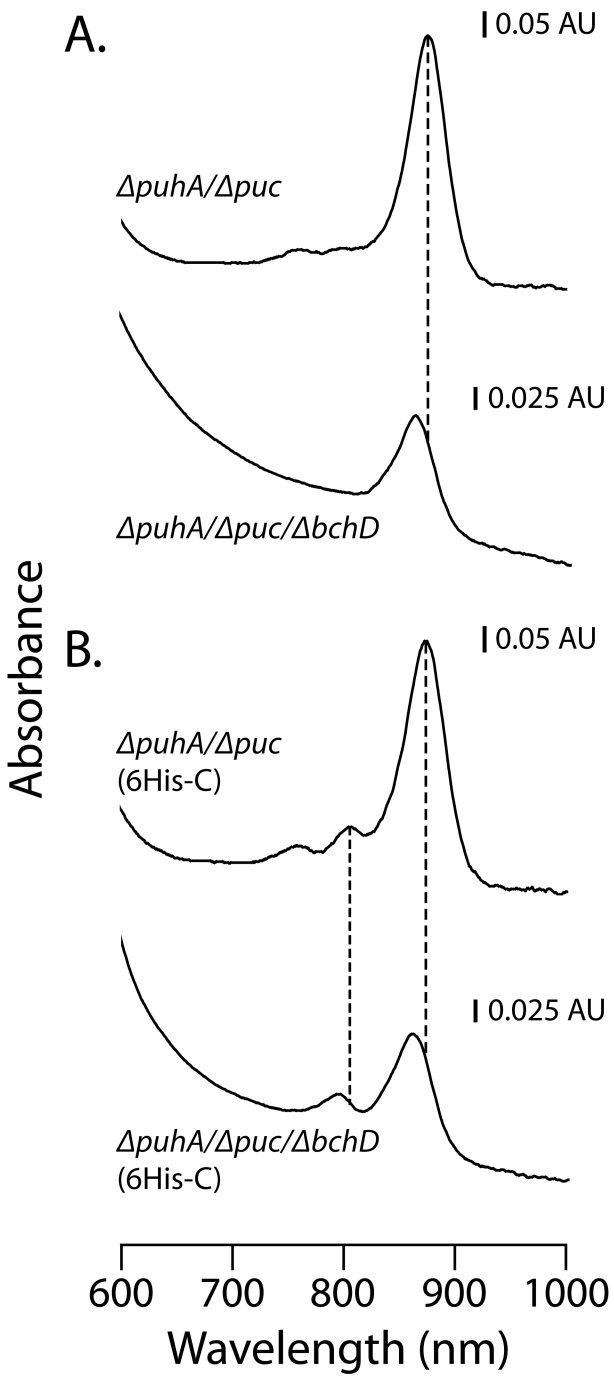

Figure 3-18. Membrane absorption spectra of *puhA*/*puc* and *puhA*/*puc*/*bchD* strains. (A) Strains with LH1 complex only. Strains lack both LH2 and RC complex. (B) Strains with RC and LH1 complexes. p6His-C, low-copy plasmid containing the *puhA* gene under control of the native *Rb. sphaeroides puc* operon promoter. Dashed lines indicate wavelengths of wt RC (804 nm) and LH1 (875 nm) complexes.

The addition of the p6His-C plasmid (and hence the *puhA* gene encoding the RC H protein) to the Δ*puhA*/Δ*puc*/Δ*bchD* strain generated the Δ*puhA*/Δ*puc*/Δ*bchD*(p6His-C) strain with an $RC^{+}LH1^{+}LH2^{-}$ phenotype. The Zn-RC was now able to assemble and the characteristic absorbance peak at 794 nm from the accessory BChls could be seen in the membrane absorption spectra (Figure 3-18B), blue-shifted from the parental strain. From the membrane spectra normalized to A_{650} and taking into account the lower extinction coefficient of Zn-BChl, Δ*puhA*/Δ*puc*/Δ*bchD*(p6His-C) had only 22% of the LH1 peak height of the parental Δ*puhA*/Δ*puc*(p6His-C). The RC peaks looked similar in height, but both were so small and overlapping with the LH1 peak as to make comparison difficult. The absorption spectrum of Δ*puhA*/Δ*puc*/Δ*bchD*(p6His-C) now resembled that of *Ac. rubrum* very closely (Wakao et al. 1996), although with much lower amounts of LH1. Despite these promising spectra, growth experiments again showed that the *bchD* phenotype strain Δ*puhA*/Δ*puc* /Δ*bchD*(p6His-C) could not grow photosynthetically (data not shown).

3.3.3. The effect of oxygen and light on *bchD* mutant growth.

To evaluate the possibility of photoactive species inhibiting the growth of the *bchD* mutant in the presence of light, I compared the number and appearance of CFUs spread on plates that were grown aerobically in the light and dark for both the wt and *bchD* mutant strains.

The results of three experiments were first analyzed to see if the data was normally distributed. All three data sets did not satisfy the conditions of the Kolmogorov-Smirnov one-sample normality test (Smirnov 1939) and were therefore subsequently analyzed with the non-parametric two-independent sample Wilcoxon rank sum test which did not assume normality of the data (Mann & Whitney 1947; Stephens 2004). This test showed no significant difference in number of CFUs between the light and dark conditions at α=0.05 (two-tailed) for the wt and *bchD* mutant strains (Appendix III). These results indicated that the possibility of damaging photoactive species accumulating within the wt or *bchD* mutant strains under these conditions seemed unlikely.

Qualitatively, the colonies for both the wt and *bchD* mutant strains grown in the light were smaller than those grown in the dark, indicating that there could be some

oxidative stress caused by growth in the light in the presence of full aeration (recall that growth in the light is usually anaerobic), but this effect was not more pronounced in one strain over the other.

3.3.4. The adaptation of blue-native polyacrylamide gel electrophoresis for use with *Rb. sphaeroides*.

Although photosynthetic apparatus levels in the *bchD* mutant were much lower than in the wt strain, ALA-synthase mutants have shown that photosynthetic growth is possible with comparably low amounts of photosynthetic apparatus (Neidle & Kaplan 1993). This suggested that perhaps the physical association of the LH2, LH1 and RC complexes in the *bchD* mutant had been disrupted, and was preventing their cooperative activity to enable photosynthetic growth. Several available methods to study the photosynthetic apparatus superstructure in a native context already existed.

Early work searching for a method of mildly denaturing electrophoresis to study pigment protein complexes from *Rb. sphaeroides* resulted in development of lithium-dodecyl sulfate electrophoresis at low temperatures as a gentle way to separate intact protein complexes from *Rb. sphaeroides* while still retaining resolution similar to SDS-PAGE. These efforts met with some success as various oligomeric complexes of LH1 and LH2 were resolved, as well as a partially denatured RC particle containing only the RC L and M proteins (Broglie et al. 1980; Hunter et al. 1988). Free pigment was seen to migrate on the gel system and therefore some destruction of complexes occurred during the run. Since their development, these methods have not been widely adopted by the *Rb. sphaeroides* research community, possibly because of their limited utility with regards to separation of other membrane complexes (such as cytochrome bc_1 and the ATPase).

More recently, the technique of blue-native polyacrylamide electrophoresis (BN-PAGE) has been used in plant and algae systems to analyze membrane protein assembly and structure under non-denaturing conditions (Kugler et al. 1997; Rokka et al. 2005). I decided to adapt the BN-PAGE system for use with *Rb. sphaeroides* so that I could analyze the structure of the intact *bchD* mutant photosynthetic apparatus in an attempt to discover why the cells could not grow photosynthetically. The wt strain was used initially

because it expresses 10-fold greater amounts of photosynthetic complexes than the *bchD* mutant, and would ensure the highest chance of success with this technique.

Two different detergents were tried initially to solubilize the ICM. Titration of dodecyl maltoside (DDM) and octyl-β-D-thioglucopyranoside (OBTG) showed that both would solubilize membranes, but that they had several key differences in their effective concentration, as well as in the complexes that they solubilized (Figure 3-19). DDM solubilized well at low concentrations and started producing dissociation products (for example, in Figure 3-19, a band appeared below the red band at 242 kDa at 2.00% DDM and greater) only at very high detergent concentrations (Figure 3-19A). OBTG did not solubilize well at low concentrations and had a very narrow range of action before bands became distorted (Figure 3-19B). I decided that 1.50% DDM gave the best compromise between solubilization of multiprotein complexes (MPC) and disruption of larger complexes that I wanted to separate and visualize. This concentration was used for all following experiments. The difference in the ability of DDM and OBTG to solubilize MPCs has been seen in similar empirical analyses of other systems (Reisinger & Eichacker 2007).

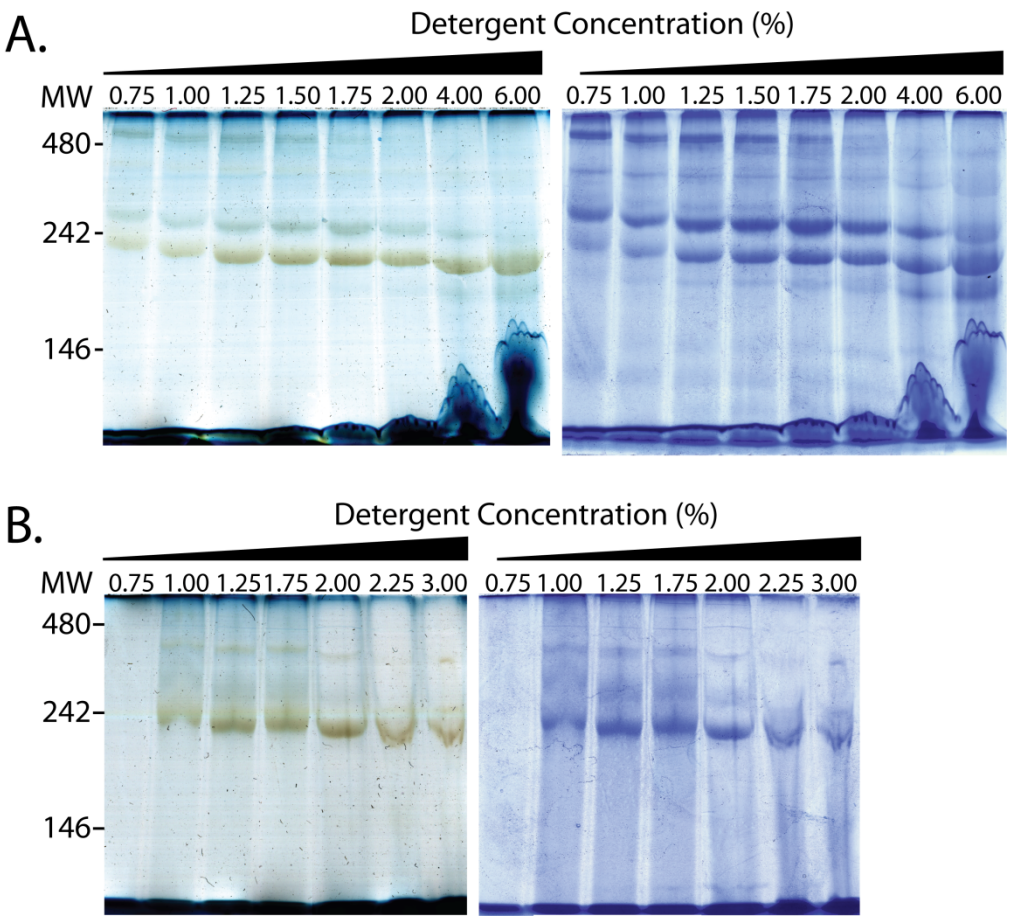

Figure 3-19. Titration of DDM and OBTG detergents shows different solubilization characteristics of *Rb. sphaeroides* ICMs on BN-PAGE. (A) DDM, (B) OBTG. Left gel, after electrophoresis and methanol fixing (showing pigments); right gel, after Coomassie stain. Gels were 3.5% stacking/6% resolving. MW, molecular weight marker (kDa). 100 μg membrane protein loaded per lane.

Next, I wanted to discover the identity of the MPCs represented by the bands on the gels. To do this I ran membranes from the wt strain alongside that of an LH2-knockout strain (ΔRCLH::pESHPUF), which would help me to resolve which bands were due to the LH2 complex. As a second method of band identification, I excised several bands of interest from the gel and then performed absorption spectroscopy directly on the MPCs *in situ* to identify those that contained photosynthetic complexes by their distinctive absorption spectra. The results of this multi-pronged analysis showed that five bands in the wt strain and two in the ΔRCLH::pESHPUF strain contained MPCs that had absorption spectra that matched photosynthetic complexes (Figure 3-20). There appeared to be at

least three forms of LH2, corresponding well to predicted masses for a trimer (297 kDa) and dimer (198 kDa) complex. The smallest form of LH2 on the gel (band 5) was too large to be the monomer (99 kDa). The RC-LH1-PufX core-complex was seen in both strains and the migrations seemed to correspond to dimer (503.4 kDa) and monomer forms (251.7 kDa).

In another approach to assigning bands on the BN-PAGE gels to different photosynthetic MPCs, I performed a first dimension separation on BN-PAGE followed by a second dimension denaturing separation on tricine-SDS-PAGE. Proteins from the second dimension were transferred to a membrane and probed with antibodies against various photosynthetic proteins. The RC-LH1-PufX core complex had both a monomer and dimer form, and revealed that both contained the PufX protein (Figure 3-21). RC proteins associated with the core-complex MPCs, but the LH2 proteins did not. The LH2 dimer band migrated just below the RC-LH1-PufX monomer. Furthermore, the 'naked' RC (no LH1) could be seen at the bottom of the first dimension gel in both the wt and ΔRCLH::pESHPUF. The PufX and LH2 proteins were not associated with this form of the RC complex. No photosynthetic proteins could be seen in the ΔRCLH strain, as expected, because it contains deletions in the *puhA, pufQBALMX*, and *pucBA* genes, which code for the RC, PufX, LH1, and LH2 proteins. The LH2 proteins were confined to only one band in the wt strain, but this may have been due to variation in the solubilization process in this experiment, which seems to have abolished the trimer form of the LH2 complex seen above in Figure 3-20. Furthermore, the LH2 antibody used was raised against the closely related *Rb. capsulatus* proteins and as a result only cross-reacted with the smaller β subunit of the *Rb. sphaeroides* proteins.

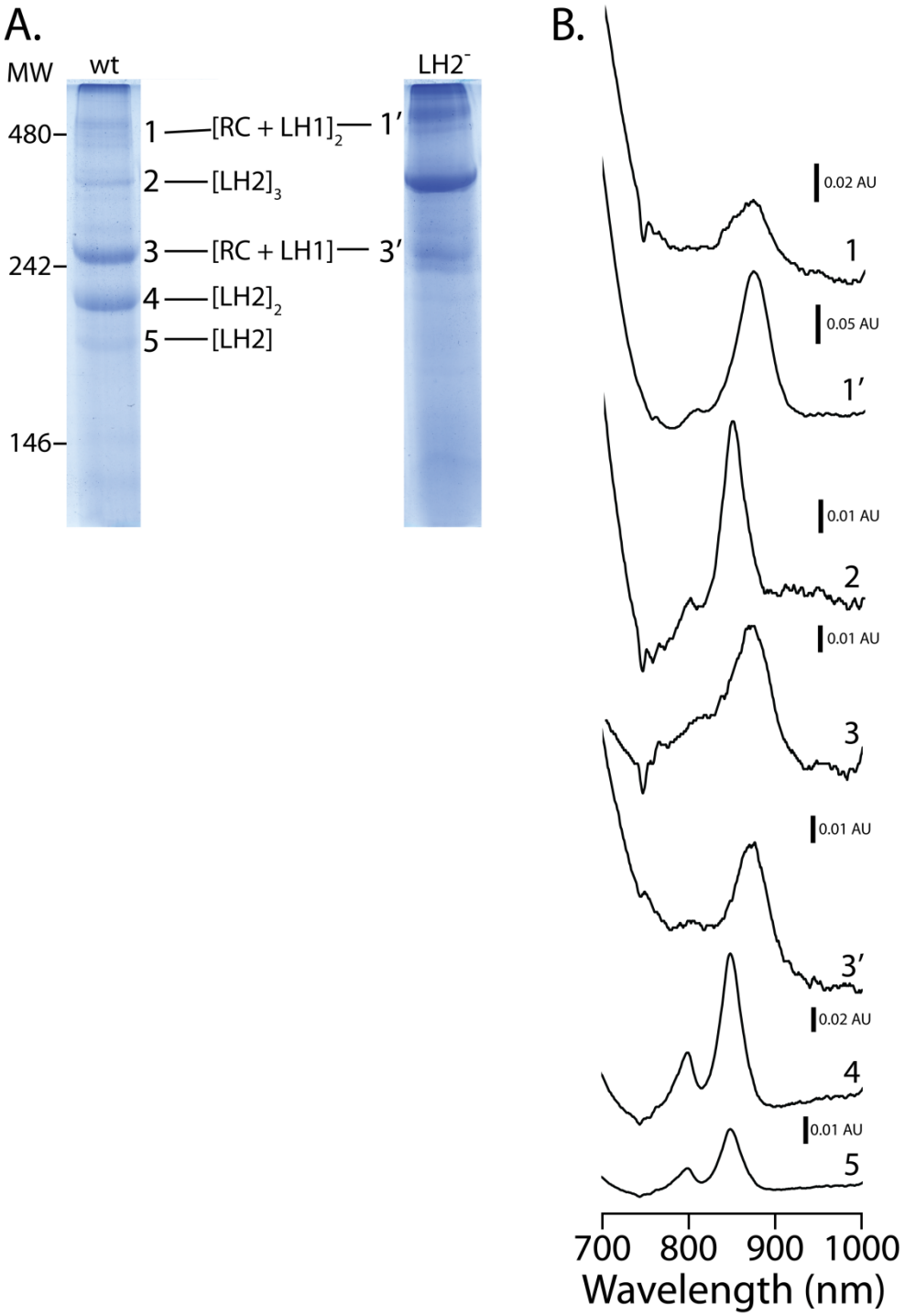

Figure 3-20. Separation of MPCs of wt and ΔRCLH::pESHPUF (LH2$^-$) and identification through *in situ* absorption spectroscopy. (A) BN-PAGE (3.5% stacking/6% resolving) separation of solubilized MPCs from membranes of wt and ΔRCLH::pESHPUF strains. (B) Absorption spectroscopy analysis of excised bands from part (A). Thin bands were excised at regular intervals from the top of each lane to the 146 kDa marker, but only bands that exhibited absorption spectra similar to known photosystem complexes are indicated. 100 μg membrane protein loaded per lane.

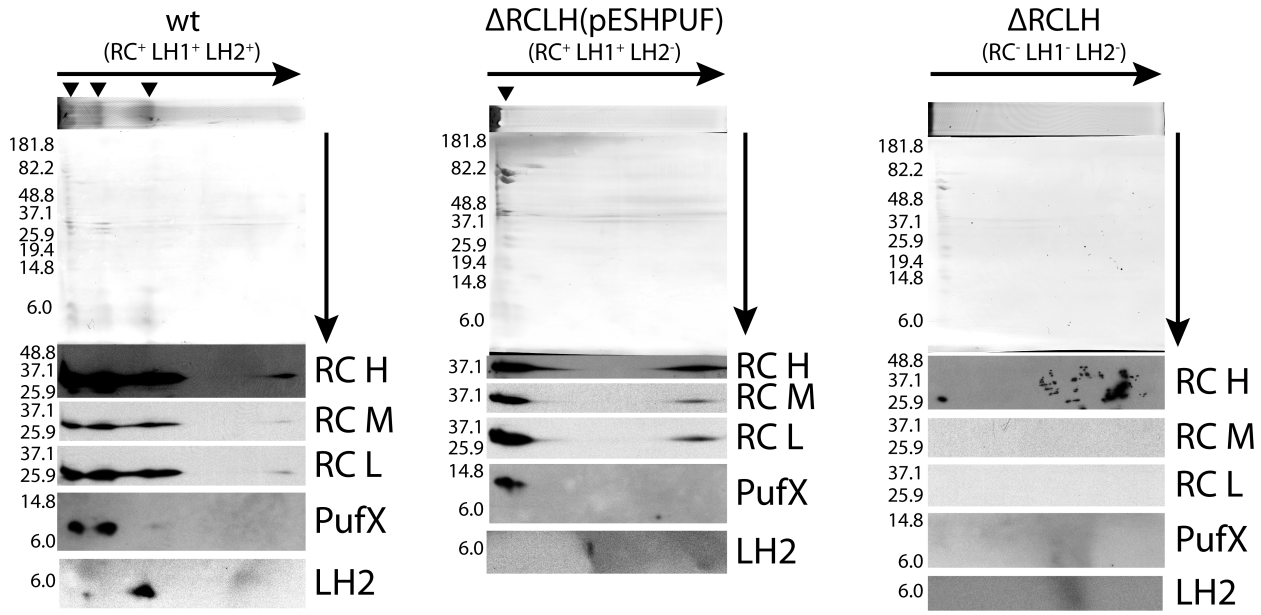

Figure 3-21. Two-dimensional separation of MPCs from membranes of *Rb. sphaeroides* strains that lack LH2 and that lack the RC, LH1 and LH2 complexes. For each strain a first-dimension separation on BN-PAGE (stacking 3.5%/resolving 6%) was followed by lane excision, incubation in 1% SDS/1% mercaptoethanol, and then layering over a second tricine-SDS-PAGE gel (stacking 4%/resolving 13%) at a right angle. Following the second dimension separation the gel was transferred to a nitrocellulose membrane and stained for total protein. Panels below represent serial probing of membrane with antibodies raised against the indicated proteins. ▼, identified MPC bands in first dimension gel. Arrows indicate direction of electrophoretic migration for each dimension. 100 μg solubilized membrane protein loaded per first dimension lane.

These results fit well with a recently published paper that took the same BN-PAGE techniques shown here and extended them by adding mass spectrometry (D'Amici et al. 2010). Their findings agree with my own, as the authors visualized and located the RC-LH1-PufX core-complex monomer and dimer, and several oligomeric forms of LH2. Additionally, they found the 'naked' RC complex migrating to a similar location on the gel as I did (Figure 3-21). With the aid of mass spectrometry they were also able to identify non-photosynthetic MPCs, such as the ATPase and cytochrome bc_1 complex. Additionally, they utilized a related technique to BN-PAGE, called clear-native polyacrylamide gel electrophoresis, which separates complexes using only their intrinsic charge, without the

addition of Coomassie dye. These techniques seem to hold much promise for studying photosynthetic complexes in *Rb. sphaeroides*.

One application of the BN-PAGE system that the work in this thesis extended beyond others was the identification of RC-LH1-PufX core-complex assembly in the absence of the LH2 complex. As seen on the gel in Figure 3-20 the RC-LH1-PufX core complex did not seem to be perturbed by the loss of the LH2 complex, although a band containing unidentified proteins migrating at 395 kDa became much more abundant than in the wt strain. This change in abundance could have been due to the difference in the composition of the membranes separated on the gel. The ΔRCLH::pESHPUF strain, which lacks LH2, forms tubular and less differentiated ICMs than the wt strain (Chory et al. 1984; Kiley et al. 1988). As a result, the membrane samples isolated from the ΔRCLH::pESHPUF strain could have an increased proportion of cytoplasmic membrane contaminants, not normally found in ICM preparations. This would have caused an increase in the amounts of MPCs in the ICM preparations that are normally found in the cytoplasmic membrane (Geyer & Helms 2006; Tucker et al. 2010). Unfortunately, project priorities did not allow the *bchD* mutant membranes to be analyzed during the time-frame of this thesis.

3.4. Characterization of the zinc-bacteriochlorophyll biosynthetic pathway

After my initial discovery that the *bchD* mutant could make Zn-BChl I set out to uncover the biosynthetic pathway of this rare chlorophyll. Only one other group of bacteria, members of the genus *Acidiphilium*, are known to synthesize and use Zn-BChl, and they do so through a mechanism that makes normal Mg-BChl, somehow removes the metal to generate BPhe, and then inserts Zn^{2+} (Hiraishi & Shimada 2001; Masuda et al. 1999). I suggested that the mechanism in the *Rb. sphaeroides bchD* mutant was likely different than that used by *Ac. rubrum* because the *bchD* mutation, which knocked out one of the key components of the Mg-chelatase complex necessary for function (Gibson et al. 1995), precluded the synthesis of Mg-BChl to be converted into BPhe and then Zn-BChl. Instead, I hypothesized a "Zn-early" pathway, with Zn^{2+} introduced into PPIX, to generate Zn-PPIX.

Although the *bchD* gene was disrupted in the *bchD* strain, the *bchH* and *bchI* genes were not. Evidence from a *Chlamydomonas CHLH*-disrupted strain showed that the BchD-

and BchI-homologous ChlD and ChlI proteins were expressed to similar levels as in wild type cells, although the enzymes were not assayed for function (Chekounova et al. 2001). Experiments on the *Rb. sphaeroides bchHID* genes expressed in *E. coli* showed no Mg-chelatase activity without the *bchD* gene product present in the assay (Gibson et al. 1995). Importantly, there was no trace of Zn-PPIX created from assays containing only the *bchH* and *bchI E. coli* lysates, which presumably contained Zn^{2+}. Although this observation was not proof, it provided *in vitro* evidence that the Mg-chelatase remnant structure was unlikely to carry out Zn^{2+} chelation. Because Zn-PPIX has been observed in organisms lacking the Mg-chelatase, such as yeast, rats and humans (Jacobs et al. 1998; Labbe et al. 1999; Pretlow & Sherman 1967), this pointed to another source for the molecule.

Ferrochelatase seemed to be a likely candidate to catalyze Zn^{2+} chelation because it had been known for some time that *Rb. sphaeroides* ferrochelatase, given favorable conditions *in vitro*, inserted Zn^{2+} into PPIX at approximately 75% the rate of Fe^{2+}insertion (Neuberger & Tait 1964). I hypothesize that once Zn-PPIX is generated in the *bchD* mutant strain, its similarity to Mg-PPIX, which is normally produced in the wt, allows it to be a substrate for the subsequent enzymes in the BChl-biosynthetic pathway. This process would then funnel Zn-containing intermediates all the way through the remaining enzymes of the BChl-biosynthetic pathway (see Figure 1-5 and Figure 1-6), resulting in Zn-BChl instead of Mg-BChl.

3.4.1. Analysis of porphyrins in the wt and *bchD* mutant strain.

I examined *bchD* cells to see if a pool of Zn-PPIX that could be used for Zn-BChl biosynthesis could be detected. Since no Zn-PPIX can be detected in wt *Rb. sphaeroides* cells (Masuda et al. 1999), finding this molecule in the *bchD* mutant would support the early addition of Zn^{2+} model of the pathway. I isolated a crude preparation of metalloporphyrins from wt and *bchD* cells by extracting with a 9/1 mixture of acetone/0.1 N NH_4OH, followed by washing with hexane to remove the carotenoids, and extracting the remaining fraction with ether (Rebeiz 2002). The ether fraction was analyzed by absorption and fluorescence spectroscopy versus authentic Mg- and Zn-PPIX standards.

This analysis showed that the wt strain contained metalloporphyrins that had spectral characteristics resembling those of Mg-PPIX, whereas metalloporphyrins in the *bchD* mutant resembled Zn-PPIX (Figure 3-22A). The wt extract exhibited a major absorption peak at 418 nm and smaller 553 nm and 590 nm peaks characteristic of Mg-PPIX. However, the *bchD* mutant extract yielded peaks blue-shifted from those of the wt and matching Zn-PPIX, with a 414 nm absorption peak and smaller 543 nm and 582 nm peaks. The fluorescence spectra of the ether extracts confirmed the results of the absorption spectra: excitation at 418 nm produced unique emission patterns for both extracts, 595 nm for wt and 589 nm for the *bchD* mutant strain. These spectral characteristics closely matched the corresponding Mg- and Zn-PPIX standards with 596 nm and 588 nm emission maxima, respectively (Figure 3-22B).

This simple experiment highlighted the difference between the wt and *bchD* mutant strains: all other *Rb. sphaeroides* strains studied to date accumulated Mg-PPIX rather than Zn-PPIX in their cells. Since Mg- and Zn-PPIX have nearly identical absorption spectra to their structural derivatives, such as the monomethyl ester, HPLC separation was used to further narrow down the identity of the components in the crude extraction.

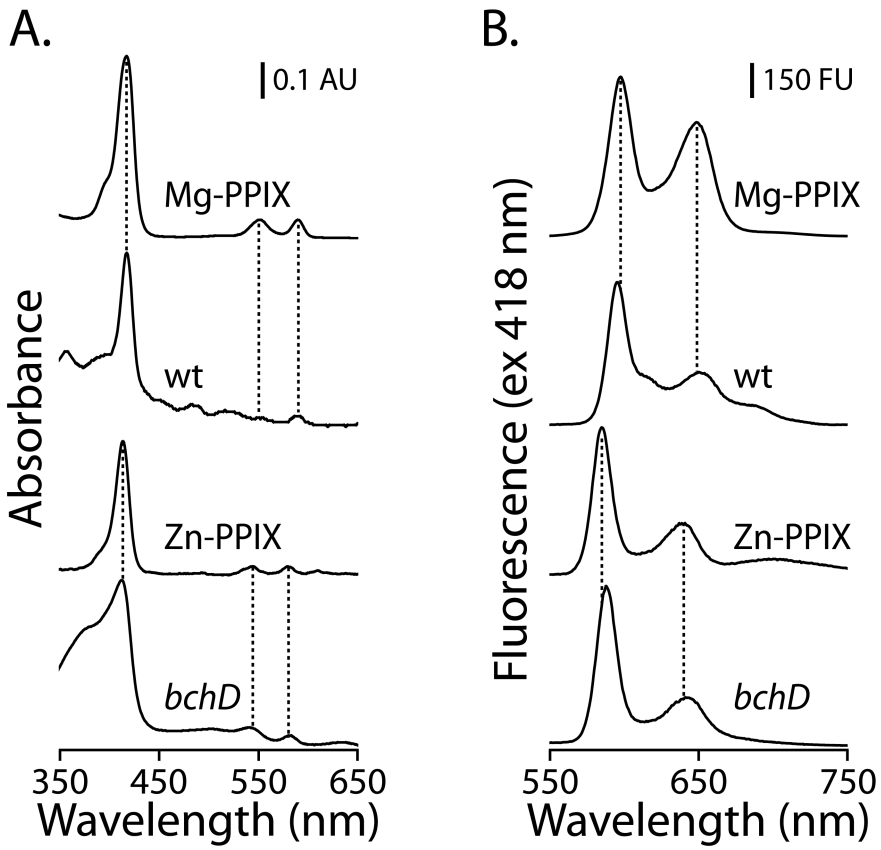

Figure 3-22. Spectral characteristics of crude porphyrin extractions from wt and *bchD* mutant. (A) Absorption spectra of extracts and authentic standards in ether. (B) Fluorescence emission spectra of extracts and authentic standards in ether, excited at 418 nm. Dotted lines highlight peaks with similar wavelength maxima between spectra.

3.4.4. Isolation and identification of the Zn-BChl biosynthetic pathway intermediate Zn-protoporphyrin IX monomethyl ester.

With the knowledge that there was a pool of Zn-PPIX in the *bchD* mutant analogous to the Mg-PPIX pool normally seen in the wt strain (Masuda et al. 1999), isolation of the second intermediate of the BChl-biosynthetic pathway in the *bchD* mutant became a goal of the project, to see if it contained Zn^{2+} rather than Mg^{2+}. To accomplish this I separated crude ether extracts on HPLC to confirm the identities of the metalloporphyrins by comparison to authentic standards.

The results of this HPLC separation showed that the wt strain extract contained Mg-PPIX and a metalloporphyrin with 3.1 min longer retention time (Figure 3-23A, top two traces). The longer retained molecule has been shown to be magnesium-protoporphyrin

IX monomethyl ester (Mg-PPIX-MME) (Masuda et al. 1999), the product of the second enzyme in the BChl biosynthetic pathway. In contrast, the *bchD* mutant extracts contained two species, one with a retention time that matched that of Zn-PPIX, confirming the presence of this compound in *bchD* cells, and a second with a 2.1 min longer retention time (Figure 3-23A, bottom two traces).

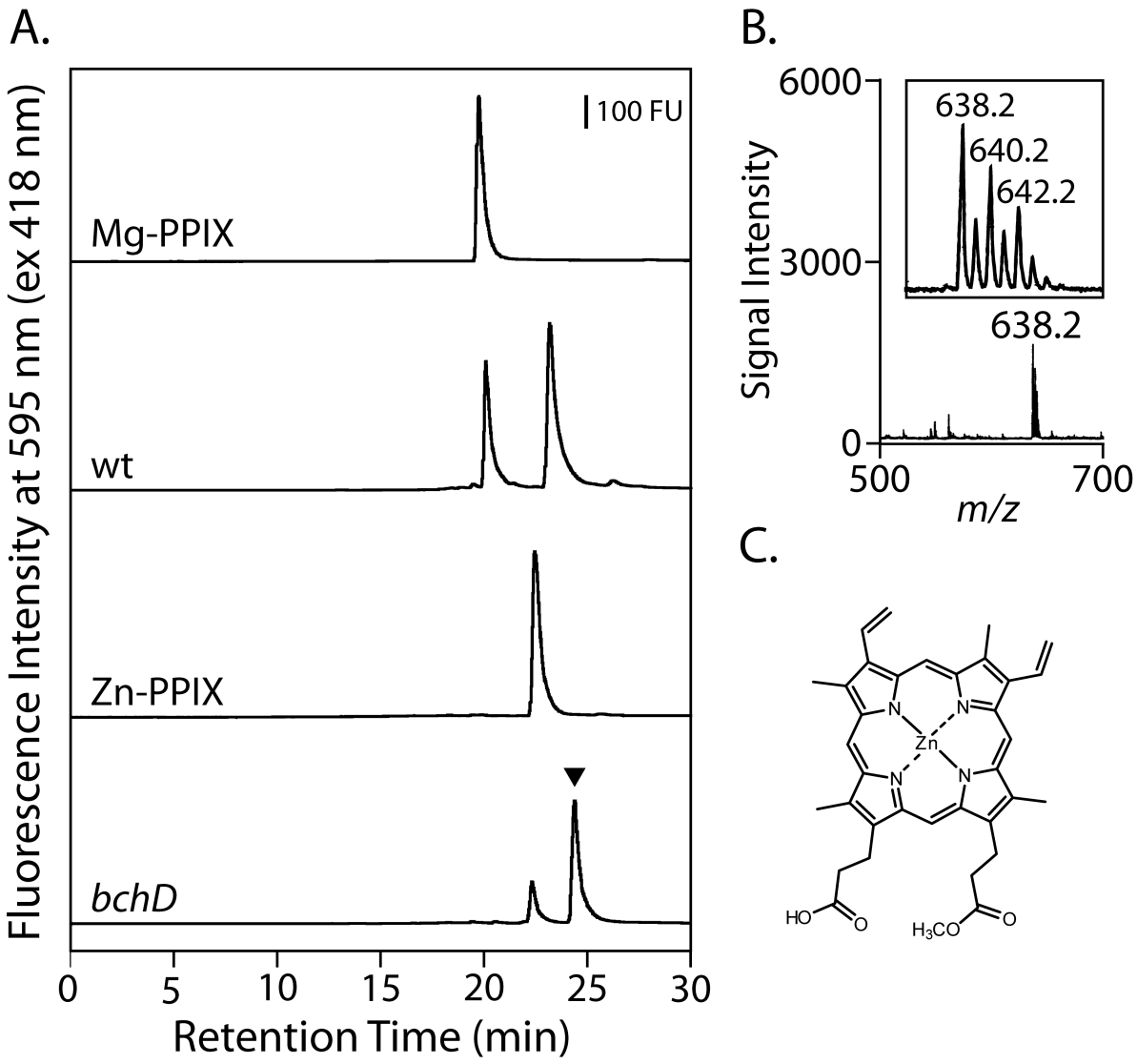

Figure 3-23. HPLC separation and mass spectrometry of crude porphyrin extracts shows *bchD* mutant contains Zn-PPIX-MME. (A) HPLC separation of wt and *bchD* mutant ether extracts and metalloprotoporphyrins IX standards. ▼, peak collected for mass spectrometry analysis. (B) Mass spectrometry of collected peak from *bchD* mutant. Inset is expanded view of region around 638.2 *m/z* peak. (C) Proposed structure of collected peak, zinc-protoporphyrin IX monomethyl ester.

This second species was isolated and subjected to mass spectrometry analysis, which showed a peak at 638.2 *m/z* (Figure 3-23B) corresponding to the predicted mass of zinc-protoporphyrin IX monomethyl ester (Zn-PPIX-MME). Additionally, the isotopic splitting pattern of the 638.2 *m/z* peak (Figure 3-23B, inset) matched that of a zinc-containing compound (see Section 3.1.3 for an explanation of this pattern). The combination of *m/z* value and zinc isotopic pattern of the isolated material, leads me to conclude that the material isolated from the *bchD* mutant was Zn-PPIX-MME. The proposed structure of this compound is shown in Figure 3-23C. To the best of my knowledge this compound has never been identified in an organism before and is not listed in the PubChem database of the National Center for Biotechnology Information (NCBI 2010).

The results of mass spectrometry revealed that the *bchD* mutant synthesized a zinc intermediate analogous to the magnesium intermediate normally produced by wt *Rb. sphaeroides* cells after the BchM enzyme methylates the carboxyl group on the 13-propionate side chain of Mg-PPIX. As described in this section, the isolation and identification of the second intermediate of the BChl-biosynthetic pathway, containing Zn^{2+} rather than Mg^{2+}, confirms my hypothesis that Zn-containing intermediates proceed through the otherwise normal BChl-biosynthetic pathway.

3.4.5. Isolation and identification of Zn-BChl pathway intermediate divinyl-zinc-protochlorophyllide.

To further prove the 'Zn-early' hypothesis I treated the wt and *bchD* mutant strain with a BChl-pathway specific inhibitor, to isolate a BChl biosynthetic intermediate farther down the pathway. Nicotinamide is a known inhibitor of the BChl-biosynthetic pathway enzymatic activity that converts divinyl-protochlorophyllide to monovinyl-protochlorophyllide because *Rb. sphaeroides* cultures treated with this inhibitor were found to accumulate divinyl-magnesium-protochlorophyllide (DV-Mg-PChlide) (Shioi et al. 1988) (see Figure 1-6).

Cultures of the wt and *bchD* mutant strain were grown semiaerobically in the presence of 12 mM nicotinamide and cell pellets were extracted. Absorption spectrometry of ether extracts from the wt strain showed clearly the appearance of an absorption peak

at 438 nm in the nicotinamide-treated cells, whereas no peak was visible in the extract from untreated cells (Figure 3-24A, top two spectra). The fluorescence emission spectrum from 440 nm excitation light showed a similar difference, with a major emission peak at 634 nm present only in the treated cells (Figure 3-24B, top two spectra). This accumulating molecule was identified as DV-Mg-PChlide by comparison to the absorption and fluorescence peaks of values in the literature (Rebeiz 2002; Shioi et al. 1988). In the *bchD* mutant the absorption spectrum showed a difference upon nicotinamide treatment, but there was no distinctive peak as in the wt spectrum (Figure 3-24A, bottom two spectra). The fluorescence spectra of the same ether extracts gave a much clearer picture, because fewer substances in the extract are fluorescent and the background was greatly reduced. The nicotinamide-treated extract of the *bchD* mutant excited by 440 nm light showed an emission peak at 630 nm, which was blue-shifted from the emission of the wt extract by 4 nm (Figure 3-24B, bottom two spectra). By analogy to the Zn-PPIX-MME and Zn-BChl spectral characteristics (see above), this blue-shift indicated that the intermediate accumulating in the *bchD* mutant was almost the same as in the wt (DV-Mg-PChlide) but it contained Zn instead of Mg.

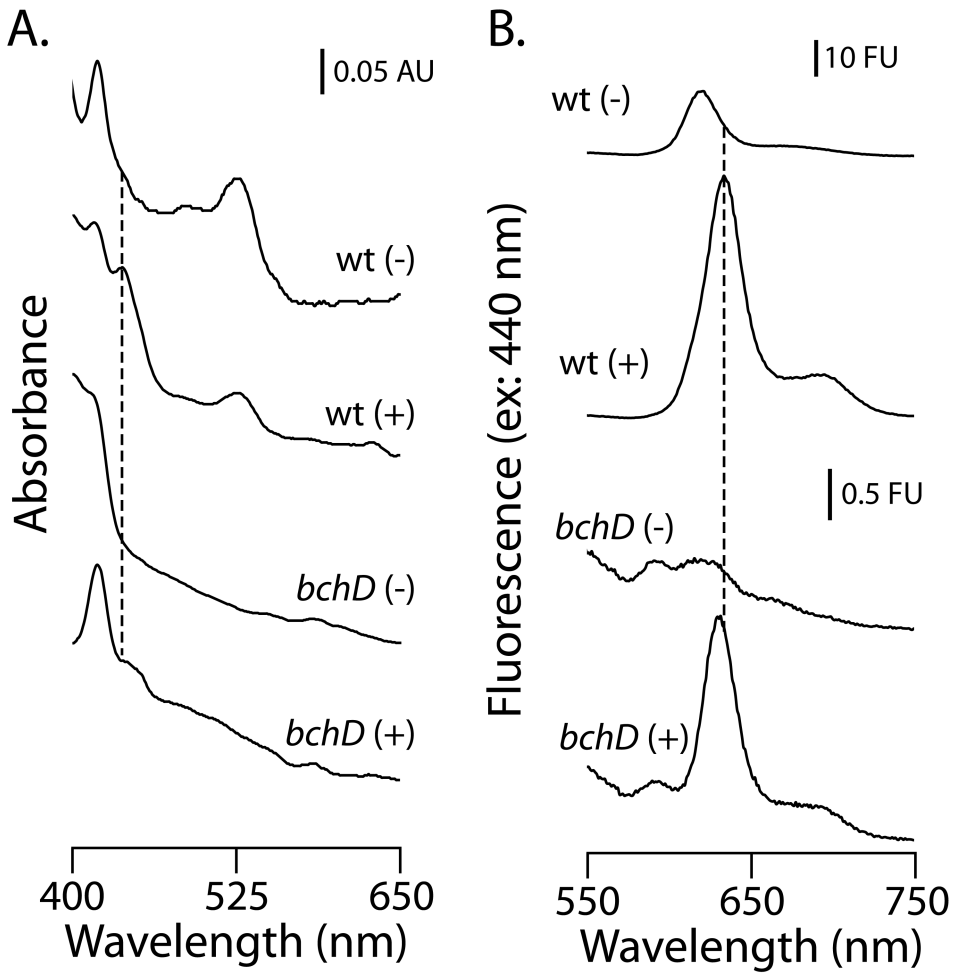

Figure 3-24. Absorption and fluorescence spectra of nicotinamide treated wt and *bchD* mutant extracts. (A) Absorption spectra in ether. (B) Fluorescence emission spectra in ether. Excitation at 440 nm. Extracts obtained from wt and *bchD* mutant cells grown either with 12 mM nicotinamide in culture medium (+), or with no added nicotinamide (-). Dashed line indicates peaks attributed to DV-Mg-PChlide in the wt spectra.

To confirm that the substance accumulating in the *bchD* mutant was DV-Zn-PChlide, I extracted wt and *bchD* cells with a 9/1 solution of acetone/0.1N NH_4OH, removed carotenoids with hexane, and injected the extracts into a HPLC system. The separation was monitored at 440 nm (the Soret peak of DV-PChlide). The HPLC trace from the wt strain showed one major species with a retention time of 22.3 min (Figure 3-25A). The absorption spectrum of this fraction matched that for DV-Mg-PChlide from the literature (Shioi et al. 1988), with peaks at 441, 579, 630 nm (Figure 3-25B, upper trace). Separation of the *bchD* mutant extract showed two peaks eluting at 19.2 and 24.0 min (Figure 3-25A). The

absorption spectrum of the first (19.2 min) peak matched that of PPIX with peaks at 398, 504, 629 nm (data not shown). The second peak, with 24.0 min retention time, had an absorption spectrum that closely matched DV-Mg-PChlide: a Soret peak at 438 nm, blue-shifted from the Mg-PChlide peak by 3 nm; a minor peak at 575 nm, blue-shifted by 4 nm; and a 624 nm peak, blue-shifted by 6 nm (Figure 3-25B, lower trace). In addition to the blue-shifted absorption spectrum of the 24.0 min peak, the 1.7 min longer retention time than the DV-Mg-PChlide peak from the wt strain agreed well with the relative retention times of the Zn-containing analogs of Mg-PPIX, Mg-PPIX-MME, and Mg-BChl seen above.

The material in the 24.0 min HPLC peak of the *bchD* mutant extract was collected and subjected to mass spectrometry using similar conditions as for Zn-PPIX-MME analysis. A peak with mass of 650.2 *m/z* was seen, which corresponded with the predicted mass of 650.2 predicted for divinyl-protochlorophyllide with the Mg^{2+} bound to the porphyrin macrocycle replaced by Zn^{2+} (DV-Zn-PChlide) (Figure 3-25C). Although the mass spectrum intensities were very weak, causing the peak heights of the largest mass and the peak two mass units less to be nearly the same height, the isotopic pattern was more similar to that seen in Zn-containing versus C-, N-, O-, or Mg-containing compounds, as detailed above in Section 3.1.3. The proposed structure of the isolated DV-Zn-PChlide intermediate is shown in Figure 3-25D. To the best of my knowledge this compound has never been identified in an organism before and is not listed in the PubChem database of the National Center for Biotechnology Information (NCBI 2010).

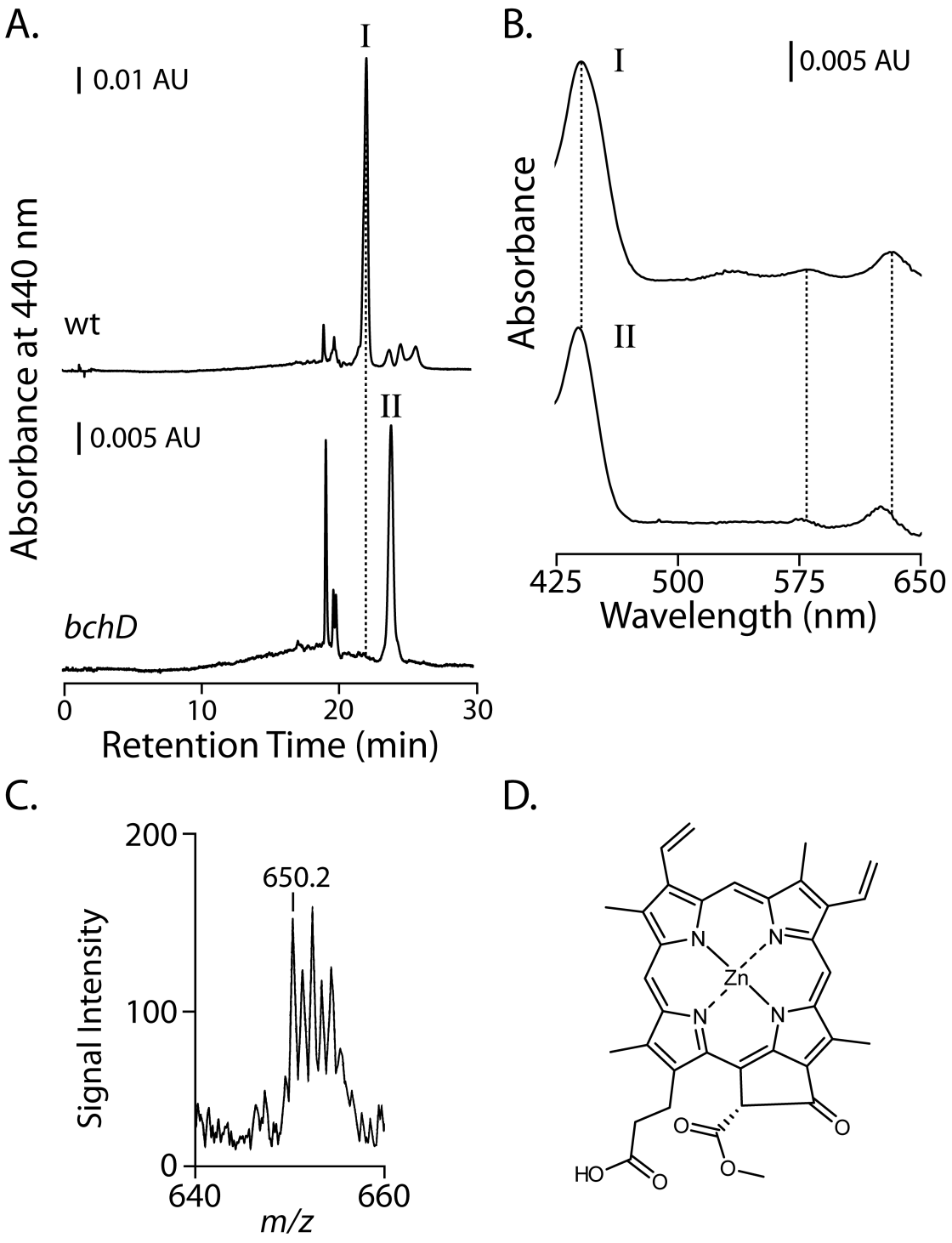

Figure 3-25. Separation and identification of DV-PChlide accumulation in nicotinamide treated wt and *bchD* mutant cells. (A) HPLC separation of cell extracts. Dotted line indicates DV-Mg-PChlide peak. (B) Absorption spectra of peaks I and II in methanol. Dotted lines indicate DV-Mg-PChlide peaks at 441, 579, and 630 nm. (C) Mass spectrometry of isolated peak II. (D) Proposed structure of peak II, divinyl-zinc-protochlorophyllide.

The presence of DV-Zn-PChlide in the *bchD* mutant, confirmed through both absorption and fluorescence spectra, and mass spectrometry data, further supports the existence of a Zn-early BChl-biosynthetic pathway operating in the *bchD* mutant. I next embarked on an attempt to isolate a further intermediate in the pathway, utilizing a genetic method to cause biosynthetic intermediates to accumulate instead of a chemical inhibitor.

3.4.6. Analysis of Zn-BChl biosynthetic intermediates in a *bchD/bchG* double mutant strain.

In an attempt to isolate and identify an additional Zn-containing intermediate in the Zn-BChl-biosynthetic pathway, I made a double knockout strain from another Tn5 mutant made at the same time as the *bchD* mutant, the *bchG* mutant (Coomber et al. 1990). The BchG protein is BChl-synthase, the penultimate enzyme in the BChl-biosynthetic pathway (Figure 1-6), and the *bchG* mutant accumulates large quantities of bacteriochlorophyllide (BChlide) and bacteriopheophorbide (BPheide), the biosynthetic intermediate (and its demetallated derivative) upstream of the BchG step (Addlesee et al. 2000). The additional *bchD* lesion in the *bchG* strain was accomplished through insertion of the Ω cartridge into the *bchD* gene using the pNHG1::*bchD*Ω suicide vector (Figure 2-1). The double mutant created is designated as the *bchG/bchD* strain.

Analysis of the *bchG/bchD* strain initially consisted of examining the absorption spectra of ether extracts from the cells (Figure 3-26A). In the spectra it was apparent that the *bchG/bchD* mutant contained considerably less of the intermediate than the single *bchG* mutant, and that it appeared to be a single peak with absorption maximum at 766 nm as opposed to absorption maxima at 740 and 753 nm in the *bchG* mutant. The red-shift seen in the intermediate accumulating in the *bchG/bchD* mutant compared to the *bchG* mutant may be due to the fact that Zn-containing porphyrins are much more resistant to demetallation than their Mg-analogs (Kobayashi et al. 1998), whereas metal-loss results in blue-shifts to the absorption spectra such as seen in comparison of Mg-BChl (771 nm) to BPhe (750 nm). If the *bchG* mutant were accumulating mostly BPheide and the *bchG/bchD* mutant were mainly accumulating Zn-BChlide, it would appear that the double mutant was accumulating a red-shifted molecule rather than blue-shifted, as

has been seen previously for intermediates in the *bchD* mutant background. Since Zn-BChlide is expected to have a far-red absorbance peak at the same wavelength as Zn-BChl (766 nm), the *bchG/bchD* mutant may be accumulating the predicted Zn-BChlide intermediate.

HPLC separation of extracts monitored at 750 nm absorbance (Figure 3-26B) showed that the *bchG* mutant material had four major peaks with retention times of 16.6, 17.1, 17.6, and 18.4 min, designated peaks 1-4, respectively. The absorption characteristics of peaks 1, 3, and 4 seemed to match demetallated porphyrins, likely BPheide-derivatives because of the 750 nm far-red peaks which were identical to BPhe. Peak 2 with its 765 nm far-red peak (Figure 3-26C) seemed to be intermediate between demetallated BPheide (750 nm) and metallated BChlide which should have a peak at the same wavelength as Mg-BChl (771 nm) (Figure 3-26C). The intermediate absorbance band of peak 2 (524 nm) matched that of peaks 1, 3, and 4 rather than Mg-BChl (Figure 3-26C).

HPLC analysis revealed that there was a single major elution peak at 15.4 min retention time in the *bchG/bchD* mutant (Figure 3-26B), which was shorter than the retention time of all the HPLC peaks in the *bchG* mutant extract. Recall that in the previous HPLC separations, Zn-containing intermediates ran slower than Mg-containing intermediates. Therefore, the relative retention times of the *bchG* and *bchG/bchD* mutants only made sense if all the *bchG* single mutant intermediates were demetallated, because these types of molecules would run slower on the solvent system than metallated molecules. This trend would also have also made sense if the *bchG/bchD* mutant was not accumulating a Zn-containing intermediate. Examination of the spectrum of peak 5 showed it was very similar to that of Zn-BChl, with both 766 nm and 568 nm peaks matching perfectly (Figure 3-26C). Currently I am trying to isolate enough of the accumulating intermediate in the double *bchG/bchD* mutant to analyze with mass spectrometry.

Having isolated and identified Zn-containing intermediates from throughout the Zn-BChl pathway, the origin of Zn-PPIX was investigated next to answer the question of how this pathway begins.

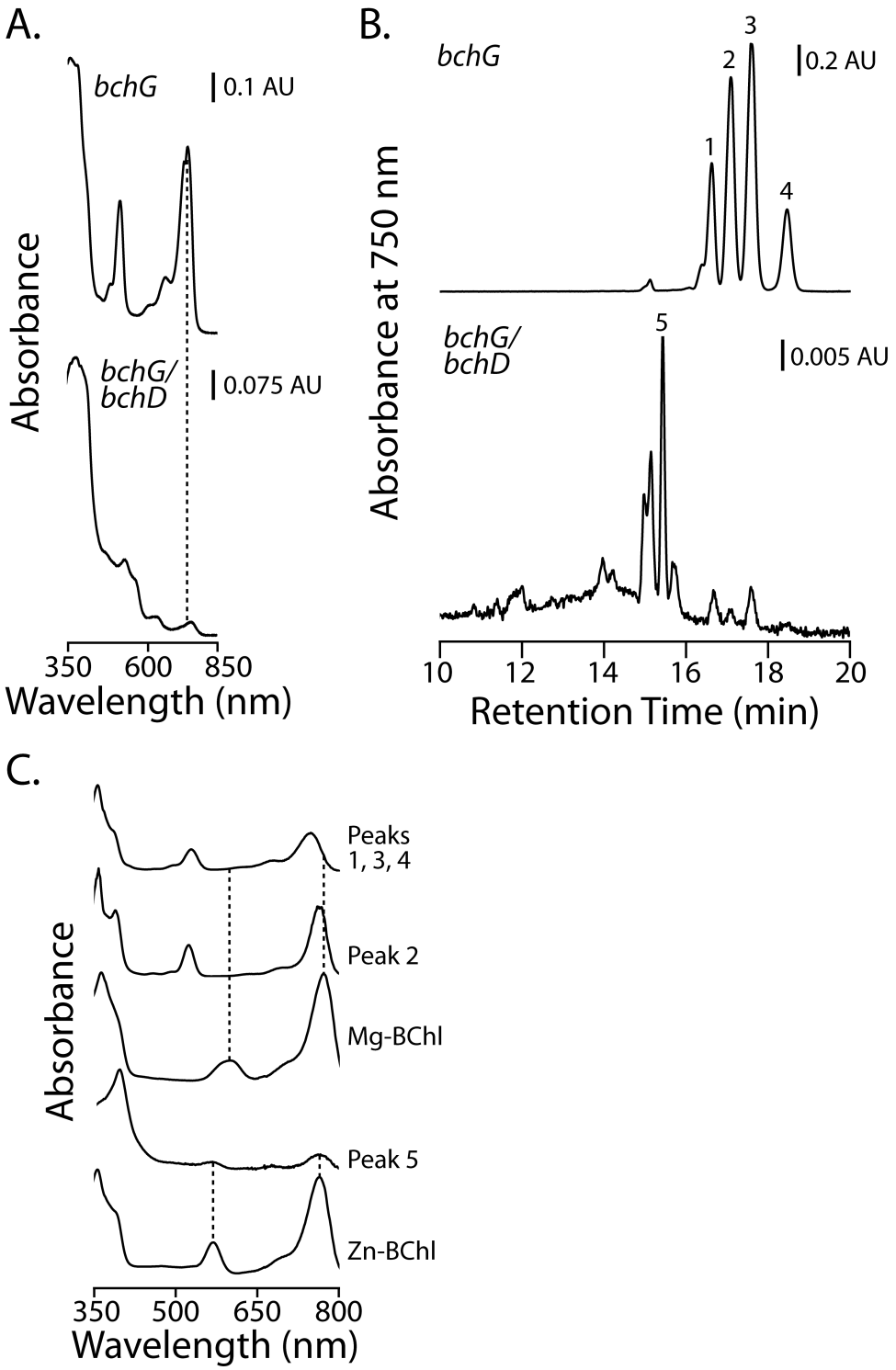

Figure 3-26. Separation and spectral characteristics of ether extracted porphyrins from the *bchG* and *bchG/bchD* mutants. (A) Absorption spectra. (B) HPLC separation. (C) Absorption spectra of major peaks from HPLC separation and Mg- and Zn-BChl standards in methanol. Dotted lines represent characteristic peaks of Mg- and Zn-BChl standards.

3.4.7. Role of ferrochelatase in Zn-PPIX and Zn-BChl biosynthesis.

Zn-PPIX in the *bchD* mutant is likely to be synthesized from one of two sources: either ferrochelatase, adding Zn^{2+} rather than Fe^{2+} into PPIX; or the remaining two proteins of the Mg-chelatase, BchH and BchI, which could conceivably form a complex in the absence of the BchD protein and catalyze the insertion of Zn^{2+} rather than Mg^{2+} into PPIX. To test the involvement of ferrochelatase in the production of Zn-PPIX and Zn-BChl in the *bchD* mutant, I utilized a chemical inhibitor called N-methylprotoporphyrin IX (NMPP). This inhibitor acts as a transition state analog of heme and competitively inhibits the *Rb. sphaeroides* ferrochelatase enzyme (Moody & Dailey 1985).

I grew wt and *bchD* cultures aerobically so that they were replete with heme and cytochromes, but contained little or no BChl, because this pathway is repressed by aerobic conditions. The cultures were then shifted to semiaerobic growth to induce BChl production with the simultaneous addition of NMPP of varying concentrations. After three days of growth, the wt and *bchD* cells were harvested and I measured the amount of PPIX and heme in both strains, and Mg-PPIX and Mg-BChl in the wt strain, and Zn-PPIX and Zn-BChl in the *bchD* mutant strain.

The results are presented (Figure 3-27) in reverse order to the BChl pathway, starting with BChl and following with metalloprotoporphyrins IX and PPIX. Additionally, the data are presented as ratios of the amount of the measured molecule in each of the treated conditions divided by the untreated condition, so that the relative effect of the inhibitor on the wt and *bchD* mutant strains can be seen. In the wt strain, Mg-BChl levels *increased* upon treatment with NMPP, up to 1.7-fold above untreated levels (Figure 3-27A). This effect in the wt strain has been previously observed from an NMPP analog added to cultures (Houghton et al. 1982). In contrast, the Zn-BChl levels of the *bchD* mutant responded to ferrochelatase inhibition in an equal but opposite manner to that seen for Mg-BChl in the wt strain. Zn-BChl levels in the *bchD* mutant exhibited a biphasic response *decreasing* sharply to 30% of untreated levels upon addition of 0.25 µM NMPP, and then slowly going down to 10% of untreated levels at the highest amount of NMPP (Figure 3-27A).

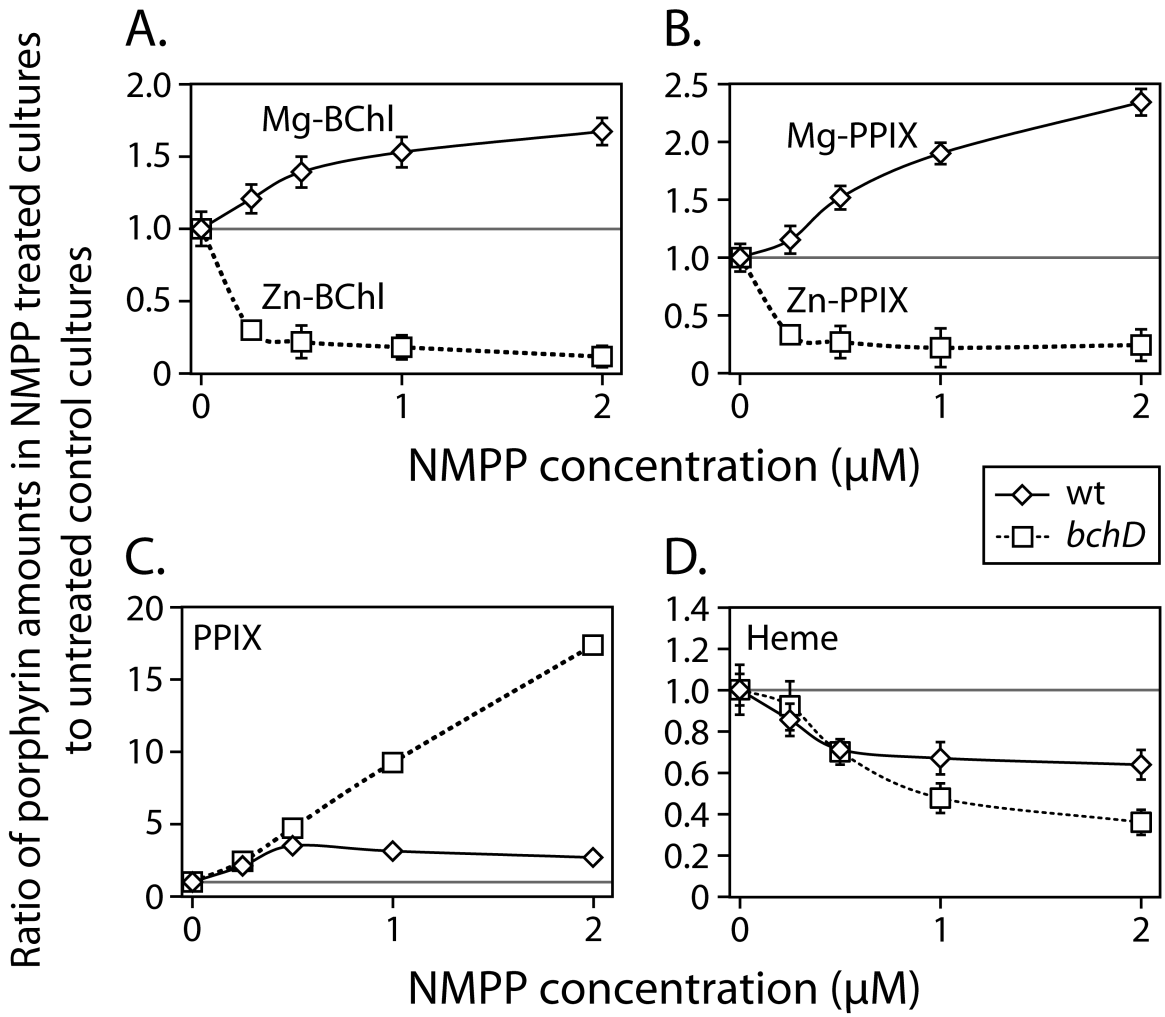

Figure 3-27. Effect of ferrochelatase inhibition on porphyrin amounts in the wt and *bchD* mutant strains. (A) Mg- and Zn-BChls. (B) Mg- and Zn-metalloprotoporphyrins IX. (C) PPIX. (D) Heme. Horizontal line denotes a 1:1 ratio; therefore points above the line indicate that cellular concentrations of this molecule increase upon ferrochelatase inhibition, whereas points below the line denote lowered cellular levels upon ferrochelatase inhibition.

Measurements to quantify the amounts of the metalloprotoporphyrins IX at the start of the BChl biosynthetic pathway showed that Mg-PPIX (wt) and Zn-PPIX (*bchD* mutant) exhibited similar responses to that seen for Mg-BChl and Zn-BChl, respectively (Figure 3-27B). The decline of Zn-PPIX levels in the *bchD* mutant when ferrochelatase was inhibited was similar to what is seen in ALA-fed rat hepatocytes that produce Zn-PPIX (Jacobs et al. 1998). By increasing the flux of porphyrins by adding the precursor to PPIX (ALA), they produced excess PPIX, but also Zn-PPIX. But, when the hepatocytes were also

treated with NMPP, the levels of Zn-PPIX were reduced (Jacobs et al. 1998), pointing to ferrochelatase as the source of Zn-PPIX in the hepatocytes. The similarity between the results seen in the *bchD* mutant and rat hepatocytes indicates that the effect observed in this experiment is robust and consistent across phyla, as well as pointing to ferrochelatase as the biological source of Zn-PPIX in the *bchD* mutant.

Together, these results strongly support the idea that ferrochelatase, as opposed to Mg-chelatase, is needed for production of Zn-PPIX. If the Mg-chelatase complex were involved instead of ferrochelatase, the levels of Zn-PPIX and Zn-BChl in the *bchD* mutant should follow the same trend as Mg-PPIX and Mg-BChl levels in the wt strain (Figure 3-27A and B). Instead, the effect is opposite, showing that the wt Mg-chelatase is not inhibited by NMPP, whereas the enzyme in the *bchD* mutant responsible for Zn-PPIX and Zn-BChl production is inhibited by NMPP.

The changes in PPIX levels caused by NMPP treatment showed a different relationship between the wt and *bchD* mutant strain than for metalloporphyrins IX or BChl, but reinforced the difference between the wt and *bchD* porphyrin pathways. The wt strain PPIX levels increased up to 3.5-fold upon treatment with NMPP, similar to the increase in Mg-BChl and Mg-PPIX levels upon similar treatment (Figure 3-27C). In sharp contrast, the *bchD* mutant had a dramatic 17.6-fold increase in PPIX levels under NMPP inhibition of the ferrochelatase (Figure 3-27C). This result is consistent with the explanation that upon ferrochelatase inhibition in the wt strain, the excess PPIX that would normally be used by the ferrochelatase to make heme was re-routed through the Mg-chelatase to generate the increased amounts of Mg-BChl and Mg-PPIX seen. Because the *bchD* mutant does not have a functional Mg-chelatase, the excess PPIX generated in this strain when ferrochelatase was inhibited could not be re-routed, and instead built up to the remarkable levels seen in Figure 3-27C. The buildup likely continued to such an extent because lowered heme levels (see below) signaled ALA-synthase to make more ALA, which was converted to PPIX (Burnham & Lascelles 1963; Yubisui & Yoneyama 1972).

Heme levels declined in both the wt and *bchD* mutant strains treated with NMPP, but the *bchD* mutant showed a slightly larger decrease (Figure 3-27D). The decrease in heme was due to the combined effect of inhibition of new heme synthesis as well as dilution of the existing heme pool present in the semiaerobic culture inoculum that was

grown under high aeration (replete with heme). The reductions in heme levels are consistent with other work using similar inhibitors (Chekounova et al. 2001; Houghton et al. 1982; Jacobs et al. 1998). The larger decline in heme levels in the *bchD* mutant compared to the wt strain could have been due to the lower cell density in the *bchD* mutant cultures (see Section 3.1.1), resulting in a higher concentration of NMPP per cell than in wt cultures, and more complete inhibition of ferrochelatase.

The ferrochelatase inhibition experiments highlighted the necessity of this enzyme for Zn-PPIX and Zn-BChl production in the *bchD* mutant, as well as a fundamental difference between the porphyrin biosynthetic pathways in the wt and *bchD* mutant strains. While the wt strain has two pathways (Mg and Fe) that use PPIX as a substrate, the *bchD* mutant only has one, and the function of this pathway is consistent with the Zn and Fe pathway catalyzed by ferrochelatase. Furthermore, the function of ferrochelatase is necessary for Zn-BChl synthesis in the *bchD* mutant, but not for Mg-BChl synthesis in the wt strain.

3.4.8. Time-course of porphyrin levels in the wt and *bchD* mutant strains.

The next step after discovering the source of Zn-PPIX in the *bchD* mutant was to quantitatively determine the concentration of Zn-PPIX in mutant cells to determine whether it was sufficient to supply the amounts of Zn-BChl measured. To this end I performed a time-course to evaluate the changes to porphyrin levels over a transition from aerobic to semiaerobic growth. Cultures were grown aerobically, shifted to semiaerobic growth, and samples were removed at time points. For each time point, the levels of PPIX, Mg-PPIX (wt) and Zn-PPIX (*bchD*), and Mg-BChl (wt) and Zn-BChl (*bchD*), were measured. The Mg- and Zn-PPIX measurements represented an aggregate of both the metalloprotoporphyrin IX and the monomethyl ester, because these are indistinguishable spectroscopically.

The results of the time-course showed a similar general trend between the wt and the *bchD* mutant strains over the course of the experiment, but with several interesting differences. In the wt strain, Mg-PPIX and PPIX peaked within 40 hours of transition to semiaerobic growth, which corresponded with a period of rapid Mg-BChl synthesis

(Figure 3-28A, top panel). As Mg-BChl levels plateaued, Mg-PPIX and PPIX rapidly dropped down to levels lower than that occur initially. In contrast to the wt strain, the *bchD* mutant strain showed a 50-hour lag period where all porphyrins measured stayed at the same level or increased slightly. This period was followed (as earlier in the wt strain) by a rapid increase in all porphyrin levels, then a slight drop-off in levels of Zn-PPIX and PPIX, while Zn-BChl levels plateaued (Figure 3-28B, top panels).

While the general trend of changes was similar between the strains, the starting levels of the porphyrins stood in stark contrast. While PPIX at 5.5 hours post-shift was slightly higher in the wt strain, Zn-PPIX levels in the *bchD* mutant strain were 5-fold greater than Mg-PPIX levels in the wt, and Zn-BChl was only 3% of wt Mg-BChl levels (Figure 3-28, top panel). After the first time point, PPIX and Zn-PPIX in the *bchD* mutant increased rapidly to more than 14-fold and 20-fold of levels in the wt strain, respectively. Production of Zn-BChl in the *bchD* mutant lagged so severely behind that of Mg-BChl in the wt that even by 169 hours, the *bchD* mutant still had less per cell than the wt strain had at the first time-point (Figure 3-28, top panels).

The growth curves for the wt and the *bchD* mutant cultures during this time-course followed a very similar shape. Despite the similarity in the growth curve progression, the cell density in the *bchD* mutant culture at every time point was about half that of the wt strain (Figure 3-28, bottom panels).

Although Zn-PPIX and Zn-BChl levels appeared to change over the growth phase in a similar way to their analogs in the wt strain (i.e., Zn-PPIX peaked at the time that Zn-BChl levels were beginning to rise), Mg-PPIX was at all times below 5% of Mg-BChl levels, while Zn-PPIX was between 20-170% of Zn-BChl levels in the *bchD* mutant strain. If the hypothesized Zn-BChl biosynthetic pathway is indeed using Zn-PPIX as a substrate, there seems to be a significant bottleneck somewhere in the pathway during conversion of Zn-PPIX to Zn-BChl.

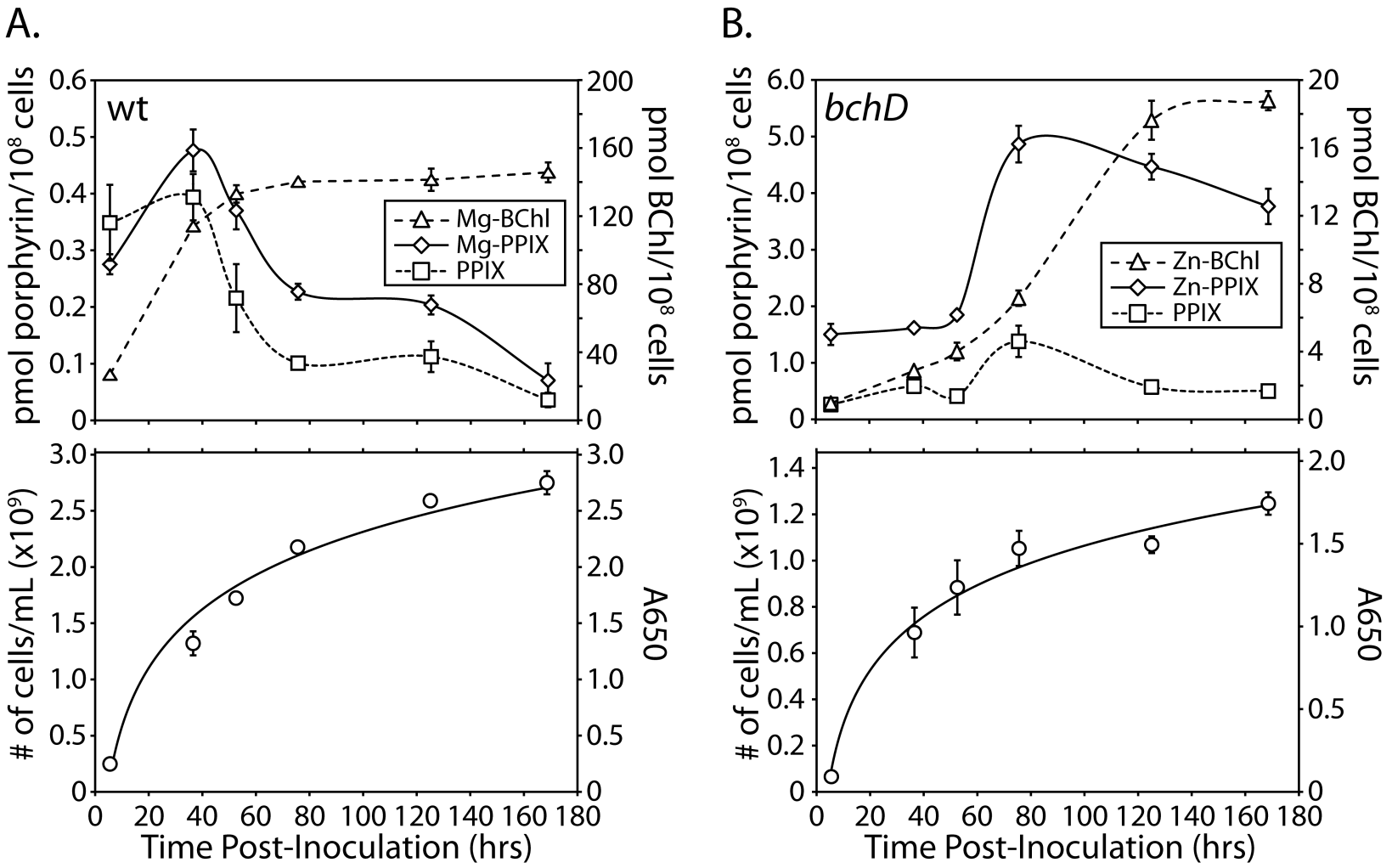

Figure 3-28. Porphyrin time-course during changeover from aerobic to semiaerobic growth. Porphyrin levels and culture density for (A) wt, (B) *bchD* mutant. Cultures grown aerobically, then at zero-time inoculated into a new flask filled 80% and shaken at 150 RPM. Top, metalloprotoporphyrins IX and PPIX represented on left y-axis, BChls on right y-axis. Bottom, number of cells per mL (calculated from A_{650} measurement using equation from Appendix I) represented on left axis, measured absorbance of culture at 650 nm on right axis. Error bars represent standard deviation of 3-4 biological replicates.

3.4.9. Elucidation of the Zn-BChl biosynthetic pathway bottleneck.

One fundamental question that remained to be answered about the Zn-BChl biosynthetic pathway in the *bchD* mutant was why *early* intermediates (Zn-PPIX) were present at such high levels relative to the *end* product (Zn-BChl), compared to the wt strain.

3.4.9.1. Ferrochelatase.

From the time-course in Figure 3-28, the early precursor, Zn-PPIX, is between 5 and 54 times *more* abundant per cell than Mg-PPIX is in the wt strain, while end product Zn-BChl is 3 to 10 times *less* abundant than Mg-BChl in the wt strain. These data indicate strongly that ferrochelatase that produces Zn-PPIX in the *bchD* mutant is not the bottleneck in the pathway.

3.4.9.2. BchM methyltransferase.

Moving down the pathway from the beginning to the end, I attempted to narrow down where the bottleneck in the biosynthetic pathway was occurring by comparing the ratio of the product (Mg- or Zn-PPIX-MME) to the substrate (Mg- or Zn-PPIX) of the second enzyme in the pathway, BchM. The difference in the ratio between the wt strain and the *bchD* mutant would allow me to determine if BchM were able to use Zn-PPIX as efficiently as Mg-PPIX. If BchM were the bottleneck in the Zn-BChl biosynthetic pathway in the *bchD* mutant I would have expected to see a large excess of Zn-PPIX over Zn-PPIX-MME, resulting in a Zn-PPIX-MME/Zn-PPIX ratio below 1. Extractions from the wt and *bchD* mutant strains grown semiaerobically to the same cell density were analyzed on HPLC. The wt strain showed a Mg-PPIX-MME product to Mg-PPIX substrate ratio of 2.5 ± 0.8 (n=4), whereas the *bchD* mutant product to substrate ratio was 4.4 ± 0.6 (n=8). Since I see a greater proportion of the monomethyl ester accumulating in the *bchD* mutant compared to the wt strain, I could say with confidence that the bottleneck in the Zn-BChl pathway was downstream of BchM.

3.4.9.3. AcsF and BchE cyclases.

The enzymatic step directly downstream of BchM is catalyzed by both AcsF and BchE, the cyclases that generate the fifth isocyclic ring of (B)Chls. It is likely that under the semiaerobic conditions utilized in this work only BchE was active (Hunter & Coomber 1988; Oh et al. 2000), and therefore only this enzyme will be mentioned in further discussion. If BchE were the limiting step in Zn-BChl biosynthesis I would have expected two results: first, there would be a buildup of large amounts of Zn-PPIX-MME, the substrate for BchE; second, there would be very low amounts of DV-Zn-PChlide, the product of the cyclization reaction. As detailed in the preceding section, the *bchD* mutant accumulated a large excess of Zn-PPIX-MME over the substrate Zn-PPIX, satisfying the first condition implicating BchE as a bottleneck in the pathway.

To determine the relative amounts of the product of the cyclization reaction, DV-PChlide, I used a deconvolution technique similar to that used previously for PPIX levels and re-analyzed HEAR samples from the time-course (see Figure 3-28). Unfortunately, I did not have DV-PChlide standards with which to create standard curves and so the data were expressed as fluorescence emission units rather than moles. The fluorescence units have been normalized for the relative fluorescence yields of Mg-PPIX and Zn-PPIX, assuming the same relative difference exists for the DV-PChlides.

The results of this quantification showed that in the wt strain, as was seen for all the other porphyrins except for Mg-BChl, there was a steady 3.5-fold decline in DV-Mg-PChlide levels per cell over the growth phase (Figure 3-29). In contrast, DV-Zn-PChlide in the *bchD* mutant rose slightly and then fell back to starting levels (Figure 3-29). However, the amount of DV-Zn-PChlide ranged from 2.2 up to 8.5-fold more than wt DV-Mg-PChlide levels. Although DV-Zn-PChlide still accumulated in excess to DV-Mg-PChlide levels, the relative difference between *bchD* and wt was lower than for prior intermediates. This could indicate an inflection point for the pathway where metabolite levels start to decline down to Zn-BChl. Caution must be used though when interpreting these data because the relative fluorescence yield of DV-Zn-PChlide to DV-Mg-PChlide may be quite different than Mg- and Zn-PPIX (Mg-PPIX fluorescence is 6.2-fold greater intensity per molecule than Zn-PPIX). The normalization had a large effect on the values and could even reverse

the relationship, but if they are accurate, this finding suggests that the cyclization reaction functions well in the *bchD* mutant. This would be manifest in DV-Zn-PChlide production at a faster rate than the downstream enzymes could convert it to Zn-BChl, resulting in an accumulation of the intermediate to a greater extent than seen in the wt strain.

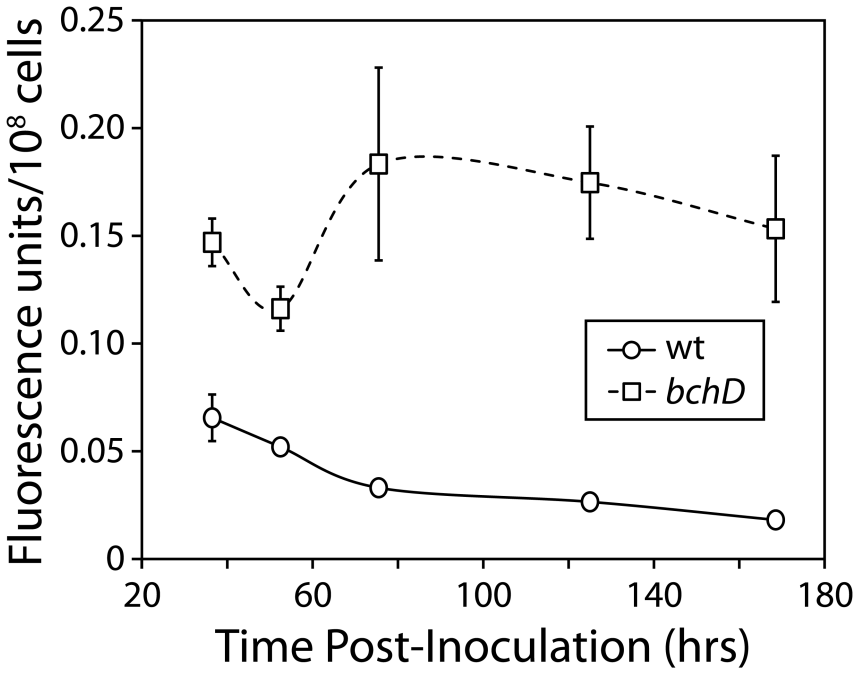

Figure 3-29. DV-PChlide level time-course in the wt and *bchD* strains. Fluorescence units are deconvoluted emissions units from 638 nm in wt and 634 nm in the *bchD* mutant, normalized for relative fluorescence of DV-Mg-PChlide versus DV-Zn-PChlide. Error bars are standard deviations of 3-4 biological replicates.

4. Discussion

The work in this thesis was performed to address two main aims: (1) elucidation of the Zn-BChl biosynthetic pathway in the *bchD* mutant; and (2) utilization of this biosynthesis as a tool to probe aspects of Zn-containing photosynthetic apparatus function. Initial experiments established that the *bchD* mutant was unable to grow photosynthetically and had additional defects in other growth modes. Levels of photosystem proteins were decreased from the wt strain but those proteins that were present assembled into LH2, LH1, and RC complexes that bound Zn-BChl instead of Mg-BChl. The RC complex from the *bchD* mutant bound 6 Zn-BChl instead of the 4 Mg-BChls and 2 BPhe found in the WT-RC. Moreover, BPhe was absent from both the Zn-RC and *bchD* cells. Despite these major changes from the WT-RC, the Zn-RC maintained similar ET rates and yields, revealing the importance of tetracoordination versus pentacoordination on the redox potential of BChls. Finally, experiments on the biosynthesis of Zn-BChl showed ferrochelatase was required to make the first (Zn-PPIX) and last (Zn-BChl) metabolites of the pathway. The Zn-BChl biosynthetic pathway progressed through a unique route via Zn^{2+}-containing intermediates, two of which were isolated and identified as Zn-PPIX-MME and DV-Zn-PChlide. Further analysis revealed large amounts of intermediates building up before the BchE cyclase step, while lowered amounts were found downstream of this step, implicating this enzyme as a likely bottleneck in the pathway.

4.1. Biosynthesis of Zn-BChl in the *bchD* mutant.

This is the first report of Zn-BChl produced in a purple photosynthetic bacterium that normally assembles LH and RC complexes containing Mg-BChl. It may appear surprising that this was discovered in a mutant lacking the enzyme of the first step in the BChl-biosynthetic pathway, but I suggest below that the absence of a functional Mg-chelatase was a major factor in both the synthesis and detection of Zn-BChl.

4.1.1. The role of ferrochelatase.

Experiments in this thesis have shown that both the precursor (Zn-PPIX) and the end product (Zn-BChl) of the Zn-BChl biosynthetic pathway in the *bchD* mutant were dependent on the function of ferrochelatase, the enzyme that normally synthesizes heme. Although the possibility that the remnant of the Mg-chelatase in the *bchD* mutant could somehow chelate Zn^{2+} into PPIX cannot be definitively ruled out, the fundamental difference between the response of the wt and *bchD* strains to ferrochelatase inhibition makes this possibility extremely unlikely (Figure 3-27). Together, these results strongly support a model of the Zn-BChl biosynthetic pathway that I originally, in which ferrochelatase synthesizes Zn-PPIX from PPIX and Zn^{2+}, and that this molecule feeds into the existing BChl-biosynthetic enzymes to create Zn-BChl.

The structure and origin of ferrochelatase and Mg-chelatase are very different despite catalyzing similar reactions. While ferrochelatase is a single subunit of 115 kDa (Dailey 1982), the Mg-chelatase is a 1.1-1.2 MDa complex consisting of 2-3 copies of BchH, 6 copies of BchI, and 6 copies of BchD (Lundqvist et al. 2010). Although both enzymes are located in the cytoplasm, the ferrochelatase may be membrane-associated (Dailey 1982; Gibson et al. 1995). Finally, both enzymes catalyze the insertion of a divalent cation. However, the ferrochelatase seems to be able to catalyze the reaction in the absence of ATP (Dailey 1982), whereas Mg-chelatase requires ~15 ATP per insertion event (Reid & Hunter 2004). The Mg-chelatase is related to other AAA+-chelatases such as the aerobic cobaltochelatase formed by CobNST (Lundqvist et al. 2009), while the ferrochelatase is instead part of a second class of chelatases together with the anaerobic cobaltochelatases CbiK and CbiX (Beck et al. 1997; Raux et al. 1997). Due to the numerous differences between these two enzymes, it is surprising that the non-homologous ferrochelatase can overlap with the BChl-biosynthetic pathway that Mg-chelatase is usually associated with. This may be because of the similar cellular localization of the chelatases and relaxed specificity of the BChl-biosynthetic enzymes, or it could indicate some deeper association between heme and BChl biosynthesis, as discussed in Section 4.3.

4.1.2. Comparison to other Zn-BChl producing organisms.

There are two other cases where Zn^{2+} is substituted for Mg^{2+} in (B)Chls *in vivo*. One is the unicellular alga *Chlorella kessleri*, which produces Zn-Chl only when grown heterotrophically to late-stationary phase in acidic media containing more than 2000 times the usual concentration of Zn^{2+}(>16.8 mM) (Ikegami et al. 2005). The second case is the purple phototrophic acidophile *Ac. rubrum* (Wakao et al. 1996). In both cases, the organisms grow under acidic conditions, possess functional Mg-chelatases, and are believed to produce Zn-(B)Chl using Mg-(B)Chl as a substrate with culture conditions forcing Zn^{2+} into (B)Phe (Ikegami et al. 2005; Masuda et al. 1999; Wakao et al. 1996). Because *Ac. rubrum* and *Ch. kessleri* can presumably make (B)Phe from Mg-(B)Chl they do not have to dechelate the Zn-(B)Chl derivative. These cases are in sharp contrast to the *bchD* mutant, which grows at neutral pH where Zn^{2+} is less soluble, synthesizes Zn-BChl without first producing Mg-BChl or BPhe, and utilizes Zn^{2+} as a physiological substrate.

4.1.3. The Zn-BChl pathway bottleneck.

Looking at the differences between pathway intermediate levels in the wt and *bchD* strains highlights the preference of the BChl-biosynthetic pathway enzymes for Mg^{2+} versus Zn^{2+} in the macrocycle of the substrate. This effect is revealed in several interesting trends between the intermediate levels in the wt and *bchD* strain. Firstly, while the *bchD* mutant contained between 4.3-17.5 fold *more* intermediate than the wt for every intermediate measured, the Zn-BChl end product was 10-fold *less* in the *bchD* mutant (Figure 4-1, middle section). Secondly, the relative disparity between intermediate levels in the *bchD* mutant and the wt increased at each step up to a peak at Zn-PPIX-MME, which was on average 17.5-fold greater in the *bchD* mutant. Following this step though, DV-Zn-PChlide in the *bchD* mutant was on average only 4.3-fold more than DV-Mg-PChlide in the wt, indicating a potential change in the trend of the pathway at this step (Figure 4-1, middle section).

The relative range of intermediate levels over the time-course of induction within each strain reveals an additional difference between the wt and *bchD* strains. Within the wt pathway intermediate levels changed greatly during the growth phase, from 4-13 fold,

with DV-Mg-PChlide changing the least, and PPIX changing the most (Figure 4-1, numbers above intermediates in top section). In contrast, the ranges of intermediate concentrations in the *bchD* mutant were dampened, with intermediates fluctuating only 2-6 fold (Figure 4-1, numbers below intermediates in bottom section). As with the wt strain, DV-Zn-PChlide changed the least and PPIX changed the most over the time-course (Figure 4-1).

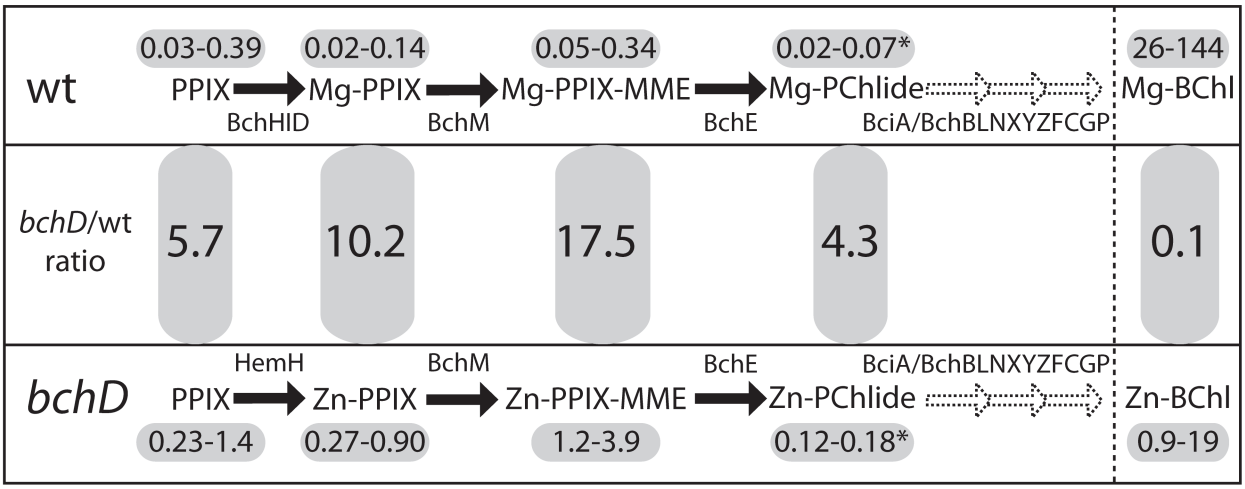

Figure 4-1. Summary of amounts of intermediates in the Zn-BChl biosynthetic pathway. BChl-biosynthetic pathway intermediates and enzymes that catalyze the reaction, wt (top) and *bchD* mutant (bottom). Values above and below intermediates represent range of intermediate concentration over the growth cycle (concentrations in pmol/10^8 cells, except for PChlide which is fluorescence/10^8 cells, indicated by asterix). Mg- and Zn-PPIX and monomethyl ester values derived from time-course values by applying the ratio of monomethyl ester quantified from HPLC experiment in Section 3.4.9.2. The average ratio of *bchD* mutant to wt strain intermediate levels is shown in the center section.

That the relative intermediate levels started to decline after BchM suggests that the BchE enzymatic step is a turning point in the pathway after which intermediate levels decline, rather than increase. The BchE cyclase step in the *bchD* mutant seemed to be less efficient compared to its counterpart in the wt strain, otherwise we would have seen a much higher accumulation of DV-Zn-PChlide, rather than the Zn-PPIX-MME that is seen. Furthermore, when nicotinamide was used to inhibit the conversion of DV-PChlide to monovinyl-protochlorophyllide, the amounts of DV-Zn-PChlide that accumulated in the *bchD* mutant were much less than DV-Mg-PChlide in the wt strain. Together, these data point to BchE as a contributor to the bottleneck in the Zn-BChl biosynthetic pathway. The

catalytic efficiency of BchE from *Rb. sphaeroides* using a Zn-containing substrate has never been reported so I cannot say whether the bottleneck effect in the *bchD* mutant is due to this (or the specificity of this) enzyme, or some other factor, such as lowered enzyme expression. It is interesting that the ring-closing reaction catalyzed by this enzyme is unique in the BChl biosynthetic pathway (Willows & Kriegel 2009). Moreover, it is tempting to speculate that perhaps the catalytic site of BchE is hindered in some way by Zn-containing substrates. It is conceivable that there may be other bottlenecks in addition to BchE. Further work is needed to reveal the relative efficiencies of each step in the pathway, and determine whether this hypothesis is true.

The described Zn-BChl biosynthetic pathway in the *bchD* mutant is an example of a naturally occurring "mutasynthetic" pathway where the elimination of one biosynthetic enzyme in a pathway (usually the first), is compensated for by supplying an alternative substrate (Weissman 2007; Wohlleben & Pelzer 2002). In general, this practice is used to feed cells an exogenous substrate to produce novel end products for drug discovery, but in this case *Rb. sphaeroides* itself supplies the alternative substrate endogenously. Mutasynthetic pathways are commonly limited by early substrate availabilities (Hawkins & Smolke 2008). In contrast, we see excess levels of substrates for all Zn-BChl pathway steps examined. Similar situations have been seen in metabolic engineering efforts in other organisms, such as the development of artemisinin production in *E. coli* (Keasling 2008). The general principles learned from these efforts revolve around matching enzyme levels with substrate levels so that toxic intermediates do not accumulate (Martin et al. 2003). These same principles are likely important for the *bchD* mutant, as evidenced by the poor growth rate and lowered maximum cell densities of cultures, however, enzyme levels and substrate affinity in the Zn-BChl pathway are uncharacterized.

4.1.4. Effect of porphyrin buildup on growth of the *bchD* mutant.

Links between Zn-PPIX accumulation, cytochrome biogenesis deficiency, and growth rate deficiencies have been found in other mutants. In yeast mutants that accumulate Zn-PPIX, cytochrome biogenesis is strongly inhibited, as is respiratory adaptation when the cells transition from anaerobic to aerobic growth (Gilardi et al. 1971). Furthermore, *E. coli* cells

fed exogenous Zn-PPIX showed a cytochromes *c* biogenesis-deficiency directly proportional to Zn-PPIX levels (Richard-Fogal et al. 2007).

The differential growth of the *bchD* mutant in three major growth modes of *Rb. sphaeroides* leads directly to a hypothesis that the defect may be in cytochrome biogenesis or function. In *Rb. sphaeroides* the aa_3 cytochrome *c* oxidase complex is used mainly for high aeration growth (Shapleigh et al. 1992), while the cbb_3 cytochrome *c* oxidase is used for microaerophilic oxygen growth modes, such as the semiaerobic growth protocol used here (Garcia-Horsman et al. 1994). If cytochrome *c* or *b* biogenesis was affected more than *a*-type, this may explain the lower efficiency of semiaerobic growth in the *bchD* mutant. It is possible that, as in the yeast and *E. coli* mutants, when Zn-PPIX levels rise over the growth phase, they inhibit the ability of *bchD* cells to respire and grow. Although I did not measure concentrations of Zn-PPIX during aerobic growth, the first time-point of the porphyrin time-course (Figure 3-28), where cells were still adapting from aerobic to semiaerobic growth, revealed that: (1) Zn-PPIX was present; (2) Zn-PPIX levels were already in excess of PPIX levels.

The severe photosynthetic growth deficit in the *bchD* mutant may be a combination of low photosynthetic apparatus levels coupled with deficiencies in the *c*-type cytochromes used in both the cytochrome bc_1 complex and c_2 protein. The results generated from the combination *bchD* and LH2-knockout strain Δ*puhA*/Δ*puc*/Δ*bchD*(p6His-C) seemed to rule out interference from the LH2 complex as a potential cause of the photosynthetic deficiency in the *bchD* mutant, at least within the context of the low amounts of RC and LH1 seen in the mutant. A minimal threshold of RC could still be the reason strains with the *bchD* mutation could not grow photosynthetically, but results from *hemAT* (ALA-synthase) mutants that contain similar amounts of WT-RC to the amounts of Zn-RC found in the *bchD* mutant, suggests another explanation (Neidle & Kaplan 1993). Additionally, I cannot rule out interference from the LH1 complex. To evaluate this possibility, I am currently creating a *bchD* mutant that only expresses the RC complex.

A further factor that could be limiting photosynthetic growth in the *bchD* mutants is the accumulation of photoactive compounds in the cell. Other organisms, such as *E. coli* and *Chlamydomonas*, that have mutations in the ferrochelatase or Mg-chelatase, and that

accumulate PPIX, are extremely sensitive to light (Chekounova et al. 2001; Miyamoto et al. 1992). This effect is believed to be caused by the interaction of oxygen and light with PPIX to generate reactive oxygen species (Hsu et al. 1971). The *bchD* mutant accumulated only 3.6-fold more PPIX than the wt strain at their peak values, which is much lower than the 175-300 fold increase in the *Chlamydomonas CHLH* mutant or the 150-fold increase in the *hemH E. coli* mutant (Chekounova et al. 2001; Miyamoto et al. 1992). Additionally, my experiments that probed the effect of both light and oxygen on the growth of the *bchD* mutant (Section 3.3.3) clearly showed no detrimental effects, indicating that photoactive species did not limit photosynthetic growth. While the *bchD* cells were being grown in the presence of oxygen and light, the oxygen levels were likely kept lower in the *bchD* mutant than in the *Chlamydomonas* mutant because the photosynthetic apparatus of *Rb. sphaeroides* does not evolve oxygen as it does in *Chlamydomonas*. In fact, *Rb. sphaeroides* cells in colonies reduce the oxygen concentration in the microenvironment because of respiration.

Modeling of the electron transport chain of *Rb. sphaeroides* when grown in the presence of both light and oxygen showed that respiration overrides phototrophy. Qualitatively, the cells should act the same when grown aerobically in the light or darkness (Klamt et al. 2008). These results fit well with my experimental results, despite the authors' caution that their model did not include the effect of toxic radicals. My results indicated that these species had little effect on the fitness of either the wt or *bchD* strains of *Rb. sphaeroides* under the experimental conditions utilized.

4.2. The Zn-BChl photosynthetic apparatus of the *bchD* mutant.

4.2.1. The LH and RC proteins.

The reduced pool of RC and LH proteins in the *bchD* mutant may have resulted from a shortage of Zn-BChl which both reduced the amount of complexes assembled, and increased the degradation of non-complexed proteins. Previous work showed that the absence of BChl decreases the steady-state levels of LH and RC proteins in the ICM, presumably because of degradation of non-complexed proteins (Brand & Drews 1997; Varga & Kaplan 1993). Furthermore, pulse-chase experiments on a *Rb. capsulatus bchH*

mutant showed loss of LH proteins from the ICM fraction, with the LH1/2 β proteins lost at a faster rate than the LH1/2 α proteins (Brand & Drews 1997). This differential stability is consistent with the LH protein levels seen in the *bchD* mutant (Table 3-1, bottom two rows), where the relative amounts of α proteins were greater than the β proteins. Moreover the RC protein amounts (M>L>H) in the *bchD* mutant followed the same pattern as the proposed stabilities determined from RC single gene knockouts (Tehrani & Beatty 2004), which may be due to the inherent stabilities of the non-complexed proteins.

The co-purification of RC proteins using a 6His tag on the RC H protein showed that the H, M and L proteins formed a complex in the *bchD* mutant (Figure 3-3), and therefore Zn-BChl functioned in place of BChl for *in vivo* assembly of the *Rb. sphaeroides* RC. Furthermore, the absence of BPhe in the *bchD* mutant showed that BPhe was not needed for the *in vivo* assembly of a RC that contained the other cofactors.

4.2.2. Characteristics of LH complexes.

Although Zn-BChl incorporation into an LH1-type complex has been reported for *Ac. rubrum* (Wakao et al. 1996), the presence of Zn-BChl in the *Rb. sphaeroides* LH2-type complex described in this work is new. In the *bchD* mutant, the LH2 complex accumulated to a lesser extent than LH1, which may have been due to preferential targeting of limited amounts of Zn-BChl to the LH1 complex, rather than inefficient or unstable assembly of the LH2 complex with Zn-BChl. The low ratio of LH2/LH1 in the *bchD* mutant resembled the ratio in wt cells when low amounts of BChl limit photosynthetic apparatus development. In wt cultures undergoing a shift from high to low aeration, when BChl production first begins, the core RC-LH1 complex is assembled first, followed by the LH2 complex later in the maturation process (Koblizek et al. 2005).

More relevant to the *bchD* mutant steady-state situation are the results obtained with *Rb. sphaeroides* ALA-synthase mutants (Neidle & Kaplan 1993). In order for ALA-synthase mutants to produce BChl they must be fed exogenous ALA, allowing the modulation of the amount of BChl produced by altering the amount of ALA added. When only small amounts of ALA were given to the cells, limiting BChl production, the LH2:LH1 ratios were similar to what is seen for the *bchD* mutant (Neidle & Kaplan 1993). This effect

may also be linked to the lower cell densities in the *bchD* mutant cultures, which could have resulted in skewed LH development from higher oxygen levels.

4.2.3. The lack of photosynthetic proteins in other *bch* mutants.

Two other *bch* mutants were investigated and neither was found to have significant accumulation of RC or LH proteins. The absence of photosynthetic proteins in the *bchG* mutant could be explained from feedback inhibition from the accumulating bacteriochlorophyllide (BChlide) intermediate on the RC and LH genes. The structure of BChlide is identical to BChl, but lacking the hydrophobic phytol tail. Although the phytol tail of BChl is a significant part of the structure (see Figure 1-6), the macrocycle of BChlide is identical to that of fully formed BChl, and is one of the binding determinants in the RC pockets (Camara-Artigas et al. 2002; Fyfe et al. 2007). Nevertheless, BChlide may have had difficulties accessing the RC proteins in the membrane because of the much more polar nature of the molecule when it lacks phytol. Additionally, research has shown that the C-17[3] carboxylic acid group of BChlide, which is normally esterified to phytol in BChl, undergoes an intramolecular chelation of the central Mg^{2+} which may have implications for its ability to bind to the RC (Fiedor et al. 2008). It would be interesting to search for secondary mutants that allowed RC proteins to accumulate in the *bchG* mutant to see if they would assemble a photosynthetic apparatus with BChlide. The RC M protein found alone in the *bchY* mutant was likely not capable of binding any cofactors. The structure of the accumulating chlorophyllide intermediate is slightly different from BChl and would be expected to be able to bind to the RC.

Overall, these results seem to point towards the *bchD* mutant being a unique case, where deletion of a subunit of the first enzyme of the BChl-biosynthetic pathway is different than a deletion of *bch* genes that encode enzymes further down the pathway. In light of the results of the *bchY* and *bchG* mutants it is also interesting to speculate on whether the *bchD* mutant's phenotype is due solely to the loss of the BchD protein, or to the loss of the Mg-chelatase. It is known that the BchH protein has a different role from the other members of the Mg-chelatase, as it binds to the PPIX substrate (Sawicki &

Willows 2008). It would be interesting to see if *bchI* and *bchH* mutant strains exhibit the same phenotype as the *bchD* mutant.

4.2.3.1. Adaptation of blue-native PAGE for *Rb. sphaeroides*.

The successful adaptation of blue-native PAGE could have far reaching applications for the study of photosynthetic complexes in *Rb. sphaeroides* because it allows rapid and parallel visualization of photosystem complex abundance and composition. Furthermore, it will allow us to investigate the assembly process of the photosystem by taking time-point samples as cultures are shifted from photosystem repressing (aerobic) to inducing (anaerobic) conditions. Similarly, the many existing mutants of *Rb. sphaeroides* and *Rb. capsulatus* that have photosystem assembly defects (Aklujkar et al. 2000; Aklujkar et al. 2005a; Aklujkar et al. 2005b; Aklujkar et al. 2006; LeBlanc & Beatty 1996; Young et al. 1998) can be investigated with this technique, shedding fuller light on fundamental assembly processes of the photosynthetic machinery. A similar analysis has been successfully performed using these techniques on the cytochrome cbb_3 complex in *Rb. capsulatus* (Kulajta et al. 2006).

4.2.4. The origin of BPhe.

In all biological systems, BPhe has only ever been found in the type 2 RC complexes. Site-directed mutants of RC proteins have caused BPhe to assemble into the special pair sites (Bylina & Youvan 1988a; Kirmaier et al. 1988), and $B_{A,B}$ sites (Katilius et al. 2004; Katilius et al. 1999). This was accomplished by substituting a His residue, that normally ligates Mg^{2+} of the BChl macrocycle, to a Leu. The reverse has also be reported: substituting the Leu residues in the $H_{A,B}$ sites to His residues, results in the substitution of Mg-BChl in place of BPhe (Kirmaier et al. 1991; Watson et al. 2005). Nevertheless, these experiments do not establish whether the Leu residue itself dechelates BChl to BPhe as has been suggested previously (Jaschke & Beatty 2007). It is possible that molecules of BPhe and BChl are both present in the membrane and it is binding affinity that determines which are found in each site of the RC.

My results in this thesis support the affinity argument. Analysis of several mutants of *Rb. sphaeroides* (Section 3.1.6) lacking the *puhA*, *puf*, or *puc* genes, revealed that they still made BPhe, indicating that the RC complex was not necessary for BPhe production. These results also pointed towards a dechelatase activity that did not rely on the *puhA*, *puf*, or *puc* genes. RC pigment exchange experiments also support this hypothesis: BChls are always exchanged into $B_{A,B}$ sites and BPhes are always exchanged into the $H_{A,B}$ sites (Scheer & Hartwich 1995). BPhe likely binds to the $H_{A,B}$ sites because the steric occlusion caused by the Leu residue prevents entry of a water molecule that could ligate the Mg^{2+} of BChl.

Therefore, I suggest that the lack of BPhe in the *bchD* mutant was due to the inability of a dedicated dechelatase enzyme (outside of the aforementioned operons) to remove the strongly bound Zn^{2+} from Zn-BChl. It is known that an early step in BChl degradation in *Rb. sphaeroides* is dechelation of BChl to BPhe. However, the enzyme involved has never been identified (Haidl et al. 1985). It is possible that the disrupted Mg-chelatase enzyme itself has a role in the dechelation reaction, although this seems less likely because of the differing structures of PPIX and BChl. Finally, a non-enzymatic route to generating BPhe is conceivable, which would be hampered by the increased binding strength of Zn^{2+} to the chlorin and neutral pH of the growth conditions used in my work. Because Zn-BChl is much more resistant to pheophytinization (dechelation) than is BChl (Kobayashi et al. 1998), this property is likely responsible for the absence of BPhe.

4.2.5. The Zn-RC.

Based on the data collected in these experiments, I propose that the Zn-RC from the *bchD* mutant contains 6 Zn-BChl molecules: two of these make up P, two occupy the B positions and two occupy the H positions. The Zn-BChls are likely in very similar environments as the BChls and BPhes in the WT-RC, as the RC has proven to be structurally robust to alterations, including substitution of BPhe for BChl in the heterodimer mutant (Camara-Artigas et al. 2002). Furthermore, the spectral differences observed in the Q_X region were due to differences in the metal coordination state in the Zn-BChl molecules occupying the P and B positions compared to those occupying the H positions. Since there was no

protein ligand in the H_A and H_B sites for a fifth coordination to the metal in these Zn-BChl molecules (Allen et al. 1987), their Q_X band remained at a wavelength similar to that observed for tetracoordinated Zn-BChl in organic solvent (Hartwich et al. 1998). There are two BPhe Q_x bands in the WT-RC thought to arise from differences in hydrogen bonding (Bylina & Youvan 1988b), and so the similarity of the Q_x transitions for both Zn-BChls in the H-sites of the Zn-RC, as shown by one sharp band as opposed to the two separate bands in the WT-RC (Figure 3-10A), indicates that the hydrogen bonding is similar for both H site Zn-BChls in the Zn-RC.

Past work on *Rb. sphaeroides* RCs reconstituted *in vitro* with Zn-BChl derivatives bound to the $B_{A,B}$ sites indicated no significant changes in the binding, relative to Mg-BChl (Kobayashi et al. 2004). In another study, Zn-BChl was reconstituted into the *Rb. sphaeroides* RC P and $B_{A,B}$ sites, although only 30% occupancy was achieved. The absorption spectra of these partially reconstituted RCs yielded peaks at 864 nm for the special pair and 800 nm for the accessory BChls (Tomi et al. 2007). These values differ from the peaks attributed to the special pair (855 nm) and the accessory BChls (795 nm) in the RC purified from the *bchD* mutant, and in fact more closely resemble wild type RC peaks. The discrepancy is probably due to the low occupancy of Zn-BChl and incomplete removal of BChl in the reconstituted RCs in the other work (Tomi et al. 2007).

In contrast, the RC isolated from *Ac. rubrum*, which has RC proteins homologous to *Rb. sphaeroides* but assembles with four Zn-BChls *in vivo* (Haffa et al. 2002), has an absorption spectrum more similar to that of the RC isolated from the *bchD* mutant: the *Ac. rubrum* special pair peak is at 859 nm (vs. 855 nm for the *bchD* RC) and the accessory BChls peak is at 792 nm (vs. 795 nm). Evidently these absorption peak differences reflect amino acid sequence differences in the RC proteins. It was suggested that the difference in the amino acid at position 168 of the RC L protein (His versus Glu), between *Rb. sphaeroides* and *Ac. rubrum*, changes the electronic character of the special pair, allowing the *Ac. rubrum* RC with Zn-BChl to function similarly to the *Rb. sphaeroides* native RC (Tomi et al. 2007). Experiments on a RC L 168 His → Glu *Rb. sphaeroides* mutant RC showed a weakening or flattening of the special pair absorption peak compared to the native RC, similar to that seen in *Ac. rubrum* (Haffa et al. 2002; Tomi et al. 2007). My results support the idea that residue RC L 168 affects the electronic coupling of the special pair, because the special pair

to accessory BChl peak ratio in the *bchD* RC is more similar to the *Rb. sphaeroides* native RC than to the *Ac. rubrum* RC.

4.2.6. Speculation on the coordination state of the Zn-BChl bound to the H-sites of the Zn-RC.

From the position of the Q_X band in the Zn-RC spectrum, it appears that Zn-BChl in the H-site is tetracoordinated. This is very interesting because Mg-BChl and Zn-BChls have been observed exclusively in pentacoordinated states in all RCs studied to date (Tomi et al. 2007; Yeates et al. 1988). Evidence for the tetracoordination of the H-site Zn-BChls comes from the 560 nm peak position in the Zn-RC, which is similar to the Q_X band of tetracoordinated Zn-BChl in solution (Hartwich et al. 1998). The 775 nm band of this H-site Zn-BChl is somewhat red-shifted relative to the Zn-BChl Q_Y band in solution (normally 762 nm) (Hartwich et al. 1998), evidently because of protein-pigment interactions. A study of BChls containing different metals in organic solvents concluded that tetracoordination of the central Zn^{2+} in Zn-BChl results in a Q_X band in the 560 nm region, whereas a large red shift of this band (to around 580 nm) was observed in pentacoordinated Zn-BChl (Hartwich et al. 1998). This analysis reveals yet another unique aspect of the Zn-RC: not only are two Zn-BChl molecules binding to sites where only BPhe have been observed, but they are in a tetracoordination state not found in any other type 2 RC.

4.2.7. ET rates in the Zn-RC may be influenced more by the P→ B_A than by the B_A→ H_A transfer step.

The weak sensitivity of the primary ET rates to the difference in cofactor composition between the Zn-RC and WT-RC is remarkable considering the inherent energetic differences between BChl and BPhe molecules (Noy et al. 1998). However, as explained below, the observed similarity between the Zn-RC and WT-RC in the kinetics for the formation of the $P^+H_A^-$ state could be because the measured time constant for the $P^*H_A \rightarrow P^+H_A$-ET is more sensitive to the microscopic rate constant of the $P^* \rightarrow P^+B_A^-$ reaction than of the $P^+B_A^-H_A \rightarrow P^+B_AH_A^-$ reaction. If the two-step model ($P^*B_AH_A \rightarrow P^+B_A^-H_A \rightarrow P^+B_AH_A^-$) for ET holds (Arlt et al. 1993), then ET from P* to B takes 3 ps, whereas the transfer from B_A^- to H_A takes less than 1 ps, and so the first ET step is rate-limiting. One would expect that the P*

→ $P^+B_A^-$ step would be similar in the Zn-RC and the *Ac. rubrum* RC because the two RCs consist of homologous proteins and both share the identical cofactors in the P and B sites. Because the *Ac. rubrum* and *Rb. sphaeroides* WT-RCs have the same kinetics, it would not be surprising for the Zn-RC and the WT-RC to have the same kinetics for the initial ET. Therefore a moderate change in the kinetics of $P^+B_A^-$ → $P^+H_A^-$ would not affect the observed P* kinetics significantly. In other words, the energy of $P^+H_A^-$ can be varied to a certain extent without causing a major change in the P* to H_A ET rate. This explanation agrees with a study of RC mutants indicating that the initial ET rate is more sensitive to the energy changes in B and less sensitive to changes in H (Kirmaier et al. 1995).

The fact that the kinetics of ET are almost unaffected by simultaneously replacing Mg^{2+} with Zn^{2+} in all BChl cofactors and replacing BPhe with Zn-BChl is more difficult to explain than the changes in the ground state absorption spectrum. Previous studies showed that the replacement of cofactors at either the H or B positions has a great impact on ET kinetics, and can even alter the ET pathways (Katilius et al. 1999; Kirmaier et al. 1991; Lin et al. 1994). In the β-mutant, BPhe at the H_A position is replaced with a BChl, and the primary ET rate from P to H_A changes from 3.5 ps in the WT-RC to 6.5 ps in the β-mutant RC (Kirmaier et al. 1991). In the so-called ϕ-mutant, the BChl at the B_B position is replaced with a BPhe, causing 35% of ET to travel through the B-side cofactors (Katilius et al. 1999). One would think that the cofactor changes in the Zn-RC would have an impact comparable to the mutants described above; however, the ET steps from P to Q_A in the Zn-RC take place with rates and yields very similar to the WT-RC.

One explanation for the conservation of function is that the Zn-RC cofactor changes may maintain relative midpoint potentials. Although the cofactors in the Zn-RC are different from those of the WT-RC, the oxidation potential of P and the reduction potential of H_A may change in a coordinated fashion due to the influence of the protein, such that the energy difference between P* and $P^+H_A^-$ (and therefore the driving force) remain essentially the same. The blue-shifted absorption band in the Zn-RC suggests a higher P* energy than that of P* in the WT-RC and the P_{Zn}/P_{Zn}^+ midpoint potential for the Zn-RC was determined to be 10 mV more positive than that of the WT-RC.

What is unclear is the magnitude of the change in redox potential when BPhe is replaced with Zn-BChl at the H positions. The redox potential of H_A in RCs cannot be

measured directly from isolated RCs in buffer because such negative potentials degrade the RC (Lin 2009). However, the metal of Zn-BChl in the H-sites is very likely tetracoordinated, as argued above. Studies on the electrochemistry of BChl and BPhe in solvents shows that the redox potential of BChl can be altered to be nearly identical to BPhe, indicating that it is possible for the environment to play a major role in the electrochemistry of the cofactor (Cotton & Vanduyne 1979). However, other studies of metal-substituted BChls showed that Zn-BChl has a 0.14-0.16 V more negative redox potential than BPhe in organic solvents (Noy et al. 1998). The same study also found that the redox potential of BChls is linearly correlated with the Q_X transition band position. In the Zn-RC the H position Q_X band peak is 560 nm, only 15 nm from the BPhe band at 545 nm in the WT-RC, as opposed to the 40 nm from the P or B bands at 600 nm. This indicates that the electronic configuration, and thus the redox potential of the Zn-BChl at the H_A site is more similar to BPhe than to that of the P or B BChls. Therefore, these data predict that the tetracoordinated H-site Zn-BChl has a similar redox potential as a BPhe and that driving force and ET rates from P* to H_A in the Zn- and WT-RCs of *Rb. sphaeroides* should be similar. The experimental data of the current work are in agreement with this prediction.

4.2.8. Insight into different evolutionary strategies of type 1 and type 2 RCs.

The results for ET in the Zn-RC are interesting because they may enable a deeper understanding of the structure, function and evolution of RCs in general. The cyanobacterial and plant type 2 RCs in photosystem 2 (PS2) have an arrangement of chlorins similar to the purple bacterial WT-RC: in both cases P is a (B)Chl dimer, B sites contain (B)Chl, and H sites contain (B)Phe (Yeates et al. 1988; Zouni et al. 2001). In contrast, the cyanobacterial and plant type 1 RCs in photosystem 1 (PS1) have six Mg-containing Chls in a similar spatial arrangement, analogous to the Zn-RC, with the A_0 Chl in the PS1 RC equivalent to the H_A Zn-BChl in the Zn-RC (Ben-Shem et al. 2003; Jordan et al. 2001). It is interesting to note that in the PS1 RC protein, in contrast to the His residues coordinating the Mg^{2+} of the Chl molecules of P700, the sulfur of a Met side chain weakly ligates the Mg^{2+} in the Chl electron acceptor A_0. This sulfur coordination of Mg^{2+} is uniquely found in RCs that naturally contain a Chl (as opposed to a pheophytin) as the primary electron

acceptor A_0 (Fromme et al. 2001; Jordan et al. 2001). It was shown that changing the Met residue at this site to His reduces the rate of ET from P to A_0, indicating that the weak ligation of the Mg^{2+} in the A_0 Chl to Met in the PS1 RC results in an interaction that resembles tetracoordination (Ramesh et al. 2007). We know this ligation is weaker and causes a similar effect on the Q_x energy of the A_0 Chl in the PS1 RC, as is seen for the Zn-RC, because *in vitro* studies on BChls in solvents that donate a fifth ligand to the Mg^{2+} in BChl show that an axial sulfur ligand, as opposed to nitrogen, displays a marked 3-25 nm blue-shift in the Q_x band (Callahan & Cotton 1987). From both these data and our results, I suggest the coordination state of BChls is a key factor in governing the midpoint potential and hence the rate of ET in RCs.

I speculate that evolution has resulted in two strategies for a high rate of ET in RCs: (1) in the type 2 RCs (as in *Rb. sphaeroides* WT-RC), the primary electron acceptor is a (B)Phe surrounded by protein that excludes (B)Chl and water from the H sites; (2) in the type 1 RCs (as in cyanobacteria and eukaryotic chloroplasts), the primary acceptor is a Chl (A_0), but this Chl functions well as the primary acceptor because the Mg^{2+} in the A_0 Chl is ligated weakly by a sulphur atom coming from the protein, endowing this Chl with tetracoordination-like electrochemical properties (Figure 4-2). This work is the first example of a RC from purple bacteria in which the energetic differences that dictate the kinetics of ET are determined predominantly by the protein environment of six identical cofactors, analogous to PS1 of plants and cyanobacteria. Thus, one may think of the Zn-RC as a combination of the protein of a type 2 RC and the cofactors of a type 1 RC.

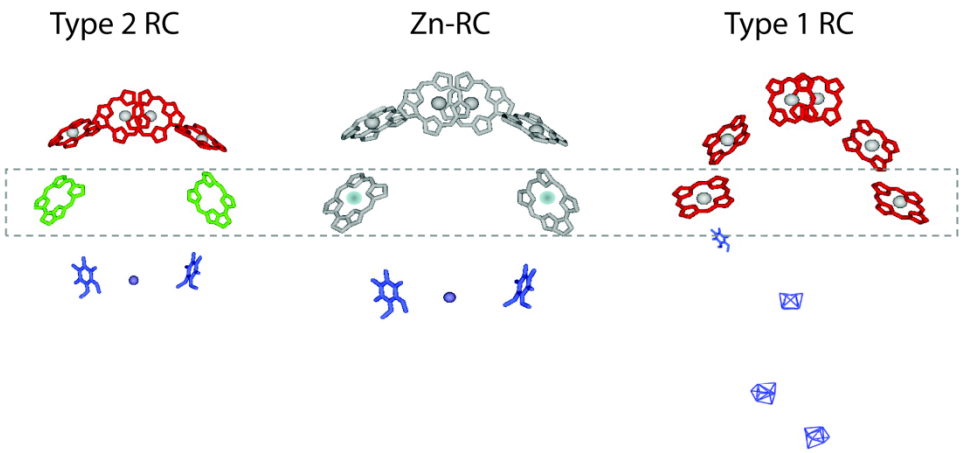

Figure 4-2. Comparison of the different RC cofactor arrangements. (B)Chls in red; BPhe in green; Zn-BChl in grey; Quinone and Fe-S protein terminal electron acceptors in blue. Cytoplasm is towards the bottom. Figure courtesy of Su Lin (Lin et al. 2009b).

4.3. Evolutionary significance of the Zn-BChl biosynthetic pathway and photosystem.

It is interesting to speculate about the significance of this alternative BChl-biosynthetic pathway. Is it merely chance that Zn-PPIX can be created by ferrochelatase under the right conditions, and then handed off to the subsequent enzymes in the BChl biosynthetic pathway? Or, is it possible that this reveals an ancestral pathway that functioned prior to the evolution of Mg-chelatase?

The ancestor of all photosynthetic organisms has been proposed to have resembled a purple bacterium, which lived in a reduced anaerobic environment containing Mg^{2+}, Fe^{2+}, and Zn^{2+} (Nisbet et al. 1995; Xiong et al. 2000). Zinc abundance under these conditions would have been highly dependent on pH with acidic conditions favoring Zn^{2+} availability, and more neutral conditions favoring the loss of soluble Zn^{2+} as ZnS, $ZnCl_2$, and $Zn(OH_2)_2$ precipitates (Lazcano & Miller 1996; Lide 2009c; Williams 1997).

It is conceivable that a ferrochelatase in this hypothetical ancestor would have led to the production of Fe-PPIX (heme), as well as some Zn-PPIX due to the proposed promiscuous nature of most early enzymes, and the present-day plasticity of substrates that are accepted by this enzyme (Dailey 1982; Jacobs et al. 1998; Jensen 1976; Jones & Jones 1970; Pretlow & Sherman 1967). With the production of Zn-PPIX, the cell could have dealt with this molecule in three general ways: (1) ferrochelatase could have evolved to

prevent Zn-PPIX from being generated, by reducing the specificity for Zn^{2+}; (2) cells could have developed mechanisms to keep Zn^{2+} away from ferrochelatase; or (3) cells could have developed regulatory mechanisms to keep PPIX levels under strict control.

In contrast, some organisms may have found a way to harness the Zn-PPIX molecule's light-absorption properties, and developed a primitive light protective system, or light-sensing system, that utilized Zn-PPIX. These systems may already have existed with PPIX, but Zn-PPIX has advantages over PPIX for these uses: (1) higher molar absorptivity (Falk 1964); (2) a 10 nm red-shift of the absorption maximum (Hay 2009) that slightly decreases the energy of absorbed photons, but increases exponentially the amount of solar energy available at that wavelength due to the uneven nature of the Sun's emission spectrum (Lide 2009b). Over time the cell that utilized Zn-PPIX could have eventually developed a type of RC that bound Zn-PPIX and generated energy through ET processes (Blankenship 1992).

In this scenario, enzymes would have subsequently evolved to decorate the carbon skeleton of Zn-PPIX, generating a variety of spectral properties that would have been advantageous to bacteria in different niches (Chew & Bryant 2007). Evidence for this step-wise alteration comes from organisms that today still use protochlorophyllides for light-harvesting (Helfrich et al. 1999; Larkum et al. 1994). The evolution of the enzymes catalyzing subsequent steps in (B)Chl synthesis appears to have occurred mainly through the common processes of gene duplication and diversification of function (Jensen 1976), from other established enzyme families. Evidence for these processes is seen in the *bchBLN* and *bchXYZ* complexes, which probably evolved from nitrogenase (Fujita & Bauer 2000; Nomata et al. 2006), and from Chl and BChl synthases, which share homology and catalyze phytol addition to the same site of their respective substrates (Kim & Lee 2010).

At some point during this billion-year process, a Mg-chelatase would have evolved. The selective advantage for Mg-chelatase development could have been due to changes to the environment, such as the pH moving more towards neutral, which would have dramatically reduced the solubility of ZnS versus MgS (Lide 2009c). The organism that developed the Mg-chelatase would have had a huge selective advantage over other groups if the change was toward a present-day ocean chemistry, because Mg^{2+} is 10^6-fold more abundant than Zn^{2+} in the present-day oceans (Lide 2009a). This adaptation would

have come to dominate in populations, with results seen today: every photosynthetic organism discovered to date synthesizes (B)Chls through a Mg-chelatase complex, except the *bchD* mutant of *Rb. sphaeroides*.

The only organisms known previously to this work to make Zn-(B)Chl, synthesize the pigment in acidic conditions (Hiraishi & Shimada 2001; Ikegami et al. 2005; Masuda et al. 1999; Wakao et al. 1996). But even these organisms use the Mg-chelatase to synthesize normal Mg-(B)Chl, and then somehow swap Mg^{2+} for Zn^{2+} via a demetallated intermediate such as BPhe (Ikegami et al. 2005; Masuda et al. 1999). The Mg-chelatase was obviously a significant and important enzyme in the development of photosynthesis.

The inefficiency of the Zn-BChl pathway that I have described in this thesis can be explained if the Mg-chelatase was 'invented' before the evolution of the terminal steps in the pathway, such that the enzymes that arose later were inefficient at using Zn-containing substrates. Such a pattern can be seen in my data (Figure 4-1), where the enzymes downstream of BchM seem to be less efficient at using Zn-substrates than those upstream. This pattern would point to the pathway having developed only up to BchM at the time of Mg-chelatase evolution. This idea does have some problems, because the Bch-homologous enzymes downstream of *ChlE* in Chl-synthesis have been shown to use Zn-containing substrates relatively efficiently (Nasrulhaqboyce et al. 1987; Rüdiger et al. 2005; Scheumann et al. 1996a; Scheumann et al. 1996b; Schoch & Ihl 1998).

It would be interesting to see if other purple photosynthetic bacteria are able to synthesize Zn-BChl when the *bchD* gene is inactivated, which will help us to determine whether this is a universal alternative biosynthetic pathway or a specialized feature of *Rb. sphaeroides*.

4.4. Summary and future directions

This thesis work began by trying to elucidate the assembly of the RC complex, but instead led to the discovery of a fascinating mutant that is able to re-route its biosynthetic pathway around a knockout in the Mg-chelatase, and produce a type of chlorophyll rarely seen in nature. I described a *bchD* mutant of *Rb. sphaeroides* from several different approaches, to investigate how this transformation affects the organism. This was done

with the goal of enabling a deeper understanding of both extant photosynthetic processes as well as the evolution of photosynthesis.

I began my research on the *bchD* mutant by examining the proteins of the photosynthetic apparatus, and found they were still expressed and assembled, only with Zn-BChl instead of Mg-BChl and BPhe. The Zn-RC from the *bchD* mutant is a unique photosynthetic complex emerging from the combination of the six identical (B)Chls of type 1 RCs, and the protein structure of type 2 RCs. Despite the hybrid structure, the Zn-RC transfers electrons with nearly the same rates as the WT-RC, highlighting the robustness of ET in this complex.

A high-resolution structure of the Zn-RC is an important future goal for this project. With such a structure we could directly visualize the coordination state of the Zn-BChls binding to the H-sites. Raman spectroscopic examination of the Zn-RC would also reveal more information about the coordination state of the H-site cofactors. This information will be important for understanding how redox potentials of (B)Chls are tuned by the protein environment.

Additionally, it would be informative to study how energy is transferred from the Zn-BChl-containing LH2 complexes to LH1 and finally to the RC. The function of a LH2 complex binding Zn-BChl has never been studied and could yield interesting results regarding the photosynthetic deficiency of the *bchD* mutant. A further avenue of study would involve construction of an RC-only strain of the *bchD* mutant. This strain would help us understand the interplay of the LH1 and RC. Could this strain be able to grow photosynthetically with only the RC? Although the Zn-RC transfers electrons similarly to the WT-RC, we know virtually nothing else, aside from the absorption spectra and levels of proteins, about the LH2 and LH1 complexes in this organism. Perhaps the blue-native- and clear-native-PAGE techniques that have been developed will help analyze the superstructure of these complexes, and uncover the reason for the photosynthetic deficiency of the *bchD* mutant.

This research could be taken further by simultaneously inhibiting ferrochelatase, to prevent Zn-PPIX synthesis in the *bchD* mutant, while feeding the cells commercially-available metalloprotoporphyrins IX containing metals such as Cd^{2+}, Pb^{2+}, Cu^{2+} and Ni^{2+}, to see if the corresponding BChl is synthesized. If all enzymes in the BChl pathway cannot

process the substrate, it would reveal valuable information on the active sites of the enzymatic step where it was blocked. If the whole pathway can process the substrate it has the potential to allow the study of the structure and function of modified photosystems that contain these novel BChls.

BIBLIOGRAPHY

Abresch, E. C., Axelrod, H. L. A., Beatty, J. T., Johnson, J. A., Nechushtai, R. & Paddock, M. L. 2005 Characterization of a highly purified, fully active, crystallizable RC-LH1-PufX core complex from *Rhodobacter sphaeroides*. *Photosynthesis Research* **86**, 61-70.

Addlesee, H. A., Fiedor, L. & Hunter, C. N. 2000 Physical mapping of *bchG*, *orf427*, and *orf177* in the photosynthesis gene cluster of *Rhodobacter sphaeroides*: functional assignment of the bacteriochlorophyll synthetase gene. *Journal of Bacteriology* **182**, 3175-3182.

Addlesee, H. A. & Hunter, C. N. 1999 Physical mapping and functional assignment of the geranylgeranyl-bacteriochlorophyll reductase gene, *bchP*, of *Rhodobacter sphaeroides*. *Journal of Bacteriology* **181**, 7248-7255.

Adelroth, P., Paddock, M. L., Tehrani, A., Beatty, J. T., Feher, G. & Okamura, M. Y. 2001 Identification of the proton pathway in bacterial reaction centers: decrease of proton transfer rate by mutation of surface histidines at H126 and H128 and chemical rescue by imidazole identifies the initial proton donors. *Biochemistry* **40**, 14538-14546.

Aklujkar, M., Harmer, A. L., Prince, R. C. & Beatty, J. T. 2000 The *orf162b* sequence of *Rhodobacter capsulatus* encodes a protein required for optimal levels of photosynthetic pigment-protein complexes. *Journal of Bacteriology* **182**, 5440-7.

Aklujkar, M., Prince, R. C. & Beatty, J. T. 2005a The PuhB protein of *Rhodobacter capsulatus* functions in photosynthetic reaction center assembly with a secondary effect on light-harvesting complex 1. *Journal of Bacteriology* **187**, 1334-43.

Aklujkar, M., Prince, R. C. & Beatty, J. T. 2005b The *puhE* gene of *Rhodobacter capsulatus* is needed for optimal transition from aerobic to photosynthetic growth and encodes a putative negative modulator of bacteriochlorophyll production. *Archives of Biochemistry and Biophysics* **437**, 186-98.

Aklujkar, M., Prince, R. C. & Beatty, J. T. 2006 The photosynthetic deficiency due to *puhC* gene deletion in *Rhodobacter capsulatus* suggests a PuhC protein-dependent process of RC/LH1/PufX complex reorganization. *Archives of Biochemistry and Biophysics* **454**, 59-71.

Allen, J. P., Artz, K., Lin, X., Williams, J. C., Ivancich, A., Albouy, D., Mattioli, T. A., Fetsch, A., Kuhn, M. & Lubitz, W. 1996 Effects of hydrogen bonding to a bacteriochlorophyll-bacteriopheophytin dimer in reaction centers from *Rhodobacter sphaeroides*. *Biochemistry* **35**, 6612-9.

Allen, J. P., Feher, G., Yeates, T. O., Komiya, H. & Rees, D. C. 1987 Structure of the reaction center from *Rhodobacter sphaeroides* R-26: the cofactors. *Proceedings of the National Academy of Sciences of the United States of America* **84**, 5730-4.

Arlt, T., Schmidt, S., Kaiser, W., Lauterwasser, C., Meyer, M., Scheer, H. & Zinth, W. 1993 The accessory bacteriochlorophyll: a real electron carrier in primary photosynthesis. *Proceedings of the National Academy of Sciences of the United States of America* **90**, 11757-61.

Bahatyrova, S., Frese, R. N., Siebert, C. A., Olsen, J. D., van der Werf, K. O., van Grondelle, R., Niederman, R. A., Bullough, P. A., Otto, C. & Hunter, C. N. 2004 The native architecture of a photosynthetic membrane. *Nature* **430**, 1058-1062.

Barrett, J. & Jones, O. T. G. 1978 Localization of ferrochelatase and of newly synthesized heme in membrane-fractions from *Rhodopseudomonas spheroides*. *Biochemical Journal* **174**, 277-281.

Beale, S. I. 1995 Biosynthesis and structures of porphyrins and hemes. In *Anoxygenic photosynthetic bacteria* (ed. R. E. Blankenship, M. T. Madigan & C. E. Bauer), pp. 153-177: Kluwer Academic Publishers.

Beatty, J. T., Johansson, B. C., Wall, J. D. & Gest, H. 1977 Nitrogen assimilation defects in a mutant of *Rhodopseudomonas capsulata* blocked in alpha-ketoglutarate generation. *FEMS Microbiology Letters* **2**, 267-270.

Beck, R., Raux, E., Thermes, C., Rambach, A. & Warren, M. 1997 CbiX: a novel metal-binding protein involved in sirohaem biosynthesis in *Bacillus megaterium*. *Biochemical Society transactions* **25**, 77S.

Belanger, F. C. & Rebeiz, C. A. 1980 Chloroplast biogenesis: detection of divinyl protochlorophyllide in higher plants. *The Journal of Biological Chemistry* **255**, 1266-1272.

Ben-Shem, A., Frolow, F. & Nelson, N. 2003 Crystal structure of plant photosystem I. *Nature* **426**, 630-5.

Bickar, D. & Reid, P. D. 1992 A high-affinity protein stain for western blots, tissue prints, and electrophoretic gels. *Analytical Biochemistry* **203**, 109-115.

Blankenship, R. E. 1992 Origin and early evolution of photosynthesis. *Photosynthesis Research* **33**, 91-111.

Bollivar, D. W., Suzuki, J. Y., Beatty, J. T., Dobrowolski, J. M. & Bauer, C. E. 1994 Directed mutational analysis of bacteriochlorophyll *a* biosynthesis in *Rhodobacter capsulatus*. *Journal of Molecular Biology* **237**, 622-640.

Brand, M. & Drews, G. 1997 The role of pigments in the assembly of photosynthetic complexes in *Rhodobacter capsulatus*. *Journal of Basic Microbiology* **37**, 235-244.

Broglie, R. M., Hunter, C. N., Delepelaire, P., Niederman, R. A., Chua, N. H. & Clayton, R. K. 1980 Isolation and characterization of the pigment-protein complexes of *Rhodopseudomonas sphaeroides* by lithium dodecyl sulfate/polyacrylamide gel electrophoresis. *Proceedings of the National Academy of Sciences of the United States of America* **77**, 87-91.

Brown, A. E., Eiserlin, F. A. & Lascelles, J. 1972 Bacteriochlorophyll synthesis and ultrastructure of wild-type and mutant strains of *Rhodopseudomonas spheroides*. *Plant Physiology* **50**, 743-746.

Bryant, D. 2010 Personal Communication.

Burke, D. H., Alberti, M. & Hearst, J. E. 1993a *bchFNBH* bacteriochlorophyll synthesis genes of *Rhodobacter capsulatus* and identification of the third subunit of light-independent protochlorophyllide reductase in bacteria and plants. *Journal of Bacteriology* **175**, 2414-2422.

Burke, D. H., Alberti, M. & Hearst, J. E. 1993b The *Rhodobacter capsulatus* chlorin reductase-encoding locus, *bchA*, consists of three genes, *bchX*, *bchY*, and *bchZ*. *Journal of Bacteriology* **175**, 2407-2413.

Burnham, B. F. & Lascelles, J. 1963 Control of porphyrin biosynthesis through a negative-feedback mechanism: studies with preparations of delta-aminolaevulate synthetase and delta-aminolaevulate dehydratase from *Rhodopseudomonas spheroides*. *Biochemical Journal* **87**, 462-465.

Bydder, M., Rahal, A., Fullerton, G. D. & Bydder, G. M. 2007 The magic angle effect: a source of artifact, determinant of image contrast, and technique for imaging. *Journal of Magnetic Resonance Imaging* **25**, 290-300.

Bylina, E. J. & Youvan, D. C. 1988a Directed Mutations Affecting Spectroscopic and Electron-Transfer Properties of the Primary Donor in the Photosynthetic Reaction Center. *Proceedings of the National Academy of Sciences of the United States of America* **85**, 7226-7230.

Bylina, E. J. & Youvan, D. C. 1988b Directed mutations affecting spectroscopic and electron transfer properties of the primary donor in the photosynthetic reaction center. *Proceedings of the National Academy of Sciences of the United States of America* **85**, 7226-7230.

Callahan, P. M. & Cotton, T. M. 1987 Assignment of bacteriochlorophyll *a* ligation state from absorption and resonance Raman spectra. *Journal of the American Chemical Society* **109**, 7001-7007.

Camara-Artigas, A., Magee, C., Goetsch, A. & Allen, J. P. 2002 The structure of the heterodimer reaction center from *Rhodobacter sphaeroides* at 2.55 Å resolution. *Photosynthesis Research* **74**, 87-93.

Che, A., Cui, J. & Dinov, I. 2009 SOCR analyses - an instructional Java web-based statistical analysis toolkit. *Journal of Online Learning and Teaching* **5**, 1-19.

Chekounova, E., Voronetskaya, V., Papenbrock, J., Grimm, B. & Beck, C. F. 2001 Characterization of *Chlamydomonas* mutants defective in the H subunit of Mg-chelatase. *Molecular Genetics and Genomics* **266**, 363-73.

Chew, A. G. M. & Bryant, D. A. 2007 Chlorophyll biosynthesis in bacteria: the origins of structural and functional diversity. *Annual Review of Microbiology* **61**, 113-129.

Chory, J., Donohue, T. J., Varga, A. R., Staehelin, L. A. & Kaplan, S. 1984 Induction of the photosynthetic membranes of *Rhodopseudomonas sphaeroides*: biochemical and morphological studies. *Journal of Bacteriology* **159**, 540-554.

Choudhary, M., Zanhua, X., Fu, Y. X. & Kaplan, S. 2007 Genome analyses of three strains of *Rhodobacter sphaeroides*: evidence of rapid evolution of chromosome II. *Journal of Bacteriology* **189**, 1914-21.

Coomber, S. A., Chaudhri, M., Connor, A., Britton, G. & Hunter, C. N. 1990 Localized transposon Tn5 mutagenesis of the photosynthetic gene cluster of *Rhodobacter sphaeroides*. *Molecular Microbiology* **4**, 977-989.

Cotton, T. M. & Vanduyne, R. P. 1979 Electrochemical investigation of the redox properties of bacteriochlorophyll and bacteriopheophytin in aprotic-solvents. *Journal of the American Chemical Society* **101**, 7605-7612.

D'Amici, G. M., Rinalducci, S., Murgiano, L., Italiano, F. & Zolla, L. 2010 Oligomeric characterization of the photosynthetic apparatus of *Rhodobacter sphaeroides* R26.1 by nondenaturing electrophoresis methods. *Journal of Proteome Research* **9**, 192-203.

Dailey, H. A. 1982 Purification and characterization of membrane-bound ferrochelatase from *Rhodopseudomonas sphaeroides*. *The Journal of Biological Chemistry* **257**, 14714-8.

Dawson, R. M. C., Elliott, D. C., Elliott, W. H. & M., J. K. 1986 Porphyrins and related compounds. In *Data for biochemical research*, pp. 213-238: Oxford University Press.

Eichacker, L. A., Soll, J., Lauterbach, P., Rüdiger, W., Klein, R. R. & Mullet, J. E. 1990 *In vitro* synthesis of chlorophyll *a* in the dark triggers accumulation of chlorophyll *a* apoproteins in barley etioplasts. *The Journal of Biological Chemistry* **265**, 13566-13571.

Falk, J. E. 1964 *Porphyrins and metalloporphyrins: their general, physical and coordination chemistry, and laboratory methods.* B.B.A. Library. Amsterdam: Elsevier Publishing Company.

Feher, G., Allen, J. P., Okamura, M. Y. & Rees, D. C. 1989 Structure and function of bacterial photosynthetic reaction centers. *Nature* **339**, 111-116.

Fellay, R., Frey, J. & Krisch, H. 1987 Interposon mutagenesis of soil and water bacteria: a family of DNA fragments designed for *in vitro* insertional mutagenesis of gram-negative bacteria. *Gene* **52**, 147-54.

Fiedor, L., Kania, A., Mysliwa-Kurdziel, B., Orzel, L. & Stochel, G. 2008 Understanding chlorophylls: central magnesium ion and phytyl as structural determinants. *Biochimica Et Biophysica Acta* **1777**, 1491-1500.

Fodje, M. N., Hansson, A., Hansson, M., Olsen, J. G., Gough, S., Willows, R. D. & Al-Karadaghi, S. 2001 Interplay between an AAA module and an integrin I domain may regulate the function of magnesium chelatase. *Journal of Molecular Biology* **311**, 111-122.

Francia, F., Dezi, M., Rebecchi, A., Mallardi, A., Palazzo, G., Melandri, B. A. & Venturoli, G. 2004 Light-harvesting complex 1 stabilizes $P^{+}Q_{B}^{-}$ charge separation in reaction centers of *Rhodobacter sphaeroides*. *Biochemistry* **43**, 14199-14210.

Fromme, P., Jordan, P. & Krauss, N. 2001 Structure of photosystem I. *Biochimica Et Biophysica Acta* **1507**, 5-31.

Fujita, Y. & Bauer, C. E. 2000 Reconstitution of light-independent protochlorophyllide reductase from purified Bchl and BchN-BchB subunits. *In vitro* confirmation of nitrogenase-like features of a bacteriochlorophyll biosynthesis enzyme. *The Journal of Biological Chemistry* **275**, 23583-8.

Fyfe, P. K., Potter, J. A., Cheng, J., Williams, C. M., Watson, A. J. & Jones, M. R. 2007 Structural responses to cavity-creating mutations in an integral membrane protein. *Biochemistry* **46**, 10461-72.

Garcia-Horsman, J. A., Berry, E., Shapleigh, J. P., Alben, J. O. & Gennis, R. B. 1994 A novel cytochrome c oxidase from *Rhodobacter sphaeroides* that lacks CuA. *Biochemistry* **33**, 3113-9.

Geyer, T. & Helms, V. 2006 A spatial model of the chromatophore vesicles of *Rhodobacter sphaeroides* and the position of the cytochrome bc_1 complex. *Biophysical Journal* **91**, 921-926.

Gibson, K. D., Neuberger, A. & Tait, G. H. 1963 Studies on the biosynthesis of porphyrin and bacteriochlorophyll by *Rhodopseudomonas spheroides*. 4. S-Adenosylmethionine-magnesium protoporphyrin methyltransferase. *The Biochemical Journal* **88**, 325-334.

Gibson, L. C. D. & Hunter, C. N. 1994 The bacteriochlorophyll biosynthesis gene, *bchM*, of *Rhodobacter sphaeroides* encodes S-adenosyl-L-methionine: Mg protoporphyrin IX methyltransferase. *FEBS Letters* **352**, 127-130.

Gibson, L. C. D., Willows, R. D., Kannangara, C. G., von Wettstein, D. & Hunter, C. N. 1995 Magnesium-protoporphyrin chelatase of *Rhodobacter sphaeroides*: reconstitution of activity by combining the products of the *bchH*, *-I*, and *-D* genes expressed in *Escherichia coli*. *Proceedings of the National Academy of Sciences of the United States of America* **92**, 1941-1944.

Gilardi, A., Djavadio.L, Labbe, P. & Chaix, P. 1971 Effect of Zn-protoporphyrin accumulation by yeast cells on synthesis and activity of their respiratory system. *Biochimica Et Biophysica Acta* **234**, 446-457.

Goldsmith, J. O. & Boxer, S. G. 1996 Rapid isolation of bacterial photosynthetic reaction centers with an engineered poly-histidine tag. *Biochimica Et Biophysica Acta* **1276**, 171-175.

Gough, S. P., Petersen, B. O. & Duus, J. O. 2000 Anaerobic chlorophyll isocyclic ring formation in *Rhodobacter capsulatus* requires a cobalamin cofactor. *Proceedings of the National Academy of Sciences of the United States of America* **97**, 6908-13.

Grimal, D. & Labbe-Bois, R. 1980 An enrichment method for heme-less mutants of *Saccharomyces cerevisiae* based on photodynamic properties of Zn-protoporphyrin. *Molecular and General Genetics* **178**, 713-6.

Haffa, A. L. M., Lin, S., Katilius, E., Williams, J. C., Taguchi, A. K. W., Allen, J. P. & Woodbury, N. W. 2002 The dependence of the initial electron-transfer rate on driving force in *Rhodobacter sphaeroides* reaction centers. *The Journal of Physical Chemistry. B* **106**, 7376-7384.

Haidl, H., Knodlmayr, K., Rudiger, W., Scheer, H., Schoch, S. & Ullrich, J. 1985 Degradation of bacteriochlorophyll *a* in *Rhodopseudomonas sphaeroides* R26. *Zeitschrift Fur Naturforschung C-a Journal of Biosciences* **40**, 685-692.

Hartwich, G., Fiedor, L., Simonin, I., Cmiel, E., Schafer, W., Noy, D., Scherz, A. & Scheer, H. 1998 Metal-substituted bacteriochlorophylls. 1. Preparation and influence of metal and coordination on spectra. *Journal of the American Chemical Society* **120**, 3675-3683.

Hawkins, K. M. & Smolke, C. D. 2008 Production of benzylisoquinoline alkaloids in *Saccharomyces cerevisiae*. *Nature Chemical Biology* **4**, 564-73.

Hay, J. 2009 Zn-PPIX extinction coefficient.

Heath, R. L. 1981 Table of the isotopes. In *CRC Handbook of chemistry and physics, 62nd Edtion* (ed. R. C. Weast), pp. B255-B339. Boca Raton: CRC Press.

Helfrich, M., Ross, A., King, G. C., Turner, A. G. & Larkum, A. W. D. 1999 Identification of [8-vinyl]-protochlorophyllide *a* in phototrophic prokaryotes and algae: chemical and spectroscopic properties. *Biochimica Et Biophysica Acta* **1410**, 262-272.

Hiraishi, A. & Shimada, K. 2001 Aerobic anoxygenic photosynthetic bacteria with zinc-bacteriochlorophyll. *The Journal of General and Applied Microbiology* **47**, 161-180.

Holden-Dye, K., Crouch, L. I. & Jones, M. R. 2008 Structure, function and interactions of the PufX protein. *Biochimica Et Biophysica Acta* **1777**, 613-30.

Hoogewerf, G. J., Jung, D. O. & Madigan, M. T. 2003 Evidence for limited species diversity of bacteriochlorophyll *b*-containing purple nonsulfur anoxygenic phototrophs in freshwater habitats. *FEMS microbiology letters* **218**, 359-64.

Houghton, J. D., Honeybourne, C. L., Smith, K. M., Tabba, H. D. & Jones, O. T. 1982 The use of N-methylprotoporphyrin dimethyl ester to inhibit ferrochelatase in *Rhodopseudomonas sphaeroides* and its effect in promoting biosynthesis of magnesium tetrapyrroles. *Biochemical Journal* **208**, 479–486.

Hsu, J., Goldstein, B. D. & Harber, L. C. 1971 Photoreactions associated with *in vitro* hemolysis in erythropoietic protoporphyria. *Photochemistry and Photobiology* **13**, 67-77.

Humphrey, W., Dalke, A. & Schulten, K. 1996 VMD: Visual molecular dynamics. *Journal of Molecular Graphics* **14**, 33-&.

Hunter, C. N. & Coomber, S. A. 1988 Cloning and oxygen-regulated expression of the bacteriochlorophyll biosynthesis genes *bch E, B, A,* and *C* of *Rhodobacter sphaeroides*. *Journal of General Microbiology* **134**, 1491-1497.

Hunter, C. N., Pennoyer, J. D., Sturgis, J. N., Farrelly, D. & Niederman, R. A. 1988 Oligomerization states and associations of light-harvesting pigment-protein complexes of *Rhodobacter sphaeroides* as analyzed by lithium dodecyl sulfate-polyacrylamide gel electrophoresis. *Biochemistry* **27**, 3459-3467.

Hunter, C. N., Tucker, J. D. & Niederman, R. A. 2005 The assembly and organisation of photosynthetic membranes in *Rhodobacter sphaeroides*. *Photochemical & Photobiological Sciences* **4**, 1023-1027.

Ikegami, I., Nemoto, A. & Sakashita, K. 2005 The formation of Zn-Chl *a* in *Chlorella* heterotrophically grown in the dark with an excessive amount of Zn^{2+}. *Plant & Cell Physiology* **46**, 729-735.

Itoh, S., Iwaki, M., Wakao, N., Yoshizu, K., Aoki, A. & Tazaki, K. 1998 Accumulation of Fe, Cr and Ni metals inside cells of acidophilic bacterium *Acidiphilium rubrum* that produces Zn-containing bacteriochlorophyll *a*. *Plant & Cell Physiology* **39**, 740-744.

Iyer, L. M., Leipe, D. D., Koonin, E. V. & Aravind, L. 2004 Evolutionary history and higher order classification of AAA+ ATPases. *Journal of Structural Biology* **146**, 11-31.

Jacobs, J. M., Sinclair, P. R., Sinclair, J. F., Gorman, N., Walton, H. S., Wood, S. G. & Nichols, C. 1998 Formation of zinc protoporphyrin in cultured hepatocytes: effects of ferrochelatase inhibition, iron chelation or lead. *Toxicology* **125**, 95-105.

Jaschke, P., LeBlanc, H., Lang, A. & Beatty, J. 2008 The PucC protein of *Rhodobacter capsulatus* mitigates an inhibitory effect of light-harvesting 2 α and β proteins on light-harvesting complex 1. *Photosynthesis Research* **95**, 279-284.

Jaschke, P. R. & Beatty, J. T. 2007 The photosystem of *Rhodobacter sphaeroides* assembles with zinc bacteriochlorophyll in a *bchD* (magnesium chelatase) mutant. *Biochemistry* **46**, 12491-12500.

Jaschke, P. R., Drake, I. & Beatty, J. 2009 Modification of a French pressure cell to improve microbial cell disruption. *Photosynthesis Research* **102**, 95-97.

Jeffke, T., Gropp, N. H., Kaiser, C., Grzeszik, C., Kusian, B. & Bowien, B. 1999 Mutational analysis of the *cbb*$_3$ operon (CO_2 assimilation) promoter of *Ralstonia eutropha*. *Journal of Bacteriology* **181**, 4374-4380.

Jensen, R. A. 1976 Enzyme recruitment in evolution of new function. *Annual Review of Microbiology* **30**, 409-25.

Johnson, A. & Jones, O. G. 1964 Enzymic formation of haems and other metalloporphyrins. *Biochimica Et Biophysica Acta* **93**, 171-3.

Jones, M. R. 2009 The petite purple photosynthetic powerpack. *Biochemical Society transactions* **37**, 400-7.

Jones, M. R., Visschers, R. W., Vangrondelle, R. & Hunter, C. N. 1992 Construction and characterization of a mutant of *Rhodobacter sphaeroides* with the reaction center as the sole pigment protein complex. *Biochemistry* **31**, 4458-4465.

Jones, M. S. & Jones, O. T. 1970 Ferrochelatase of *Rhodopseudomonas spheroides*. *The Biochemical Journal* **119**, 453-62.

Jordan, P., Fromme, P., Witt, H. T., Klukas, O., Saenger, W. & Krauss, N. 2001 Three-dimensional structure of cyanobacterial photosystem I at 2.5 Å resolution. *Nature* **411**, 909-17.

Kanazireva, E. & Biel, A. J. 1996 Nucleotide sequence of the *Rhodobacter capsulatus hemH* gene. *Gene* **170**, 149-150.

Kannangara, C. G., Vothknecht, U. C., Hansson, M. & von Wettstein, D. 1997 Magnesium chelatase: association with ribosomes and mutant complementation studies identify barley subunit Xantha-G as a functional counterpart of *Rhodobacter* subunit BchD. *Molecular and General Genetics* **254**, 85-92.

Katilius, E. 2009 ASUFIT http://www.public.asu.edu/~laserweb/asufit/asufit.html.

Katilius, E., Babendure, J. L., Lin, S. & Woodbury, N. W. 2004 Electron transfer dynamics in *Rhodobacter sphaeroides* reaction center mutants with a modified ligand for the monomer bacteriochlorophyll on the active side. *Photosynthesis Research* **81**, 165-180.

Katilius, E., Turanchik, T., Lin, S., Taguchi, A. K. W. & Woodbury, N. W. 1999 B-side electron transfer in a *Rhodobacter sphaeroides* reaction center mutant in which the B-side monomer bacteriochlorophyll is replaced with bacteriopheophytin. *Journal of Physical Chemistry B* **103**, 7386-7389.

Keasling, J. D. 2008 Synthetic biology for synthetic chemistry. *ACS Chemical Biology* **3**, 64-76.

Kikuchi, G., Shemin, D. & Bachmann, B. J. 1958 The enzymic synthesis of delta-aminolevulinic acid. *Biochimica Et Biophysica Acta* **28**, 219-220.

Kiley, P. J., Varga, A. & Kaplan, S. 1988 Physiological and structural analysis of light-harvesting mutants of *Rhodobacter sphaeroides*. *Journal of Bacteriology* **170**, 1103-15.

Kim, E. J. & Lee, J. K. 2010 Competitive inhibitions of the chlorophyll synthase of *Synechocystis sp*. strain PCC 6803 by bacteriochlorophyllide *a* and the bacteriochlorophyll synthase of *Rhodobacter sphaeroides* by chlorophyllide *a*. *Journal of Bacteriology* **192**, 198-207.

Kirmaier, C., Gaul, D., Debey, R., Holten, D. & Schenck, C. C. 1991 Charge separation in a reaction center incorporating bacteriochlorophyll for photoactive bacteriopheophytin. *Science* **251**, 922-927.

Kirmaier, C., Holten, D., Bylina, E. J. & Youvan, D. C. 1988 Electron-Transfer in a Genetically Modified Bacterial Reaction Center Containing a Heterodimer. *Proceedings of the National Academy of Sciences of the United States of America* **85**, 7562-7566.

Kirmaier, C., Laporte, L., Schenck, C. C. & Holten, D. 1995 The nature and dynamics of the charge-separated intermediate in reaction centers in which bacteriochlorophyll replaces the photoactive bacteriopheophytin. 2. The rates and yields of charge separation and recombination. *Journal of Physical Chemistry* **99**, 8910-8917.

Klamt, S., Grammel, H., Straube, R., Ghosh, R. & Gilles, E. D. 2008 Modeling the electron transport chain of purple non-sulfur bacteria. *Molecular Systems Biology* **4**, -.

Kleinfeld, D., Okamura, M. Y. & Feher, G. 1984 Electron-transfer in reaction centers of *Rhodopseudomonas sphaeroides*.1. Determination of the charge recombination pathway of $D^{+}Q_AQ_B^{-}$ and free-energy and kinetic relations between $Q_A^{-}Q_B$ and $Q_AQ_B^{-}$. *Biochimica Et Biophysica Acta* **766**, 126-140.

Klug, G., Liebetanz, R. & Drews, G. 1986 The influence of bacteriochlorophyll biosynthesis on formation of pigment-binding proteins and assembly of pigment protein complexes in *Rhodopseudomonas capsulata*. *Archives of Microbiology* **146**, 284-291.

Kobayashi, M., Takaya, A., Kanai, N., Ota, Y., Saito, T., Wang, Z. Y. & Nozawa, T. 2004 Reconstitution and replacement of bacteriochlorophyll *a* molecules in photosynthetic reaction centers. *The Journal of Biochemistry* **136**, 363-369.

Kobayashi, M., Yamamura, M., Akiyama, M., Kise, H., Inoue, K., Hara, M., Wakao, N., Yahara, K. & Watanabe, T. 1998 Acid resistance of Zn-bacteriochlorophyll *a* from an acidophilic bacterium *Acidiphilium rubrum*. *Analytical Sciences* **14**, 1149-1152.

Koblizek, M., Shih, J. D., Breitbart, S. I., Ratcliffe, E. C., Kolber, Z. S., Hunter, C. N. & Niederman, R. A. 2005 Sequential assembly of photosynthetic units in *Rhodobacter sphaeroides* as revealed by fast repetition rate analysis of variable bacteriochlorophyll *a* fluorescence. *Biochimica Et Biophysica Acta* **1706**, 220-231.

Koepke, J., Krammer, E. M., Klingen, A. R., Sebban, P., Ullmann, G. M. & Fritzsch, G. 2007 pH modulates the quinone position in the photosynthetic reaction center from *Rhodobacter sphaeroides* in the neutral and charge separated states. *Journal of Molecular Biology* **371**, 396-409.

Kohler, J. 2006 Single molecule spectroscopy of pigment protein complexes from purple bacteria. In *Chlorophylls and bacteriochlorophylls: biochemistry, biophysics, functions and applications*, vol. 25 (ed. B. Grimm, R. J. Porra, W. Rudiger & H. Scheer), pp. 309-321. Dordrecht: Springer.

Kugler, M., Jansch, L., Kruft, V., Schmitz, U. K. & Braun, H. P. 1997 Analysis of the chloroplast protein complexes by blue-native polyacrylamide gel electrophoresis (BN-PAGE). *Photosynthesis Research* **53**, 35-44.

Kulajta, C., Thumfart, J. O., Haid, S., Daldal, F. & Koch, H. G. 2006 Multi-step assembly pathway of the cbb_3-type cytochrome *c* oxidase complex. *Journal of Molecular Biology* **355**, 989-1004.

Kupper, H., Kupper, F. C. & Spiller, M. 2006 [Heavy metal]-chlorophylls formed *in vivo* during heavy metal stress and degradation products formed during digestion, extraction and storage of plant material. In *Chlorophylls and bacteriochlorophylls: biochemistry, biophysics, functions and applications*, vol. 25 (ed. B. Grimm, R. Porra, W. Rudiger & H. Scheer), pp. 67-77. Dordrecht: Springer.

Labbe, R. F., Vreman, H. J. & Stevenson, D. K. 1999 Zinc protoporphyrin: a metabolite with a mission. *Clinical Chemistry* **45**, 2060-2072.

Lancaster, C. R. D. & Blankenship, R. E. 1995 The structures of photosynthetic reaction centers from purple bacteria as revealed by X-ray crystallography. In *Anoxygenic photosynthetic bacteria*, pp. 503-526. Dordrecht: Kluwer Academic Publishers.

Larkum, A. W., Scaramuzzi, C., Cox, G. C., Hiller, R. G. & Turner, A. G. 1994 Light-harvesting chlorophyll *c*-like pigment in *Prochloron*. *Proceedings of the National Academy of Sciences of the United States of America* **91**, 679-83.

Lascelles, J. 1956 The synthesis of porphyrins and bacteriochlorophyll by cell suspensions of *Rhodopseudomonas spheroides*. *Biochemical Journal* **62**, 78-93.

Lascelles, J. 1968 The regulation of haem and chlorophyll synthesis. *Biochemical Society Symposium* **28**, 49-59.

Lavergne, J. & Vermeglio, A. 2009 Functional coupling between reaction centers and cytochrome bc_1 complexes. In *The purple phototrophic bacteria* (ed. C. N. Hunter, F. Daldal, M. C. Thurnauer & J. T. Beatty), pp. 509-536. Dordrecht: Springer.

Lazcano, A. & Miller, S. L. 1996 The origin and early evolution of life: prebiotic chemistry, the pre-RNA world, and time. *Cell* **85**, 793-8.

Leblanc, H. N. & Beatty, J. T. 1993 *Rhodobacter capsulatus puc* Operon - promoter location, transcript sizes and effects of deletions on photosynthetic growth. *Journal of General Microbiology* **139**, 101-109.

LeBlanc, H. N. & Beatty, J. T. 1996 Topological analysis of the *Rhodobacter capsulatus* PucC protein and effects of C-terminal deletions on light-harvesting complex II. *Journal of Bacteriology* **178**, 4801-4806.

Lide, D. R. 2009a Abundance of elements in the Earth's crust and in the sea. In *CRC handbook of chemistry and physics, 90th Edition* (ed. D. R. Lide), pp. 14-18. Boca Raton: CRC Press.

Lide, D. R. 2009b Solar spectral irradiance. In *CRC handbook of chemistry and physics, 90th Edition* (ed. D. R. Lide), pp. 14-19. Boca Raton: CRC Press.

Lide, D. R. 2009c Solubility chart. In *CRC handbook of chemistry and physics, 90th Edition* (ed. D. R. Lide), pp. 8-123. Boca Raton: CRC Press.

Lin, S. 2009 Personal Communication.

Lin, S., Jaschke, P. R., Wang, H., Paddock, M., Tufts, A., Allen, J. P., Rosell, F. I., Mauk, A. G., Woodbury, N. W. & Beatty, J. T. 2009a Electron transfer in the *Rhodobacter sphaeroides* reaction center assembled with zinc bacteriochlorophyll. *Proceedings of the National Academy of Sciences of the United States of America* **106**, 8537-8542.

Lin, S., Jaschke, P. R., Wang, H., Paddock, M., Tufts, A., Allen, J. P., Rosell, F. I., Mauk, A. G., Woodbury, N. W. & Beatty, J. T. 2009b Kinetics and energetics of electron transfer reactions in a photosynthetic bacterial reaction center assembled with zinc bacteriochlorophylls. *Annual Meeting of the Biophysical Society*.

Lin, S., Katilius, E., Haffa, A. L. M., Taguchi, A. K. W. & Woodbury, N. W. 2001 Blue light drives B-side electron transfer in bacterial photosynthetic reaction centers. *Biochemistry* **40**, 13767-13773.

Lin, S., Taguchi, A. K. W. & Woodbury, N. W. 1996 Excitation wavelength dependence of energy transfer and charge separation in reaction centers from *Rhodobacter sphaeroides*: evidence for adiabatic electron transfer. *Journal of Physical Chemistry* **100**, 17067-17078.

Lin, X., Williams, J. C., Allen, J. P. & Mathis, P. 1994 Relationship between rate and free-energy difference for electron-transfer from cytochrome c_2 to the reaction-center in *Rhodobacter sphaeroides*. *Biochemistry* **33**, 13517-13523.

Lundqvist, J., Elmlund, D., Heldt, D., Deery, E., Soderberg, C. A., Hansson, M., Warren, M. & Al-Karadaghi, S. 2009 The AAA(+) motor complex of subunits CobS and CobT of cobaltochelatase visualized by single particle electron microscopy. *Journal of Structural Biology* **167**, 227-34.

Lundqvist, J., Elmlund, H., Wulff, R. P., Berglund, L., Elmlund, D., Emanuelsson, C., Hebert, H., Willows, R. D., Hansson, M., Lindahl, M. & Al-Karadaghi, S. 2010 ATP-induced conformational dynamics in the AAA+ motor unit of magnesium chelatase. *Structure* **18**, 354-65.

Mackenzie, C., Choudhary, M., Larimer, F. W., Predki, P. F., Stilwagen, S., Armitage, J. P., Barber, R. D., Donohue, T. J., Hosler, J. P., Newman, J. E., Shapleigh, J. P., Sockett, R. E., Zeilstra-Ryalls, J. & Kaplan, S. 2001 The home stretch, a first analysis of the nearly completed genome of *Rhodobacter sphaeroides* 2.4.1. *Photosynthesis Research* **70**, 19-41.

Mann, H. B. & Whitney, D. R. 1947 On a test of whether one of 2 random variables is stochastically larger than the other. *Annals of Mathematical Statistics* **18**, 50-60.

Martin, V. J., Pitera, D. J., Withers, S. T., Newman, J. D. & Keasling, J. D. 2003 Engineering a mevalonate pathway in *Escherichia coli* for production of terpenoids. *Nature Biotechnology* **21**, 796-802.

Masuda, T., Inoue, K., Masuda, M., Nagayama, M., Tamaki, A., Ohta, H., Shimada, H. & Takamiya, K.-I. 1999 Magnesium insertion by magnesium chelatase in the

biosynthesis of zinc bacteriochlorophyll *a* in an aerobic acidophilic bacterium *Acidiphilium rubrum*. *The Journal of Biological Chemistry* **274**, 33594-33600.
Masuda, T. & Takahashi, S. 2006 Chemiluminescent-based method for heme determination by reconstitution with horseradish peroxidase apo-enzyme. *Analytical Biochemistry* **355**, 307-309.
Mazanows, A. M., Neuberger, A. & Tait, G. H. 1966 Effect of lipids and organic solvents on enzymic formation of zinc protoporphyrin and haem. *Biochemical Journal* **98**, 117-120.
McGlynn, P. & Hunter, C. N. 1993 Genetic analysis of the *bchC* gene and *bchA* gene of *Rhodobacter sphaeroides*. *Molecular & General Genetics* **236**, 227-234.
Melkozernov, A. N. & Blankenship, R. E. 2006 Photosynthetic functions of chlorophylls. In *Chlorophylls and Bacteriochlorophylls: Biochemistry, Biophysics, Functions and Applications*, vol. 25 (ed. G. B, P. R, R. W & S. H.). Dordrecht: Springer.
Michalski, T. J., Hunt, J. E., Bowman, M. K., Smith, U., Bardeen, K., Gest, H., Norris, J. R. & Katz, J. J. 1987 Bacteriopheophytin *g*: properties and some speculations on a possible primary role for bacteriochlorophyll *b* and bacteriochlorophyll *g* in the biosynthesis of chlorophylls. *Proceedings of the National Academy of Sciences of the United States of America* **84**, 2570-2574.
Miyamoto, K., Nishimura, K., Masuda, T., Tsuji, H. & Inokuchi, H. 1992 Accumulation of protoporphyrin IX in light-sensitive mutants of *Escherichia coli*. *FEBS Letters* **310**, 246-8.
Moody, M. D. & Dailey, H. A. 1985 Iron transport and its relation to heme biosynthesis in *Rhodopseudomonas sphaeroides*. *Journal of Bacteriology* **161**, 1074-1079.
Moskvin, O. V., Gomelsky, L. & Gomelsky, M. 2005 Transcriptome analysis of the *Rhodobacter sphaeroides* PpsR regulon: PpsR as a master regulator of photosystem development. *Journal of Bacteriology* **187**, 2148-2156.
Mullet, J. E., Klein, P. G. & Klein, R. R. 1990 Chlorophyll regulates accumulation of the plastid-encoded chlorophyll apoprotein-CP43 and apoprotein-D1 by increasing apoprotein stability. *Proceedings of the National Academy of Sciences of the United States of America* **87**, 4038-4042.
Muraki, N., Nomata, J., Ebata, K., Mizoguchi, T., Shiba, T., Tamiaki, H., Kurisu, G. & Fujita, Y. 2010 X-ray crystal structure of the light-independent protochlorophyllide reductase. *Nature* **465**, 110-4.
Murphy, M. J. & Siegel, L. M. 1973 Siroheme and sirohydrochlorin. The basis for a new type of porphyrin-related prosthetic group common to both assimilatory and dissimilatory sulfite reductases. *The Journal of Biological Chemistry* **248**, 6911-9.
Murphy, M. J., Siegel, L. M. & Kamin, H. 1974 Reduced nicotinamide adenine dinucleotide phosphate-sulfite reductase of enterobacteria. VI. The reaction of carbon monoxide with the *Escherichia coli* holoenzyme, the hemoprotein, and free siroheme. *The Journal of Biological Chemistry* **249**, 1610-4.
Nasrulhaqboyce, A., Griffiths, W. T. & Jones, O. T. G. 1987 The use of continuous assays to characterize the oxidative cyclase that synthesizes the chlorophyll isocyclic ring. *Biochemical Journal* **243**, 23-29.
NCBI. 2010 PubChem http://pubchem.ncbi.nlm.nih.gov/.

Neidle, E. L. & Kaplan, S. 1993 5-Aminolevulinic acid availability and control of spectral complex formation in *hemA* and *hemT* mutants of *Rhodobacter sphaeroides*. *Journal of Bacteriology* **175**, 2304-2313.

NetPrimer. 2010 http://www.premierbiosoft.com/netprimer/.

Neuberger, A. & Tait, G. H. 1964 Studies on the biosynthesis of porphyrin and bacteriochlorophyll by *Rhodopseudomonas spheroides*. *Biochemical Journal* **90**, 607-616.

Nisbet, E. G., Cann, J. R. & Vandover, C. L. 1995 Origins of Photosynthesis. *Nature* **373**, 479-480.

Nomata, J., Mizoguchi, T., Tamiaki, H. & Fujita, Y. 2006 A second nitrogenase-like enzyme for bacteriochlorophyll biosynthesis: reconstitution of chlorophyllide *a* reductase with purified X-protein (BchX) and YZ-protein (BchY-BchZ) from *Rhodobacter capsulatus*. *The Journal of Biological Chemistry* **281**, 15021-15028.

Noy, D., Fiedor, L., Hartwich, G., Scheer, H. & Scherz, A. 1998 Metal-substituted bacteriochlorophylls. 2. Changes in redox potentials and electronic transition energies are dominated by intramolecular electrostatic interactions. *Journal of the American Chemical Society* **120**, 3684-3693.

Oelze, J. 1988 Regulation of tetrapyrrole synthesis by light in chemostat cultures of *Rhodobacter sphaeroides*. *Journal of Bacteriology* **170**, 4652-4657.

Oh, J.-I., Eraso, J. M. & Kaplan, S. 2000 Interacting regulatory circuits involved in orderly control of photosynthesis gene expression in *Rhodobacter sphaeroides* 2.4.1. *Journal of Bacteriology* **182**, 3081-3087.

Oh, J. I. & Kaplan, S. 2000 Redox signaling: globalization of gene expression. *EMBO Journal* **19**, 4237-4247.

Okamura, M. Y., Paddock, M. L., Graige, M. S. & Feher, G. 2000 Proton and electron transfer in bacterial reaction centers. *Biochimica Et Biophysica Acta* **1458**, 148-163.

Oster, U., Bauer, C. E. & Rudiger, W. 1997 Characterization of chlorophyll *a* and bacteriochlorophyll *a* synthases by heterologous expression in *Escherichia coli*. *The Journal of Biological Chemistry* **272**, 9671-9676.

Ouchane, S., Steunou, A. S., Picaud, M. & Astier, C. 2004 Aerobic and anaerobic Mg-protoporphyrin monomethyl ester cyclases in purple bacteria: a strategy adopted to bypass the repressive oxygen control system. *The Journal of Biological Chemistry* **279**, 6385-94.

Paddock, M. L., Chang, C., Xu, Q., Abresch, E. C., Axelrod, H. L., Feher, G. & Okamura, M. Y. 2005 Quinone (Q_B) reduction by B-branch electron transfer in mutant bacterial reaction centers from *Rhodobacter sphaeroides*: quantum efficiency and X-ray structure. *Biochemistry* **44**, 6920-8.

Papenbrock, J., Grafe, S., Kruse, E., Hanel, F. & Grimm, B. 1997 Mg-chelatase of tobacco: identification of a *Chl D* cDNA sequence encoding a third subunit, analysis of the interaction of the three subunits with the yeast two-hybrid system, and reconstitution of the enzyme activity by co-expression of recombinant CHL D, CHL H and CHL I. *The Plant Journal* **12**, 981-990.

Papenbrock, J., Pfundel, E., Mock, H. P. & Grimm, B. 2000 Decreased and increased expression of the subunit CHL I diminishes Mg chelatase activity and reduces chlorophyll synthesis in transgenic tobacco plants. *The Plant Journal* **22**, 155-164.

Pappas, C. T., Sram, J., Moskvin, O. V., Ivanov, P. S., Mackenzie, R. C., Choudhary, M., Land, M. L., Larimer, F. W., Kaplan, S. & Gomelsky, M. 2004 Construction and validation of the

Rhodobacter sphaeroides 2.4.1 DNA microarray: transcriptome flexibility at diverse growth modes. *Journal of Bacteriology* **186**, 4748-4758.
Parson, W. W. & Warshel, A. 2009 Mechanism of charge separation in purple bacterial reaction centers. In *The purple phototrophic bacteria*, vol. 28 (ed. C. N. Hunter, F. Daldal, M. C. Thurnauer & J. T. Beatty), pp. 355-377. Dordrecht: Springer.
Paulsen, H. 2006 Reconstitution and pigment exchange. In *Chlorophylls and Bacteriochlorophylls: biochemistry, biophysics, functions and applications*, vol. 25 (ed. B. Grimm, R. J. Porra, W. Rudiger & H. Scheer), pp. 375-385. Dordrecht: Springer.
Peterson, G. L. 1983 Determination of total protein. *Methods in Enzymology* **91**, 95-119.
Porra, R. J., Schafer, W., Gad'on, N., Katheder, I., Drews, G. & Scheer, H. 1996 Origin of the two carbonyl oxygens of bacteriochlorophyll *a*: demonstration of two different pathways for the formation of ring E in *Rhodobacter sphaeroides* and *Roseobacter denitrificans*, and a common hydratase mechanism for 3-acetyl group formation. *European Journal of Biochemistry* **239**, 85-92.
Porra, R. J., Urzinger, M., Winkler, J., Bubenzer, C. & Scheer, H. 1998 Biosynthesis of the 3-acetyl and 13^1-oxo groups of bacteriochlorophyll *a* in the facultative aerobic bacterium, *Rhodovulum sulfidophilum*-the presence of both oxygenase and hydratase pathways for isocyclic ring formation. *European Journal of Biochemistry* **257**, 185-91.
Pretlow, T. P. & Sherman, F. 1967 Porphyrins and zinc porphyrins in normal and mutant strains of yeast. *Biochimica Et Biophysica Acta* **148**, 629-644.
Pudek, M. R. & Richards, W. R. 1975 A possible alternate pathway of bacteriochlorophyll biosynthesis in a mutant of *Rhodopseudomonas sphaeroides*. *Biochemistry* **14**, 3132-7.
Qian, P., Bullough, P. A. & Hunter, C. N. 2008 Three-dimensional reconstruction of a membrane-bending complex: the RC-LH1-PufX core dimer of *Rhodobacter sphaeroides*. *The Journal of Biological Chemistry* **283**, 14002-14011.
Qian, P., Hunter, C. N. & Bullough, P. A. 2005 The 8.5 angstrom projection structure of the core RC-LH1-PufX dimer of *Rhodobacter sphaeroides*. *Journal of Molecular Biology* **349**, 948-960.
Ramesh, V. M., Gibasiewicz, K., Lin, S., Bingham, S. E. & Webber, A. N. 2007 Replacement of the methionine axial ligand to the primary electron acceptor A_0 slows the A_0-reoxidation dynamics in photosystem I. *Biochimica Et Biophysica Acta* **1767**, 151-60.
Raux, E., Thermes, C., Heathcote, P., Rambach, A. & Warren, M. J. 1997 A role for *Salmonella typhimurium cbiK* in cobalamin (Vitamin B-12) and siroheme biosynthesis. *Journal of Bacteriology* **179**, 3202-3212.
Rebeiz, C. A. 2002 Analysis of intermediates and end products of the chlorophyll biosynthetic pathway. In *Heme, chlorophyll, and bilins: methods and protocols* (ed. A. G. Smith & M. Witty), pp. 111-155. Totowa: Humana Press.
Reid, J. D. & Hunter, C. N. 2004 Magnesium-dependent ATPase activity and cooperativity of magnesium chelatase from *Synechocystis sp*. PCC6803. *The Journal of Biological Chemistry* **279**, 26893-9.
Reisinger, V. & Eichacker, L. A. 2007 How to analyze protein complexes by 2D blue native SDS-PAGE. *Proteomics* **7 Suppl 1**, 6-16.
Richard-Fogal, C. L., Frawley, E. R., Feissner, R. E. & Kranz, R. G. 2007 Heme concentration dependence and metalloporphyrin inhibition of the system I and II cytochrome *c* assembly pathways. *Journal Bacteriology* **189**, 455-63.

Rokka, A., Suorsa, M., Saleem, A., Battchikova, N. & Aro, E. M. 2005 Synthesis and assembly of thylakoid protein complexes: multiple assembly steps of photosystem II. *Biochemical Journal* **388**, 159-168.

Romagnoli, S. & Tabita, R. F. 2009 Carbon dioxide metabolism and its regulation in nonsulfur purple photosynthetic bacteria. In *The purple phototrophic bacteria* (ed. C. N. Hunter, F. Daldal, M. C. Thurnauer & J. T. Beatty), pp. 563-576: Springer Science.

Rüdiger, W., Bohm, S., Helfrich, M., Schulz, S. & Schoch, S. 2005 Enzymes of the last steps of chlorophyll biosynthesis: modification of the substrate structure helps to understand the topology of the active centers. *Biochemistry* **44**, 10864-10872.

Rutherford, K., Parkhill, J., Crook, J., Horsnell, T., Rice, P., Rajandream, M. A. & Barrell, B. 2000 Artemis: sequence visualization and annotation. *Bioinformatics* **16**, 944-5.

Sarma, R., Barney, B. M., Hamilton, T. L., Jones, A., Seefeldt, L. C. & Peters, J. W. 2008 Crystal structure of the L protein of *Rhodobacter sphaeroides* light-independent protochlorophyllide reductase with MgADP bound: a homologue of the nitrogenase Fe protein. *Biochemistry* **47**, 13004-15.

Sawicki, A. & Willows, R. D. 2008 Kinetic analyses of the magnesium chelatase provide insights into the mechanism, structure, and formation of the complex. *The Journal of Biological Chemistry* **283**, 31294-31302.

Schagger, H. & von Jagow, G. 1987 Tricine sodium dodecyl sulfate-polyacrylamide gel electrophoresis for the separation of proteins in the range from 1 to 100 kDa. *Analytical Biochemistry* **166**, 368-379.

Scheer, H. 2006 An overview of chlorophylls and bacteriochlorophylls: biochemistry, biophysics, functions and applications. In *Chlorophylls and bacteriochlorophylls: biochemistry, biophysics, functions and applications*, vol. 25 (ed. B. Grimm, R. J. Porra, W. Rudiger & H. Scheer), pp. 1-26. Dordrecht: Springer.

Scheer, H. & Hartwich, G. 1995 Bacterial reaction centers with modified tetrapyrrole chromophores. In *Anoxygenic photosynthetic bacteria*, vol. 2 (ed. R. E. Blankenship, M. T. Madigan & C. E. Bauer), pp. 649-663. Dordrecht: Kluwer Academic Publishers.

Scheumann, V., Helfrich, M., Schoch, S. & Rudiger, W. 1996a Reduction of the formyl group of zinc pheophorbide *b in vitro* and *in vivo*: a model for the chlorophyll *b* to *a* transformation. *Zeitschrift Fur Naturforschung C* **51**, 185-194.

Scheumann, V., Ito, H., Tanaka, A., Schoch, S. & Rudiger, W. 1996b Substrate specificity of chlorophyll(ide) *b* reductase in etioplasts of barley (*Hordeum vulgare L*). *European Journal of Biochemistry* **242**, 163-170.

Scheuring, S., Busselez, J. & Levy, D. 2005 Structure of the dimeric PufX-containing core complex of *Rhodobacter blasticus* by *in situ* atomic force microscopy. *The Journal of Biological Chemistry* **280**, 1426-1431.

Scheuring, S., Francia, F., Busselez, J., Melandri, B. A., Rigaud, J. L. & Levy, D. 2004 Structural role of PufX in the dimerization of the photosynthetic core complex of *Rhodobacter sphaeroides*. *The Journal of Biological Chemistry* **279**, 3620-3626.

Schoch, S. & Ihl, M. 1998 Substrate specificity of chlorophyllase from different plants. *Zeitschrift Fur Naturforschung C* **53**, 21-26.

Schubert, W. D., Klukas, O., Saenger, W., Witt, H. T., Fromme, P. & Krauss, N. 1998 A common ancestor for oxygenic and anoxygenic photosynthetic systems: a comparison based on the structural model of photosystem I. *Journal of Molecular Biology* **280**, 297-314.

Sener, M. K. & Schulten, K. 2009 From atomic-level structure to supramolecular organization in the photosynthetic unit of purple bacteria. In *The purple phototrophic bacteria* (ed. C. N. Hunter, F. Daldal, M. C. Thurnauer & J. T. Beatty), pp. 275-294. Dordrecht: Springer.

Shapleigh, J. P., Hill, J. J., Alben, J. O. & Gennis, R. B. 1992 Spectroscopic and genetic evidence for two heme-Cu-containing oxidases in *Rhodobacter sphaeroides*. *Journal of Bacteriology* **174**, 2338-43.

Shioi, Y., Doi, M. & Boddi, B. 1988 Selective inhibition of chlorophyll biosynthesis by nicotinamide. *Archives of Biochemistry and Biophysics* **267**, 69-74.

Simon, R., Priefer, U. & Puhler, A. 1983 A broad host range mobilization system for *in vivo* genetic engineering transposon mutagenesis in gram-negative bacteria. *Bio/technology* **1**, 784-791.

Smirnov, N. 1939 On the estimation of the discrepancy between empirical curves of distribution for two independent samples *Bulletin Mathematique de l'Universite de Moscou* **2**.

Stephens, L. 2004 Nonparametric statistics. In *Advanced statistics demystified*. New York: McGraw-Hill Professional.

Stillman, L. C. & Gassman, M. L. 1978 Protoheme extraction from plant tissue. *Analytical Biochemistry* **91**, 166-172.

Student. 1908 The probable error of a mean. *Biometrika* **6**, 1-25.

Sturgis, J. N., Hunter, C. N. & Niederman, R. A. 1988 Spectra and extinction coefficients of near-infrared absorption bands in membranes of *Rhodobacter sphaeroides* mutants lacking light-harvesting and reaction center complexes. *Photochemistry and Photobiology* **48**, 243-247.

Suzuki, J. Y. & Bauer, C. E. 1995 Altered monovinyl and divinyl protochlorophyllide pools in *bchJ* mutants of *Rhodobacter capsulatus:* possible monovinyl substrate discrimination of light-independent protochlorophyllide reductase. *Journal of Biological Chemistry* **270**, 3732-3740.

Suzuki, J. Y., Bollivar, D. W. & Bauer, C. E. 1997 Genetic analysis of chlorophyll biosynthesis. *Annual Review of Genetics* **31**, 61-89.

Swamy, M., Kulathu, Y., Ernst, S., Reth, M. & Schamel, W. W. A. 2006 Two dimensional blue bative-/SDS-PAGE analysis of SLP family adaptor protein complexes. *Immunology Letters* **104**, 131-137.

Takahashi, S. & Masuda, T. 2009 High throughput heme assay by detection of chemiluminescence of reconstituted horseradish peroxidase. *Combinatorial Chemistry & High Throughput Screening* **12**, 532-5.

Takemoto, J. & Lascelles, J. 1973 Coupling between bacteriochlorophyll and membrane protein synthesis in *Rhodopseudomonas spheroides*. *Proceedings of the National Academy of Sciences of the United States of America* **70**, 799-803.

Tehrani, A. 2003 Structure-based functional studies of the *Rhodobacter sphaeroides* reaction centre H protein. Department of Microbiology and Immunology, Ph.D., Vancouver: University of British Columbia.

Tehrani, A. & Beatty, J. T. 2004 Effects of precise deletions in *Rhodobacter sphaeroides* reaction center genes on steady-state levels of reaction center proteins: a revised model for reaction center assembly. *Photosynthesis Research* **79**, 101-108.

Tehrani, A., Prince, R. C. & Beatty, J. T. 2003 Effects of photosynthetic reaction center H protein domain mutations on photosynthetic properties and reaction center assembly in *Rhodobacter sphaeroides*. *Biochemistry* **42**, 8919-8928.

Tichy, H. V., Albien, K. U., Gad'on, N. & Drews, G. 1991 Analysis of the *Rhodobacter capsulatus puc* operon: the *pucC* gene plays a central role in the regulation of LHII (B800-850 complex) expression. *EMBO Journal* **10**, 2949-55.

Tomi, T., Shibata, Y., Ikeda, Y., Taniguchi, S., Haik, C., Mataga, N., Shimada, K. & Itoh, S. 2007 Energy and electron transfer in the photosynthetic reaction center complex of *Acidiphilium rubrum* containing Zn-bacteriochlorophyll *a* studied by femtosecond up-conversion spectroscopy. *Biochimica Et Biophysica Acta* **1767**, 22-30.

Treynor, T. P., Yoshina-Ishii, C. & Boxer, S. G. 2004 Probing excited-state electron transfer by resonance stark spectroscopy: 4. Mutations near B_L in photosynthetic reaction centers perturb multiple factors that affect B_L^*->$B_L^+H_L^-$. *The Journal of Physical Chemistry. B* **108**, 13523-13535.

Tuboi, S., Kim, H. J. & Kikuchi, G. 1970a Differential induction of fraction I and fraction II of delta-aminolevulinate synthetase in *Rhodopseudomonas spheroides* under various incubation conditions. *Archives of Biochemistry and Biophysics* **138**, 155-158.

Tuboi, S., Kim, H. J. & Kikuchi, G. 1970b Occurrence and properties of 2 types of delta-aminolevulinate synthetase in *Rhodopseudomonas spheroides*. *Archives of Biochemistry and Biophysics* **138**, 147-&.

Tucker, J. D., Siebert, C. A., Escalante, M., Adams, P. G., Olsen, J. D., Otto, C., Stokes, D. L. & Hunter, C. N. 2010 Membrane invagination in *Rhodobacter sphaeroides* is initiated at curved regions of the cytoplasmic membrane, then forms both budded and fully detached spherical vesicles. *Molecular Microbiology*.

Varga, A. R. & Kaplan, S. 1993 Synthesis and stability of reaction center polypeptides and implications for reaction center assembly in *Rhodobacter sphaeroides*. *The Journal of Biological Chemistry* **268**, 19842-19850.

Wacker, W. E. C., Tait, G. H. & Neuberger, A. 1965 Definitive identification of enzymatically formed zinc protoporphyrin. *Biochemistry* **4**, 940-943.

Wakao, N., Yokoi, N., Isoyama, N., Hiraishi, A., Shimada, K., Kobayashi, M., Kise, H., Iwaki, M., Itoh, S., Takaichi, S. & Sakurai, Y. 1996 Discovery of natural photosynthesis using Zn-containing bacteriochlorophyll in an aerobic bacterium *Acidiphilium rubrum*. *Plant & Cell Physiology* **37**, 889-893.

Wang, H., Lin, S., Allen, J. P., Williams, J. C., Blankert, S., Laser, C. & Woodbury, N. W. 2007 Protein dynamics control the kinetics of initial electron transfer in photosynthesis. *Science* **316**, 747-750.

Watson, A. J., Fyfe, P. K., Frolov, D., Wakeham, M. C., Nabedryk, E., van Grondelle, R., Breton, J. & Jones, M. R. 2005 Replacement or exclusion of the B-branch bacteriopheophytin in the purple bacterial reaction centre: the H_B cofactor is not required for assembly or core function of the *Rhodobacter sphaeroides* complex. *Biochimica Et Biophysica Acta* **1710**, 34-46.

Weissman, K. J. 2007 Mutasynthesis - uniting chemistry and genetics for drug discovery. *Trends in Biotechnology* **25**, 139-42.

Wellington, C. L. & Beatty, J. T. 1989 Promoter mapping and nucleotide sequence of the *bchC* bacteriochlorophyll biosynthesis gene from *Rhodobacter capsulatus*. *Gene* **83**, 251-261.

Williams, J. C. & Allen, J. P. 2009 Directed modification of reaction centers from purple bacteria. In *The purple phototrophic bacteria* (ed. C. N. Hunter, F. Daldal, M. C. Thurnauer & J. T. Beatty), pp. 337-353: Springer Science.
Williams, J. C. & Taguchi, A. K. W. 1995 Genetic manipulation of purple photosynthetic bacteria. In *Anoxygenic photosynthetic bacteria*, vol. 2 (ed. R. E. Blankenship, M. T. Madigan & C. E. Bauer), pp. 1029-1065. Dordrecht: Kluwer Academic Publishers.
Williams, R. J. 1997 The natural selection of the chemical elements. *Cellular and molecular life sciences : CMLS* **53**, 816-29.
Willows, R. D. & Kriegel, A. M. 2009 Biosynthesis of bacteriochlorophylls in purple bacteria. In *The purple phototrophic bacteria* (ed. C. N. Hunter, F. Daldal, M. C. Thurnauer & J. T. Beatty), pp. 57-79: Springer Science.
Wittig, I., Braun, H. P. & Schagger, H. 2006 Blue native PAGE. *Nature Protocols* **1**, 418-28.
Wittig, I. & Schagger, H. 2008 Features and applications of blue-native and clear-native electrophoresis. *Proteomics* **8**, 3974-3990.
Wohlleben, W. & Pelzer, S. 2002 New compounds by combining "modern" genomics and "old-fashioned" mutasynthesis. *Chemistry & Biology* **9**, 1163-1164.
Woodbury, N. W., Allen, J. P. & Blankenship, R. E. 1995 Electron transfer in purple nonsulfur bacteria. In *Anoxygenic photosynthetic bacteria*, pp. 527-557. Dordrecht: Kluwer Academic Publishers.
Xiong, J., Fischer, W. M., Inoue, K., Nakahara, M. & Bauer, C. E. 2000 Molecular evidence for the early evolution of photosynthesis. *Science* **289**, 1724-30.
Yan, J. 2010 Isotope Pattern Calculator v4.0. http://www-personal.umich.edu/~junhuay/pattern.htm.
Yeates, T. O., Komiya, H., Chirino, A., Rees, D. C., Allen, J. P. & Feher, G. 1988 Structure of the reaction center from *Rhodobacter sphaeroides* R-26 and 2.4.1: protein-cofactor (bacteriochlorophyll, bacteriopheophytin, and carotenoid) interactions. *Proceedings of the National Academy of Sciences of the United States of America* **85**, 7993-7.
Young, C. S. & Beatty, J. T. 1998 Topological model of the *Rhodobacter capsulatus* light-harvesting complex I assembly protein LhaA (Previously known as ORF1696). *Journal of Bacteriology* **180**, 4742-4745.
Young, C. S., Reyes, R. C. & Beatty, J. T. 1998 Genetic complementation and kinetic analyses of *Rhodobacter capsulatus* ORF1696 mutants indicate that the ORF1696 protein enhances assembly of the light-harvesting I complex. *Journal of Bacteriology* **180**, 1759-1765.
Yubisui, T. & Yoneyama, Y. 1972 Delta-aminolevulinic acid synthetase of *Rhodopseudomonas spheroides*: purification and properties of enzyme. *Archives of Biochemistry and Biophysics* **150**, 77-80.
Zeilstra-Ryalls, J., Gomelsky, M., Eraso, J. M., Yeliseev, A., O'Gara, J. & Kaplan, S. 1998 Control of photosystem formation in *Rhodobacter sphaeroides*. *Journal of Bacteriology* **180**, 2801-2809.
Zhang, H. T., Li, J. J., Yoo, J. H., Yoo, S. C., Cho, S. H., Koh, H. J., Seo, H. S. & Paek, N. C. 2006 Rice *chlorina-1* and *chlorina-9* encode ChlD and ChlI subunits of Mg-chelatase, a key enzyme for chlorophyll synthesis and chloroplast development. *Plant Molecular Biology* **62**, 325-337.

Zouni, A., Witt, H. T., Kern, J., Fromme, P., Krauss, N., Saenger, W. & Orth, P. 2001 Crystal structure of photosystem II from *Synechococcus elongatus* at 3.8 Å resolution. *Nature* **409**, 739-43.

APPENDIX I

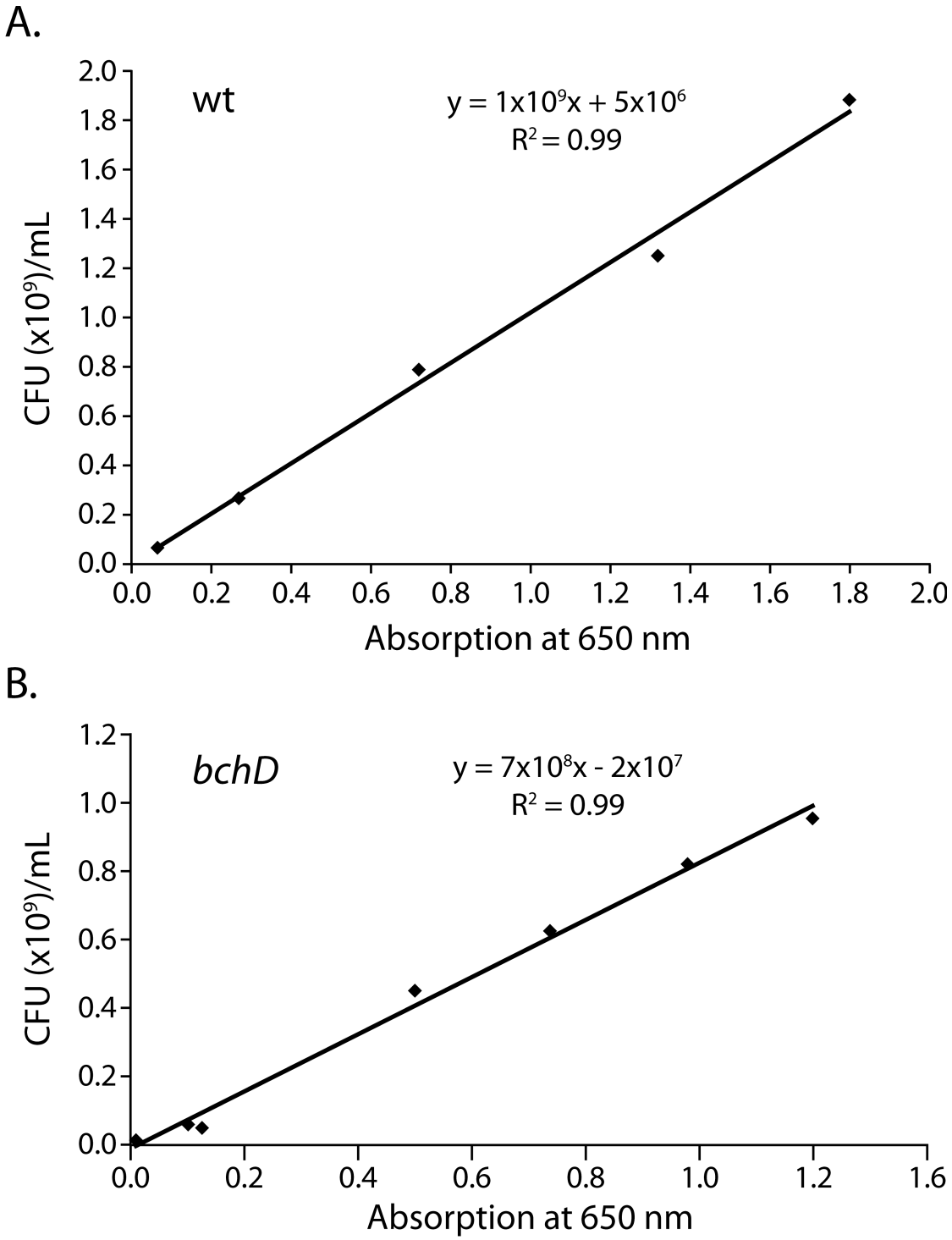

Appendix I. Comparison of numbers of CFUs per unit of absorbed light at 650 nm in wt and *bchD* mutant. (A) Wild type. (B) *bchD* mutant. Samples were taken from cultures growing semiaerobically, diluted and spread on LB plates, then colonies were counted after three days of growth at 30°C.

APPENDIX II

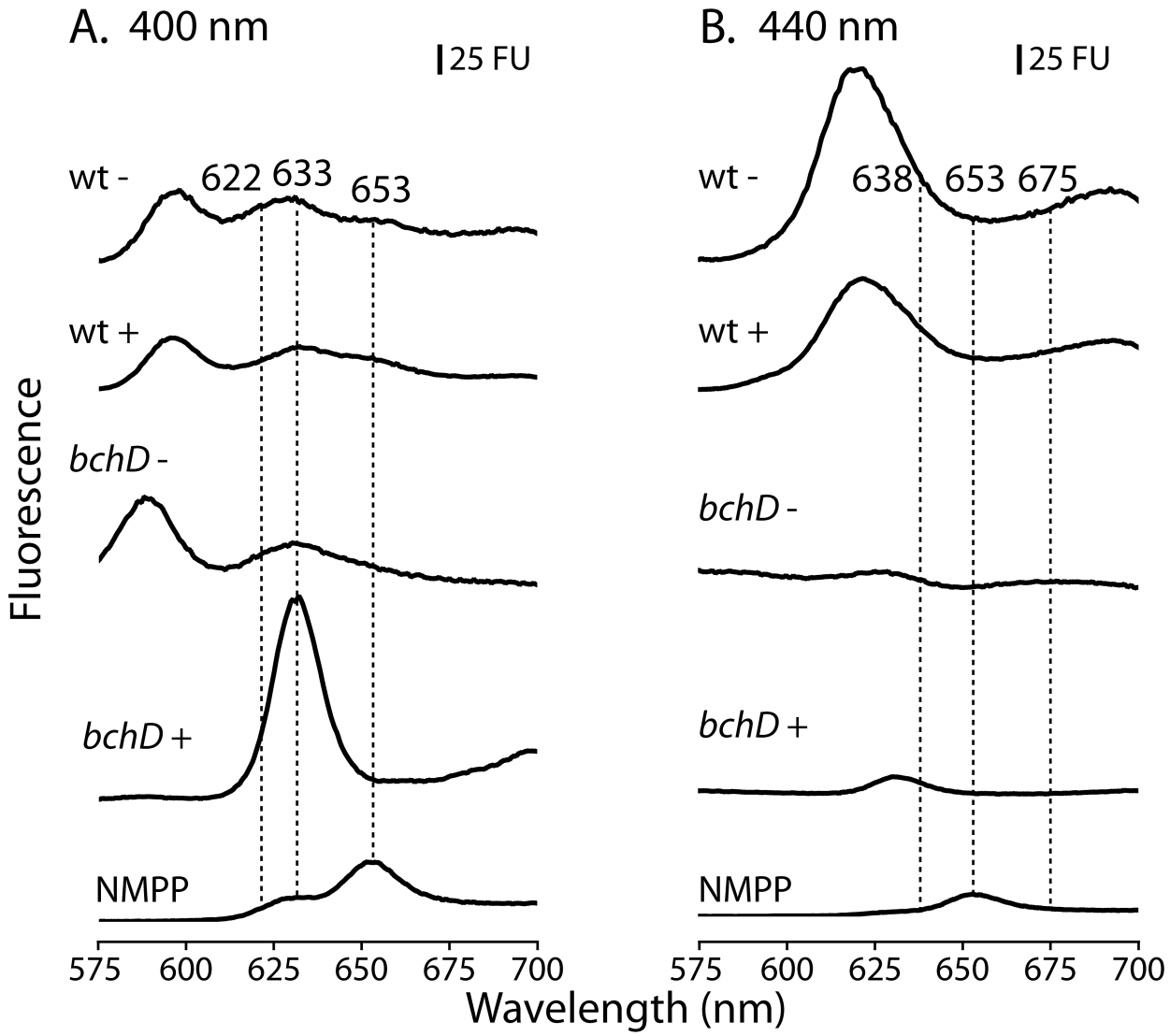

Appendix II. Fluorescence of NMPP at wavelengths used to determine PPIX concentration. (A) Excitation at 400 nm. Fluorescence emission at 622 and 633 nm used in PPIX deconvolution formula. Emission at 653 nm due to NMPP is not seen in the treated wt (+) or *bchD* (+) extracts. (B) Excitation at 440 nm. Fluorescence emission at 638 and 675 nm used in PPIX deconvolution formula. Emission at 653 nm due to NMPP is not seen in the treated wt (+) or *bchD* (+) extracts. + and -, presence or absence of 2 μM NMPP in growth medium of cells where measured extract originated. Dotted lines indicate wavelengths used in the PPIX deconvolution equation or due to NMPP fluorescence.

These data show the fluorescence traces used to calculate PPIX levels after ferrochelatase inhibition using NMPP. Since NMPP is a fluorescent molecule itself and was added to cultures at 2 μM, I wanted to show that NMPP fluorescence was not exaggerating the

amount of PPIX in the wt and *bchD* mutant measurements. For the NMPP to contribute to the fluorescence of the extract it would have to have entered the cell from the media and then been retained during the harvesting of the cells. Upon extraction of cells it would have had to be soluble in the 9/1 acetone/NH_4OH extraction and not been removed by hexane extraction. To test these assumptions I dissolved 2.0 µM NMPP into 9/1 acetone/NH_4OH and scanned it under similar conditions to those used to scan extracts from cells treated with NMPP. The emission spectra show that NMPP fluoresces at 622 and 633 nm (400 nm excitation), which are wavelengths used in the PPIX measurement, so it does have the potential to alter the amount of measured PPIX. But, if we look at where the main 653 nm emission peak of NMPP would expect to be in the extracts, we do not see it. This would indicate that the NMPP was not extracted from cells to any appreciable amount and likely did not contribute to the measured amounts of PPIX.

APPENDIX III

Exp	Strain	Condition	CFU	P-value W	P-value t	Strain	Condition	CFU	P-value W	P-value t
1	wt	L	20			*bchD*	L	10		
		L	17				L	9		
		D	26				D	19		
		D	21	0.33	0.23		D	11	0.33	0.31
2	wt	L	26			*bchD*	L	24		
		L	25				L	24		
		L	23				L	26		
		L	28				L	25		
		D	37				D	13		
		D	33				D	34		
		D	29				D	25		
		D	27	0.06	0.05		D	25	0.80	0.91
3	wt	L	3			*bchD*	L	2		
		L	3				L	1		
		L	3				L	4		
		L	3				L	7		
		D	3				D	4		
		D	2				D	3		
		D	2				D	5		
		D	4	0.43	0.62		D	2	0.83	1.00

Appendix III. Effect of light on aerobic growth in the wt and *bchD* mutant strains. Aerobically grown cultures were diluted 10^{-6} and 100 µL was spread onto dry LB plates. Plates were either wrapped in aluminum foil for the dark condition or left unwrapped for the light condition and placed in a plastic jar with partially covered lid within an aquarium light box setup for photosynthetic growth of *Rb. sphaeroides* cultures. Plates were incubated aerobically under illumination (75 µEinsteins/m^2s at 400-700 nm wavelength) and ~28°C for 4 days, followed by counting of CFUs. L, light grown plate; D, dark grown plate. P-value, two-sided for the case CFUs in dark condition is not equal to CFUs in light condition where W, tested using two-independent sample Wilcoxon rank sum test; t, tested using two-independent sample t-test.